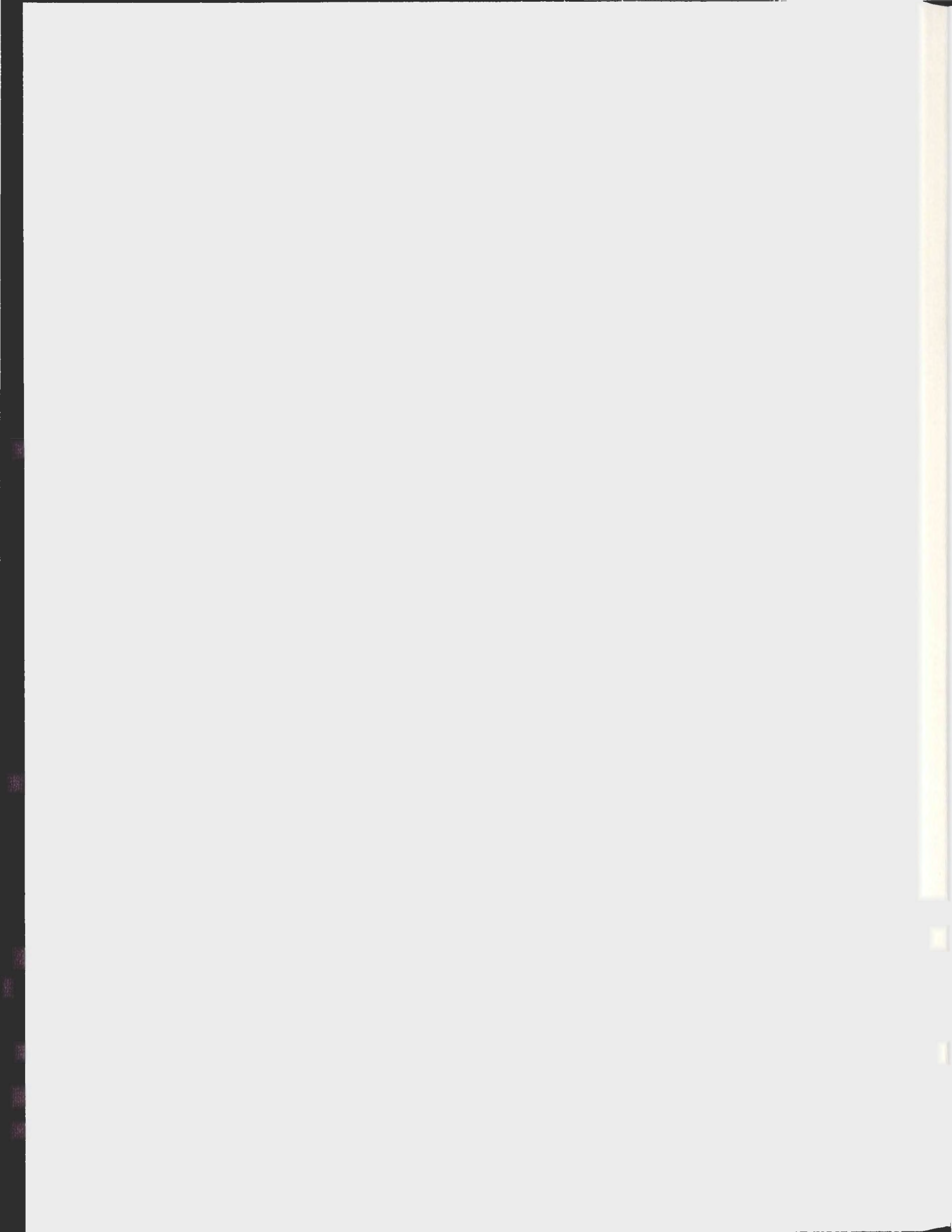


SENSOR DYNAMICS OF AUTONOMOUS
UNDERWATER GLIDERS

C.M. BISHOP



Sensor Dynamics of Autonomous Underwater Gliders

by

© C. M. Bishop
B.Sc (Physics)

A thesis submitted to the
School of Graduate Studies
in partial fulfillment of the
requirements for the degree of
Master of Science.

Environmental Science Program
Memorial University of Newfoundland

May 19th, 2008

ST. JOHN'S

NEWFOUNDLAND

Contents

Abstract	vii
Acknowledgements	ix
List of Tables	xi
List of Figures	xiv
1 Autonomous Underwater Gliders (AUGs)	1
1.1 Introduction	1
1.1.1 Henry Stommel's 'Slocum Mission'	2
1.2 Technical Specifications of the Glider	2
1.2.1 Principle of Operation	5
1.2.2 Communications	6
1.3 The Potential of AUGs	6
1.3.1 Comparison to Other Modes of Sampling	7
1.4 The Various Sensors	7
1.4.1 Limitations	8
1.4.2 Internal Sensors	9
1.4.3 Science Sensors	9

1.5	Purpose of this Project	10
2	Glider Deployments and Collected Data	12
2.1	Deployments	12
2.1.1	Introduction	12
2.1.2	Operational Test - Trinity Bay to Shelf	13
2.1.3	Oxygen optode Test	15
2.1.4	Validation Deployment	20
2.2	Collected Data	27
2.2.1	Preparation of the Data	27
2.2.2	Data Distribution	27
2.2.3	Tool Boxes	28
3	Analysis of the CTD Sensor	29
3.1	Introduction	29
3.1.1	Why Measure Temperature and Salinity?	29
3.2	Theory of Operation	31
3.3	Sensor Anomalies	31
3.3.1	The Sensor Response Problem	32
3.3.2	The Thermal Lag Problem	34
3.4	Corrections	37
3.4.1	Correcting for Sensor Response	37
3.4.2	Correcting Salinity for Thermal Lag	38
3.4.3	Comparison of Corrected Data	41
3.5	Discussion	46

4	Analysis of the Oxygen Optode Sensor	53
4.1	Introduction	53
4.1.1	Why Measure Dissolved Oxygen?	54
4.1.2	A Brief History of Oxygen Sensors	54
4.2	Theory of Operation	55
4.3	Sensor Anomalies	58
4.3.1	Sensor Response Problems	60
4.3.2	Sensitivity to Temperature	61
4.3.3	Sensitivity to Salinity	61
4.3.4	Sensitivity to Pressure	62
4.4	Corrections	63
4.4.1	Decomposition of Oxygen Concentration Data	64
4.4.2	Correction for Sensor Response	66
4.4.3	Replacing Optode Temperature with CTD Temperature	69
4.4.4	Adjusting Oxygen Data for Salinity	72
4.4.5	Adjusting Oxygen Data for Pressure	74
4.4.6	Comparison of Corrected Data	74
4.4.7	Determining new Coefficients for Calculation of DO_2	82
4.5	Discussion	83
5	Analysis of Attitude Sensor and GPS	87
5.1	Introduction	87
5.2	Estimation of Depth-Averaged Currents	88
5.3	Estimation of Surface Currents	92
5.3.1	Error Analysis	95
5.4	Slocum Gliders and Wind	96

5.4.1	Heading Information from the Attitude Sensor	98
5.4.2	Testing the Slocum's Compass	101
5.4.3	Comparison to Environment Canada Wind Data	101
5.5	Discussion	111
6	Summary	114
6.1	Summary of the CTD	114
6.1.1	Future Work and Recommendations	115
6.2	Summary of the Optode	115
6.2.1	Future Work and Recommendations	116
6.3	Summary of the Attitude/GPS	117
6.3.1	Future Work and Recommendations	117
6.4	Implications Of This Project	118
	Bibliography	119
	Appendix 1	123
A.1	Distance Calculator and Contouring	124
A.2	CTD Corrections	126
A.2.1	Fofonoff Correction for Lagged Response	126
A.2.2	Correction for Thermal-Lag	127
A.3	Optode Corrections	128
A.3.1	Back-Calculation of Phase Data	128
A.3.2	Adjusting for Lagged Response	130
A.3.3	Re-calculation of DO_2	131
A.3.4	Adjusting for Salinity	132
A.3.5	Adjusting for Pressure	133

A.4 Water Velocity Calculator 133

Abstract

Over the past decade, underwater gliders have been developed as a new autonomous sampling platform. These gliders are a type of autonomous underwater vehicle (AUV) that can be deployed in the ocean for weeks to months to collect *in situ* measurements in the world's oceans. Gliders allow us to complement traditional ship sampling by providing continuous spatial data, as opposed to ship-based casts which may be separated in the horizontal by tens to hundreds of kilometers. Oceanographic data is limited, however, by the instrument providing it.

There are several different types of underwater gliders; the glider used in this research is the Slocum battery-powered glider produced by Webb Research. At a length of 1.5 m and a mass of 52 kg, these vehicles are easily deployed by just two people and make the process of collecting *in-situ* data quick and cost-effective. By default, the Slocum glider comes with a non-pumped Conductivity-Temperature-Depth (CTD) sensor; our research group has also installed an Aanderra Dissolved Oxygen Optode sensor, with future plans of incorporating different types of sensors to extend the platform's usability. An in-depth examination of the science sensors on board the glider must be performed in order to understand the limitations of the data collected.

Here, we examine the data collected on the Newfoundland Shelf along with a study of the different sensor dynamics problems discovered during our research and field deployments. There is a well documented history of sensor dynamics issues

in operational oceanography to which the Slocum glider is not immune. This work focuses on determining the specific sensor responses of the individual instruments on board the glider, and developing post-processing algorithms for the collected data to ensure all instruments sample at the same time interval. Algorithms developed are verified by testing against other independent sensors and appear to correctly minimize sensor response issues. Also, an analysis of how our local environment (strong winds) affect the operation of our Slocum at the surface is carried out, with an emphasis on the heading data from the Attitude sensor, and GPS location. The Slocum does align with the wind, similar to a weathervane, but wind effects are negligible.

Acknowledgements

This work would not be possible without many people to whom I would like to express my gratitude.

My supervisors, Brad de Young and Ralf Bachmayer, provided many opportunities to participate in field work, and to work with many different researchers in our discipline. I was given the well rounded educational experience that I was seeking. Many different professors and research assistants have provided guidance along the way: Entcho Demirov, Daniel Bourgault, and Jack Foley.

My girlfriend, Nicole Watson, for putting up with the many late hours and keeping me fed (and sane) throughout the entire process. :) My office mates, William, Dave, Graig, Lu, Jenn, Lindsay, and many others, for providing countless distractions and making me laugh.

My parents, for allowing me to find my own path in life.

*Through me you pass in the city of woe:
Through me you pass into eternal pain:
Through me among the people lost for aye.
Justice the founder of my fabric mov'd:
To rear me was the task of power divine.
Sumpreme wisdom, and primeval love.
Before me things create were none, save things
Eternal, and eternal I endure.
All hope abandon ye who enter here.
- Dante Alighieri (1314)*

List of Tables

1.1	Technical Specifications of the Slocum Battery Glider	3
1.2	Glider Advantages and Disadvantages	8
1.3	Ship Advantages and Disadvantages	8
2.1	Mission Stats - Operational Test	15
2.2	Mission Stats - oxygen optode Test	19
2.3	Mission Stats - Validation Test	20
3.1	Differing values for τ_{Temp} and τ_{Cond} from other sources.	49
3.2	Differing values for α and τ from other sources.	50
4.1	Sensing Foil Calibration Coefficients.	66
4.2	Oxygen Optode Constants for Salinity Corrections.	72
4.3	Corrected Sensing Foil Calibration Coefficients.	83
4.4	Comparison of Raw and Corrected Glider Data to Ship-Based Data.	86
5.1	Depth-Averaged Ocean Currents - Operational Test. Data obtained from Glider unit: 49, Julian Days: 205-226, 2006.	91
5.2	Depth-Averaged Ocean Currents - Optode Test. Data obtained from Glider unit: 48, Julian Days: 267-275, 2006.	91

5.3	Surface Ocean Currents - Operational Test. Data obtained from Glider unit: 49, Julian Days: 205-226, 2006.	95
5.4	Surface Ocean Currents - Optode Test. Data obtained from Glider unit: 48, Julian Days: 267-275, 2006	95

List of Figures

1.1	The Slocum Glider	4
2.1	Map of Glider Deployments	14
2.2	Operational Test Flight - Temperature Contour	16
2.3	Operational Test Flight - Salinity Contour	17
2.4	Operational Test Flight - Density Contour	18
2.5	Optode is exposed through a 5 by 5cm hole	19
2.6	Oxygen optode Test Flight - Temperature Contour	21
2.7	Oxygen optode Test Flight - Salinity Contour	22
2.8	Oxygen optode Test Flight - Density Contour	23
2.9	Oxygen optode Test Flight - O ₂ Saturation Contour	24
2.10	Map of glider/ship route for verification of corrections.	25
2.11	A Slocum glider with accompanying Seabird Electronics 19+ CTD.	26
3.1	Location of the CTD on the Slocum Glider	30
3.2	Example of salinity downcast/upcast anomaly	33
3.3	Anomalies in Downcast/Upcast TS Data	36
3.4	Temperature profile from optode test.	39
3.5	Minimization of TS deviations.	42
3.6	Comparison of Raw Salinity to Corrected Salinity	43

3.7	Comparison of Raw Density to Corrected Density	44
3.8	Comparison of Salinity Corrections to the SBE19+.	45
3.9	Differential between downcast and upcast of corrected salinity data	47
3.10	Corrected Salinity Contour from optode Deployment.	48
3.11	Change in Salinity : Corrected - Original values	51
4.1	The Aanderaa oxygen Optode 3835	56
4.2	Dynamic Luminescence Quenching	57
4.3	Anomaly in Upcast/Downcast Oxygen Saturation Time-Series Data	59
4.4	Vertical Profile of Oxygen Saturation showing Anomalies	60
4.5	The effects of Temperature, Salinity and Pressure on oxygen Solubility	61
4.6	Oxygen Sensor Corrections Flowchart	63
4.7	Discrepancies in Original O ₂ Concentration from oxygen optode	65
4.8	Back-calculated phase data from oxygen Concentration	67
4.9	An example of lagged temperature data	69
4.10	Comparison of Temperatures from the CTD and Optode	70
4.11	Corrected Oxygen Concentration using CTD data	71
4.12	Corrected Oxygen Concentration profile using CTD data, corrected for sensor mismatch, and salinity.	73
4.13	Corrected Oxygen Concentration profile using CTD data, corrected for sensor mismatch, salinity, and pressure.	75
4.14	A comparison of corrected optode data to original optode data.	76
4.15	Comparison of Oxygen optode concentration data to Oxygen concen- tration data provided by the Seabird Electronics SBE43 profiler.	78
4.16	Corrections to optode data from verification mission.	79
4.17	Bias offset between optode and SBE43 DO ₂ data.	80

4.18	Error bars for corrected optode data compared to SBE data	81
4.19	Corrected Oxygen Saturation Contour from optode Deployment.	82
4.20	Dissolved Oxygen Calculated using new Corrected Sensing Foil Calibration Coefficients.	84
5.1	How the glider estimates depth-averaged currents	88
5.2	Calculated Depth-Averaged Currents during the Operational Test	89
5.3	Calculated Depth-Averaged Currents during the optode Test	90
5.4	Calculated Surface Currents during the Operational Test	93
5.5	Calculated Surface Currents during the Optode Test	94
5.6	Time series of U,V velocities from Operational deployment with error bars.	97
5.7	A typical surfacing event will last 6-10 minutes.	99
5.8	Heading data supplied by the Attitude sensor during surfacing events.	100
5.9	Testing the Slocum's Compass.	102
5.10	Results from the Slocum Compass Test.	103
5.11	Location of Slocum Corresponding to Wind Analysis Data	105
5.12	Comparison of Wind Speed/Direction, Slocum Heading, and Surface Drift - Operational Test, Aug 1 st , 2006	106
5.13	Comparison of Wind Speed/Direction, Slocum Heading, and Surface Drift - Operational Test, Aug 5 th , 2006	107
5.14	Scatter plot of Mean Slocum heading vs. Surface Drift	108
5.15	Scatter plot of Surface Drift vs. Direction of Wind	109
5.16	Scatter plot of Mean Slocum heading vs. Direction of the Wind	110
5.17	Hypothetical Orientation of Slocum in Response to Wind and Surface Currents	113

Chapter 1

Autonomous Underwater Gliders (AUGs)

1.1 Introduction

Over the last decade, there has been a growing need to understand global climate change, in which the world's oceans play a critical role. Ocean processes cover a wide range of scales - from eddies, to large-scale ocean gyres (covering entire ocean basins), down to micro-scale turbulent dissipation [1]. The collection and analysis of data over these scales is imperative for an in-depth understanding of global processes. This data collection is time-consuming, expensive, and often difficult; new methods and equipment are constantly being developed to help address these issues.

Over the last 15 years, Autonomous Underwater Gliders (AUGs) have been developed as a new sampling platform. Underwater gliders are Autonomous Underwater Vehicles (AUVs) that are deployed for weeks at a time to collect *in-situ* information about the ocean. These gliders are a rapidly maturing technology, with a large cost-saving potential over currently available sampling techniques - especially for long

deployments involving the collection of real-time oceanographic measurements [2].

1.1.1 Henry Stommel's 'Slocum Mission'

In 1989, Henry Stommel published an article in *Oceanography* - this narrative, written from the point of view of a scientist in the future, envisioned the first use of 'Slocums'. Slocums were described as floats which migrated vertically through the ocean by changing ballast, steering horizontally by gliding on wings, and breaching the surface 6 times a day to transmit their accumulated data [1].

Henry Stommel's vision of the future, is today being realized with the manufacturing of the Slocum Glider by Webb Research. Webb Research designs and manufactures scientific instruments for oceanographic research and monitoring, and to date has built over 100 of these Slocum gliders, which are quickly becoming established as a new and powerful tool for oceanographic data collection.

Other types of autonomous gliders exist, specifically the Spray glider developed at the Scripps Institute of Oceanography, and also, the Seaglider developed by the Applied Physics Lab at the University of Washington. However, for our research, the Slocum glider was used.

1.2 Technical Specifications of the Glider

Named after Joshua Slocum, the first person to solo circumnavigate the world, the Slocum glider is a torpedo shaped, winged vehicle, that is 1.5 m long (Figure 1.1), weighs 52 kg [3], and is easily deployed and retrieved by two people.

The Slocum glider has a maximum diving depth of 200 m, and thus is optimized for shallow-water coastal operations (see Table 1.1).

Slocum Battery Glider	
Hull	Length 150 cm, Diameter 21 cm, Mass 52 kg, Payload 3.5 kg
Lift Surfaces	Wing span (chord) 120 cm swept 45°
Batteries	250 Alkaline C cells, Energy 8 MJ, Mass 18 kg
Volume Change	Typical 450 cc, 90 W motor and single-stroke pump
Communication	Freewave Serial RS232, 5.7 Kbyte/s, 3 J/M- byte, 30 km range -or- Iridium. GPS naviga- tion, ARGOS transmitter
Operating	Max P 200 dbar, Max U 40 cm/s
Endurance	U=35 cm/s, 25° glide, Buoyancy 230 gm, Range 1000 km (estimated), Duration 42 days (estimated)
Cost	Vehicle \$70000, Refueling (new batteries) \$1200

Table 1.1: Technical Specifications of the Slocum Battery Glider.



Figure 1.1: The Slocum Glider.

1.2.1 Principle of Operation

Gliders propel themselves through the ocean by changing buoyancy (done by varying the vehicle's volume), and using wings to produce forward motion. The engine used on the Slocum Battery Glider to change its volume can ingest or expel only 250 cubic centimeters of surrounding fluid, meaning that the mass of the vehicle is only changed by ± 250 g which represents only 0.5% of its total mass. With such a limited range of mass change, it is imperative that the glider be pre-ballasted to the density of the seawater in which the vehicle will be operating [2]; this mechanism for propulsion is referred to as a 'buoyancy engine'.

Primary pitch control is achieved by the buoyancy engine in the nose cone, while fine-tuning can occur with the movement of internal masses (batteries). The combination of successive weight changes, and a change in pitch allow the wings and body to generate the hydrodynamic lift which propel the gliders horizontally and vertically through the water. We refer to this up and down motion as a saw-tooth pattern; one cycle is referred to as a yo.

Gliders dead reckon when submerged, maintaining a heading between the GPS fixes obtained at the surface. Well-trimmed gliders can fly straight through the water for a couple of hours without need for course adjustment, however they do lose positional accuracy (due to ocean currents) and must surface to verify their location with the GPS (see Chapter 5). When the Slocum surfaces, the characteristics like way points, headings, emergency procedures, dive angle, and buoyant forcing can be adjusted by a control station on shore [1]. Many different aspects of the glider's flight performance can be changed to set the path followed by the glider: this level of autonomy allows for more efficient time management on research projects. Gone are the days where researchers need to spend weeks at sea collecting data.

1.2.2 Communications

Global low-power satellite communication is a key feature for the Slocum, which allows scientists near real time access to *in-situ* oceanographic data from anywhere in the world. Communication with the Slocum is done in two different ways. During a mission, the Slocum will surface at pre-determined intervals, and is able to communicate globally using an Iridium satellite connection (2400 Baud), or, for local line-of-sight communication, a high bandwidth RF modem (≈ 115 kBaud). The antennae for communications are integrated into the tail of the glider. With the help of an inflatable bladder in the tail cone, the communication equipment is installed such that they will be at the maximum height possible during surfacing [2]. An ARGOS transmitter that provides position data roughly every 6 hours is provided for backup in the event of a failure of other communication systems.

1.3 The Potential of AUGs

Today, more than ever, there exists a keen interest in environmental monitoring and assessment. Since the Slocum is built to operate in coastal waters, it becomes a great tool in the hands of researchers. The glider can be used to study phytoplankton blooms, to track water masses, to study the effect of biological material on available oxygen content, or, even to provide an early warning for catastrophic climate change. Slocum's offer many advantages over traditional ship surveying.

Ship surveys tend to last no more than a month or two, and with rare exceptions are not repeated often enough, or over a sufficiently long duration to resolve dominant space-time variability in the ocean. The Slocum glider platform offers the promise of describing the ocean's interior with much higher resolution in space and time than is

possible with traditional ship surveys. With the Slocum we are able to get seasonal data sets, but cannot cover a large range due to the gliders slow speeds.

The real-time data return from Slocum gliders allow the possibility of adjusting sampling during the course of a mission to react to environmental conditions. This ability is referred to as ‘adaptive sampling’, which can be considered one of the key features of the Slocum glider, as it allows the researcher the ability to track any interesting features appearing in the data. In comparison, a larger research vessel usually has a set route that is not easily deviated from.

1.3.1 Comparison to Other Modes of Sampling

A glider is essentially a float with wings which provide lift and allow it to move horizontally while profiling. Gliders, however, serve a different niche than traditional ARGOS floats as scientists have some control over the horizontal position of a glider; something that cannot be done with ARGOS [1].

Traditional ship surveys are often adversely affected by bad weather conditions, something to which the Slocum seems to be immune. Slocums can be operated for a year at the same cost required for a single day of medium-sized research vessel operation; fabrication cost of a glider is equivalent to the cost of about 4 days of ship time. A comparison of advantages and disadvantages of using a Slocum glider compared to a ship survey can be found in tables 1.2 and 1.3 respectively.

1.4 The Various Sensors

Now that the Slocum glider has been introduced, it can be considered as a platform upon which one can build. The addition of different scientific sensors and probes to the Slocum allows the vehicle to be adapted for different types of missions.

Advantages	Disadvantages
Low Cost	
Real-time data interpretation	Water current limited
Not weather-limited	Power limited
Good resolution	Slow
Adaptive sampling	

Table 1.2: A comparison of the advantages and disadvantages of glider sampling.

Advantages	Disadvantages
Can carry many different sensors	Very expensive
Unlimited depth profiling	Weather limited
High Endurance	Limited horizontal resolution

Table 1.3: A comparison of the advantages and disadvantages of ship-based sampling.

1.4.1 Limitations

Slocums have constraints as to the types, and quantity of sensors that they can carry. In order to be deployed on a glider, a sensor must not only be small, it must also have low power consumption.

Ideally, in addition to the condition of being small, sensors should also not protrude beyond the external surface of the glider as to maintain hydrodynamic efficiency. Bulky sensors can be attached externally to the glider body but at the cost of mission length, as these will increase drag and thus power consumption. Sensor weight is important because of the limits in glider payload and the need to maintain the relative position of the center of mass and buoyancy within the glider. Low power consumption is another limiting factor to consider, as the power budget of the glider determines

the length of deployment [1].

1.4.2 Internal Sensors

The Slocums come with many different internal and external sensors to aid in the operation of the vehicle, these include, but are not limited to:

Altimeter - the Airmar altimeter, with a range of 0-100 m, is mounted such that the sonar is vertical to a flat sea bottom at a dive angle of nominally 26 degrees.

GPS - Used for obtaining position fixes at the surface.

Pressure Transducer - Micron strain gage transducers are used for vehicle control and dead reckoning.

Attitude Sensor - Provides the magnetic heading, pitch, and roll indications of the Glider. These inputs are used for dead reckoning the vehicle while underwater.

1.4.3 Science Sensors

Despite the practical constraints of size and power placed on the sensors, there are many different sensors from which to choose. By default, the Slocum comes with a non-pumped, low-drag Conductivity-Temperature-Depth (CTD) sensor, produced by Seabird Electronics. Our research group has also installed an oxygen optode produced by Aanderra Instruments, with future plans to install an Acoustic Doppler Current Profiler (ADCP) manufactured by Nortek. Other research groups have also installed backscatter and fluorescence sensors to measure different optical backscatter wavelengths.

1.5 Purpose of this Project

Since acquiring four Slocum gliders, the National Research Council-Institute for Ocean Technology (NRC-IOT) and Memorial University of Newfoundland (MUN) in collaboration with the Canadian Center for Ocean Gliders (CCOG) have been exploring the potential of these gliders to gather oceanographic information, in particular with application to the waters over the Newfoundland Shelf.

The data collected by these Slocums is only as good as the sensors being used - therefore it is necessary to know the limitations of the instrumentation in order to properly analyze the results. With many technological advances taking place, we need to be aware of both the capabilities and limitations of their sampling equipment [4]. Our objective here, is not only the analysis of data obtained from our glider, but also an analysis of the performance of its sensors. We will examine the data collected, along with a study of the different sensor dynamics problems discovered during our research and field deployments.

There is a well documented history of sensor dynamics issues in operational oceanography to which the Slocum glider is not immune. Perhaps the most pertinent issue is that of sensor response time. Each sensor on the Slocum has a different response function that can lead to biases and inaccuracies of the data collected. We will focus on determining the specific sensor responses of the individual instruments onboard the glider, and developing algorithms to correct for the dynamical responses to ensure all instruments sample at the same time interval. Algorithms developed will also be verified through testing against other independent measurements. We will also analyze data from our local environment, such as how our strong winds affect the operation of our Slocum at the surface. This analysis will determine if the Slocum can be used to collect detailed surface ocean current measurements.

Data analysis in the following chapters will include an in-depth study on the data obtained from the CTD and oxygen optode, as well as an examination of the Slocum's water velocity estimates. During the course of 2006/07 we have conducted several test deployments, have recorded over a month worth of data, and have flown over 800 kilometers.

This document is broken up into the following sections: Chapter 2 details and results from our various deployments. Chapter 3 offers a focus on the sensor issues and correction algorithms for the onboard CTD. Chapter 4 provides a discussion of the problems arising from the installation of the oxygen optode, and correction procedures to minimize inaccuracies. Chapter 5 includes an analysis of the GPS and attitude sensor, comparing estimates of surface currents to local wind data. Finally, in Chapter 6 we summarize our results and speculate about future possibilities.

Chapter 2

Glider Deployments and Collected Data

2.1 Deployments

2.1.1 Introduction

The deployment and retrieval of the glider can easily be carried out by two researchers. The first stage of deployment is the proper ballasting of the glider to a target density of seawater specified for the area in which it will be sampling. Once ballasted, the glider is brought to the testing area and is lowered from the research vessel into the water. While operating at the surface, the glider can be controlled, and any trouble-shooting that may be necessary can occur from a desktop computer with communication via Iridium satellite communications.

Over the course of the project, three deployments were successfully completed: 1. An operational test to see how well the Slocum would perform in our environment, 2. A test of the newly installed Aanderaa oxygen optode, and 3. A deployment with

accompanying independent instruments to test our correction algorithms. All the deployments were conducted off the coast of the Avalon peninsula of Newfoundland and Labrador, over the continental shelf (Figure 2.1).

2.1.2 Operational Test - Trinity Bay to Shelf

Description of Deployment

The first deployment of the Slocum was in July of 2006 (Table 2.1). The purpose of this mission was to assess the operational abilities of the glider in the strong currents off the coast of Newfoundland, over the continental shelf. This deployment only had a CTD onboard, with no additional sensors.

The track is out through Trinity Bay and across the continental shelf, and cuts across the inner branch of the Labrador Current (Figure 2.1). In choosing this route, there was some concern that the glider might have difficulty in flying against the strong currents (which can easily exceed 30 cm/s in the mixed layer) [2]. During this deployment, when the Slocums progress was threatened by strong surface currents, its upper climb depth was set to ≈ 30 m of depth to avoid this issue (see Chapter 5).

Results of the Deployment

Contours of temperature, salinity, and density have been created from this deployment from the raw data recorded (Figures 2.2, 2.3, 2.4); water properties in this region show substantial structure. Data is gridded every 20 m and 1 m in the horizontal and vertical directions respectively. The temperature data (Figure 2.2) shows that the glider was able to resolve both the vertical and horizontal water properties very well.

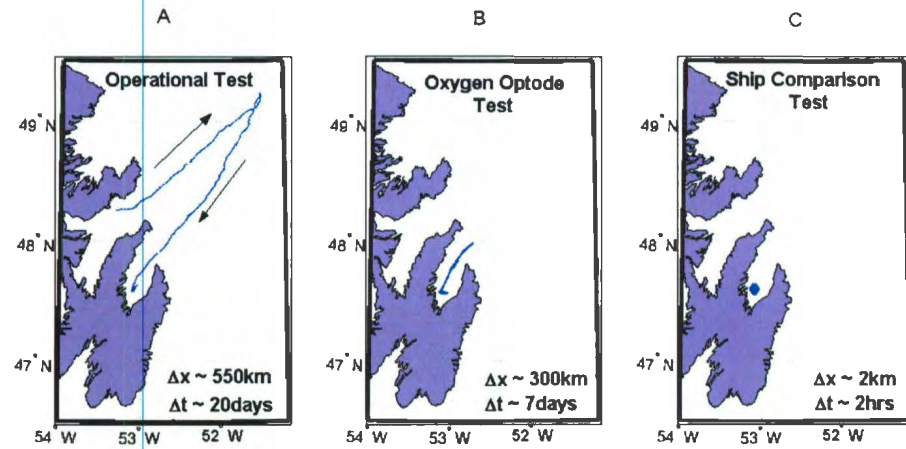


Figure 2.1: The three major deployments conducted over the summers of 2006/07. A) The operational test conducted in Trinity Bay and retrieved in Conception Bay South. Date Flown: July 26 to August 16, 2006. B) The oxygen optode test in Conception Bay South (CBS). Date flown: September 24th to October 2nd, 2006. C) A second mission conducted in CBS to compare Slocum glider data vs. traditional ship based data. Date flown: September 26th, 2007.

Mission Duration:	20 days
Distance Traveled:	550 km
Deployment Location:	Trinity Bay across continental shelf. Retrieved in Conception Bay South.
Sensors:	CTD
Rationale for Mission:	The purpose for this deployment was to assess the operational abilities of the Slocum glider in the waters off Newfoundland.

Table 2.1: Mission Stats - Operational Test

Surface temperatures reach 15 °C, while bottom temperatures are typically sub-zero. The mixed layer (Figure 2.4) is quite apparent in this figure, varying in depth from roughly 10 to 35 m. An enormous amount of detail is clear in this raw, unfiltered plot [2].

2.1.3 Oxygen optode Test

Description of Deployment

This short deployment in Conception Bay, of eight days, was to test a newly installed Aanderaa Instruments dissolved oxygen sensor: the oxygen optode 3835 (Table 2.2).

The optode was integrated into the glider in the flooded area in the tail while being exposed through a small 5 by 5 cm hole that we cut in the tail-fairing of the glider (Figure 2.5).

The response time of this oxygen sensor is much shorter than those of other oxygen sensors (such as gas tension and membrane systems which have response times on the order of minutes) [2]. While the sensor performed well, the response time of roughly

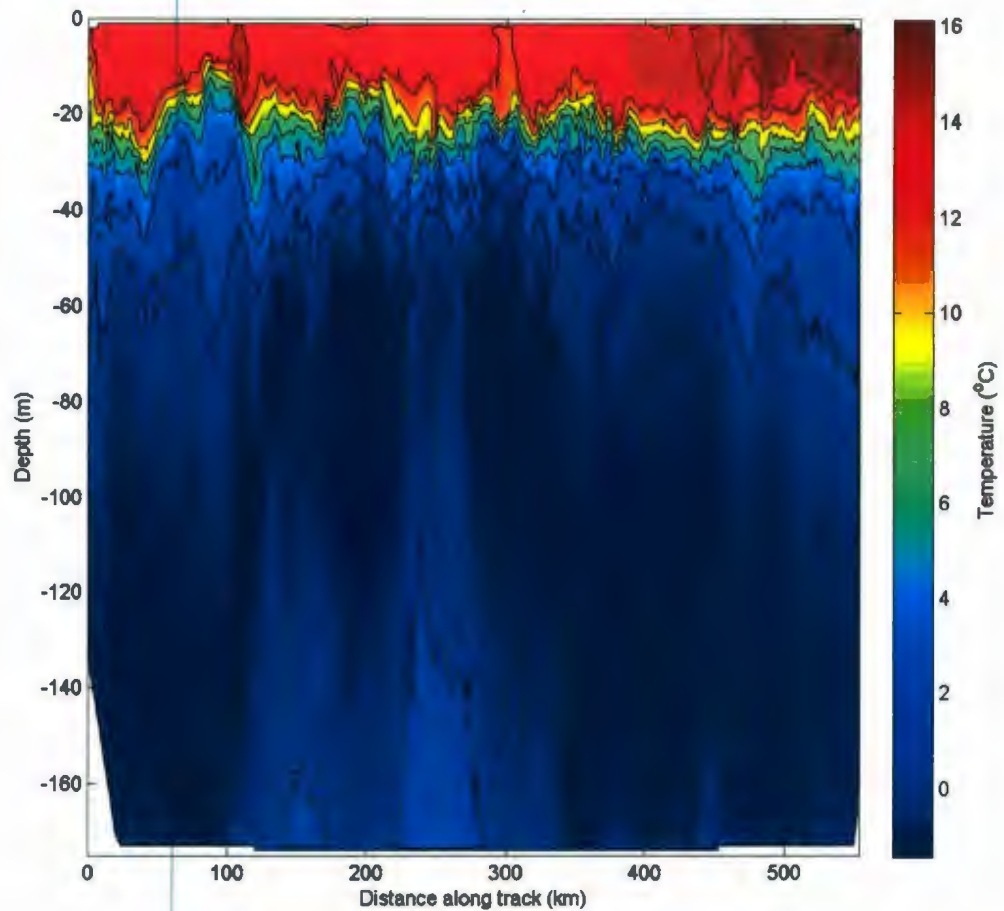


Figure 2.2: Temperature data recorded from the Operational test. Date recorded: July 26 to August 16, 2006, Distance Covered: 550 km. See figure 2.1 (left) for map of location. Contour levels are specified at -1.4, 0.5, 2.5, 4.4, 6.3, 8.3, 10.3, 12.2, and 14.2 $^{\circ}\text{C}$ respectively.

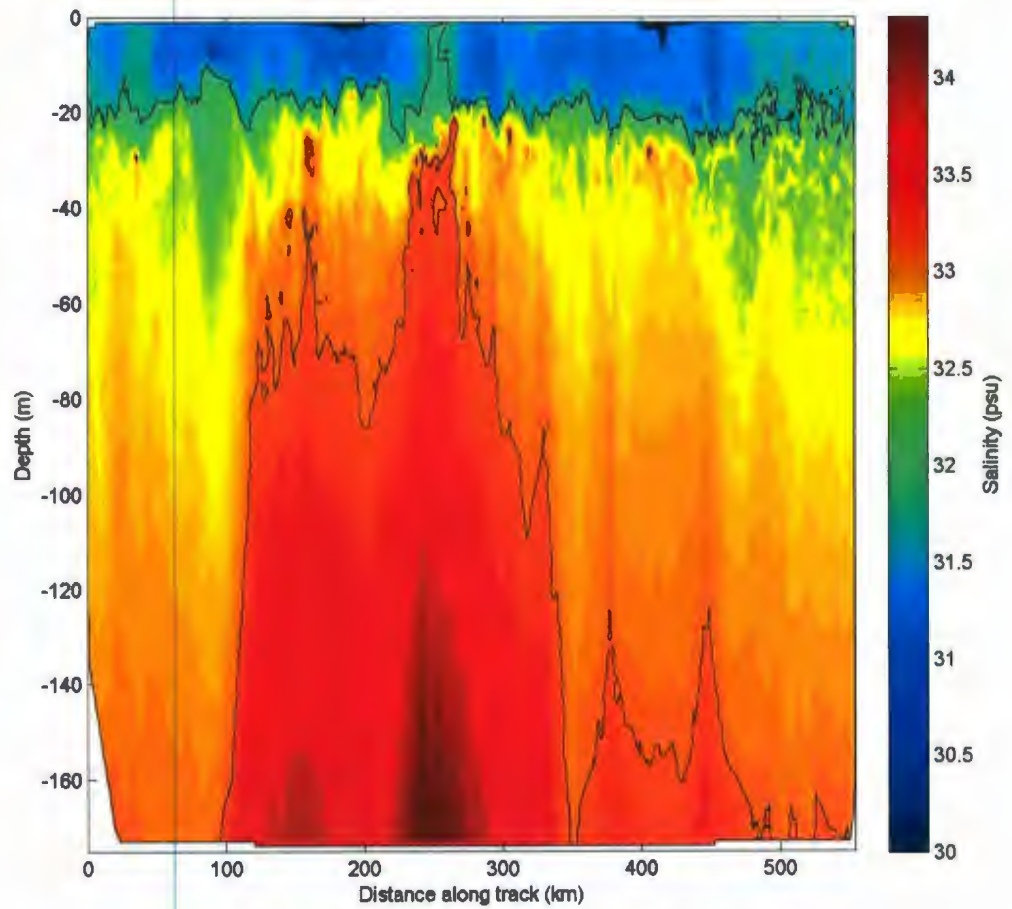


Figure 2.3: Salinity data recorded from the operational test. Date recorded: July 26 to August 16, 2006 , Distance Covered: 550 km. See figure 2.1 (left) for map of location. Contour levels are specified at 27.1, 28.3, 29.5, 30.7, 31.9, and 33.1 psu respectively.

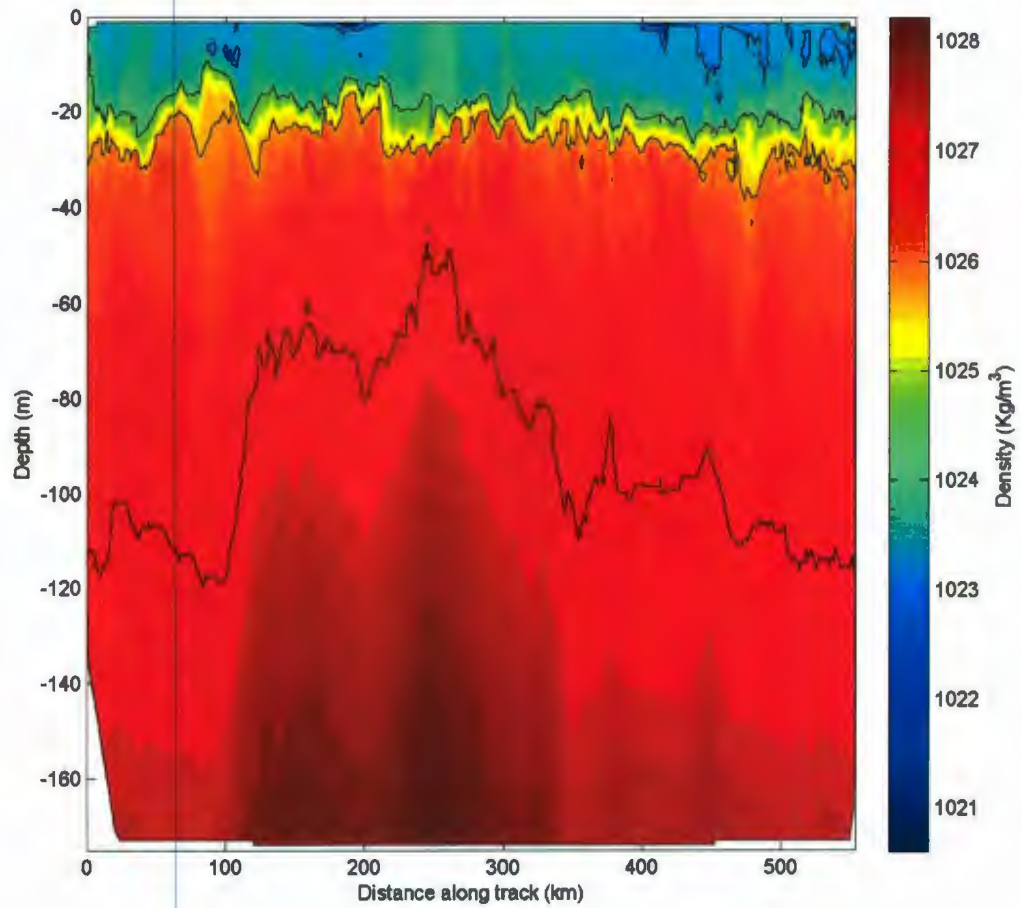


Figure 2.4: Density contour showing the clear stratification of the water above the continental shelf. Date recorded: July 26 to August 16, 2006 , Distance Covered: 550 km. See figure 2.1 (left) for map of location. Contour levels are specified at 1020.7, 1022, 1023.2, 1024.5, 1025.7, and 1027 kg/m³ respectively.



Figure 2.5: The optode is exposed in the tail section of the Slocum.

Mission Duration:	6 days
Distance Traveled:	211 km
Deployment Location:	Conception Bay South (deployment and retrieval).
Sensors:	CTD and oxygen optode
Rationale for Mission:	Primary purpose for the test flight in Conception Bay South was to test the operational abilities of the newly installed Aanderraa oxygen optode.

Table 2.2: Mission Stats - oxygen optode Test

20 seconds does pose challenges for interpreting the data profiles, and poses a problem that must be considered (see Chapter 4 for oxygen correction algorithms).

Results of the Deployment

Contours of temperature, salinity, and density were also created from this deployment (Figures 2.6, 2.7, 2.8). Surface temperatures reach $16\text{ }^{\circ}\text{C}$ (Figure 2.6), while bottom temperatures are again sub-zero. The mixed layer (Figure 2.8) is quite apparent in this figure, varying in depth from roughly 20 to 35 m. The salinity data (Figure 2.7) shows some vertical banding which is due to thermal-lag issues discussed in Chapter 3. The measured oxygen saturation varied from 80%, at 200 m, to almost 110% near the surface, typical values for coastal waters (Figure 2.9). However, the raw data from the optode contains a large offset between the downcast and upcast, which is

Mission Duration:	2 hours
Distance Traveled:	≈ 2 km
Deployment Location:	Conception Bay South (deployment and retrieval).
Sensors:	CTD and oxygen optode
Rationale for Mission:	Primary purpose for the test flight in Conception Bay South was to test and confirm algorithms developed for correcting oxygen Data.

Table 2.3: Mission Stats - Validation Test

clearly seen in the contour. Approaches to treating this offset will be discussed in Chapter 4.

2.1.4 Validation Deployment

Description of Deployment

The third field deployment that took place in September 2007 (Figure 2.1 (c)) had the primary purpose of assessing and confirming algorithms developed for correcting CTD and oxygen data (Chapters 3 and 4). In order to verify our corrected glider data, we needed a comparative data set obtained from an independent instrument. By doing several ship-based calibrated CTD casts in the same area where the glider was continually sampling, we obtained enough data for the comparison (Table 2.3). The Slocum followed the same path as the ship and traveled approximately 2 km (Figure 2.10).

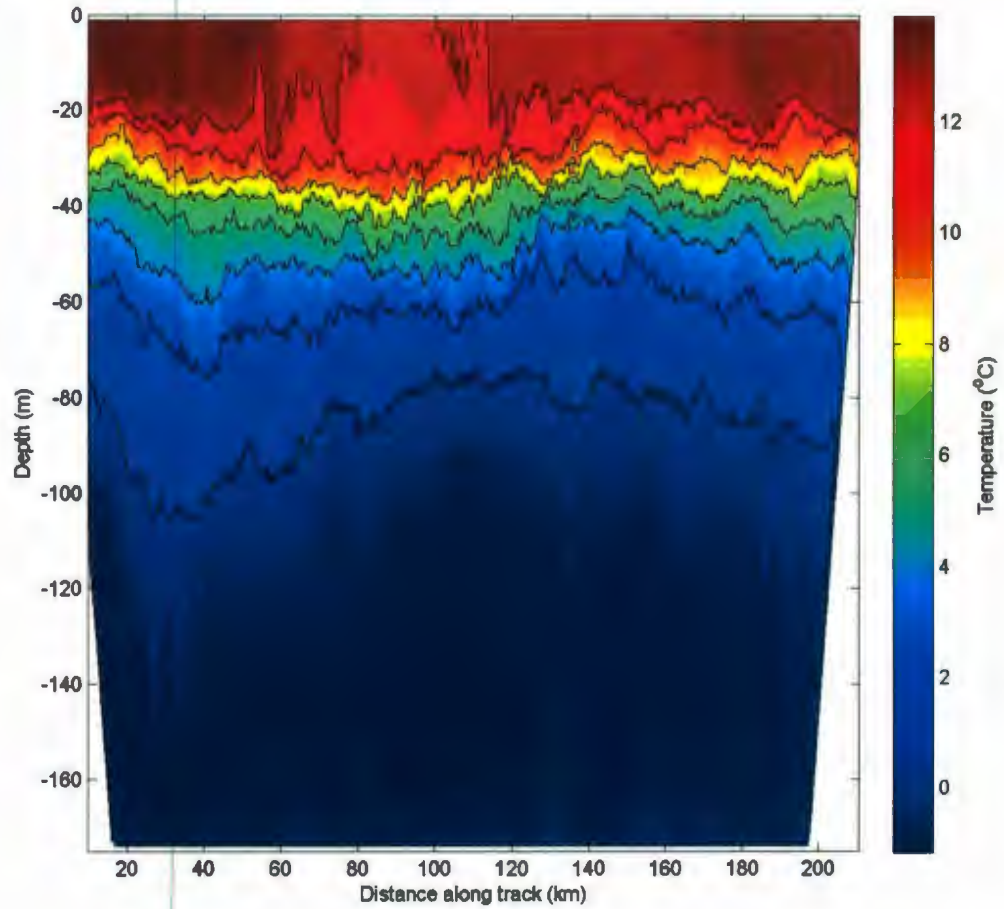


Figure 2.6: Temperature data recorded from the oxygen optode test. Date recorded: September 24th to October 2nd, 2006. Distance Covered: 211 km. See figure 2.1 (middle) for map of location. Contour levels are specified at -1.2, 0.5, 2.2, 3.8, 5.5, 7.2, 8.9, 10.5, and 12.2 °C respectively.

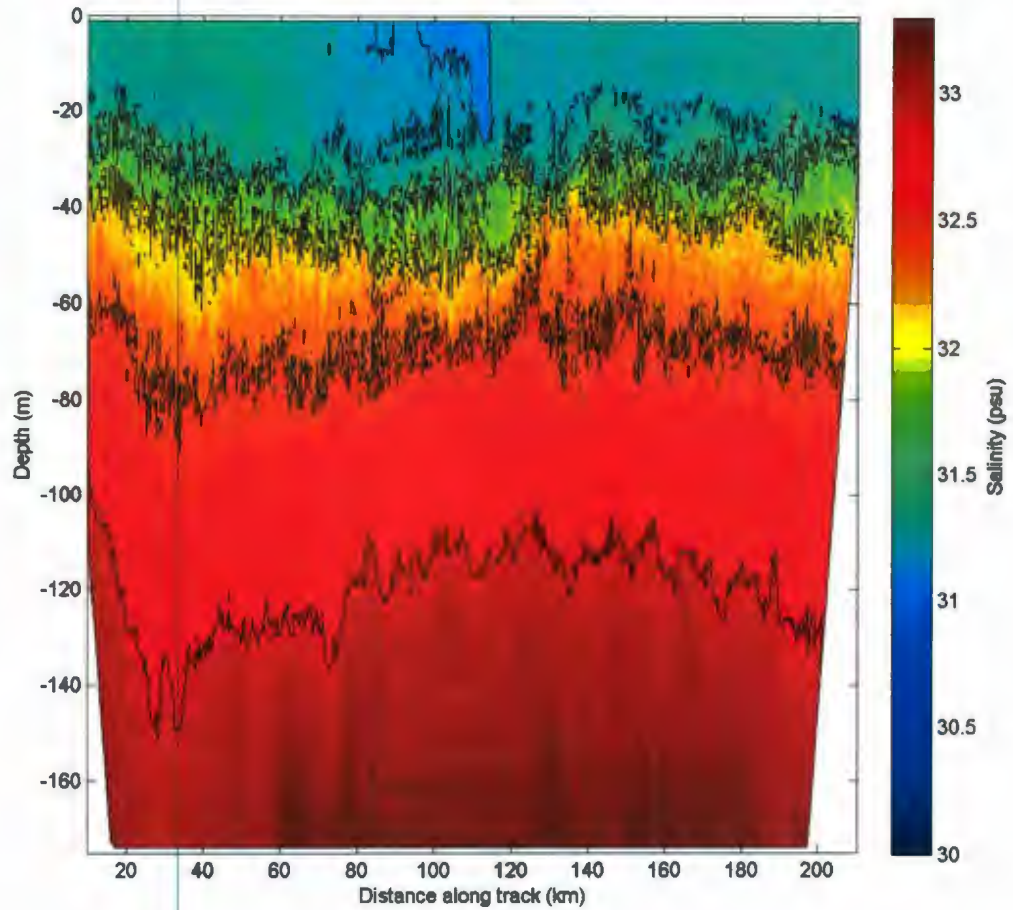


Figure 2.7: Salinity data recorded from the oxygen optode deployment. Date recorded: September 24th to October 2nd, 2006. Distance Covered: 211 km. The vertical banding is a result of an offset between the Slocum's downcast and corresponding upcast - see the following chapter for corrections. See figure 2.1 (middle) for map of location. Contour levels are specified at 30.7, 31.2, 31.6, 32.0, 32.4, and 32.9 psu respectively.

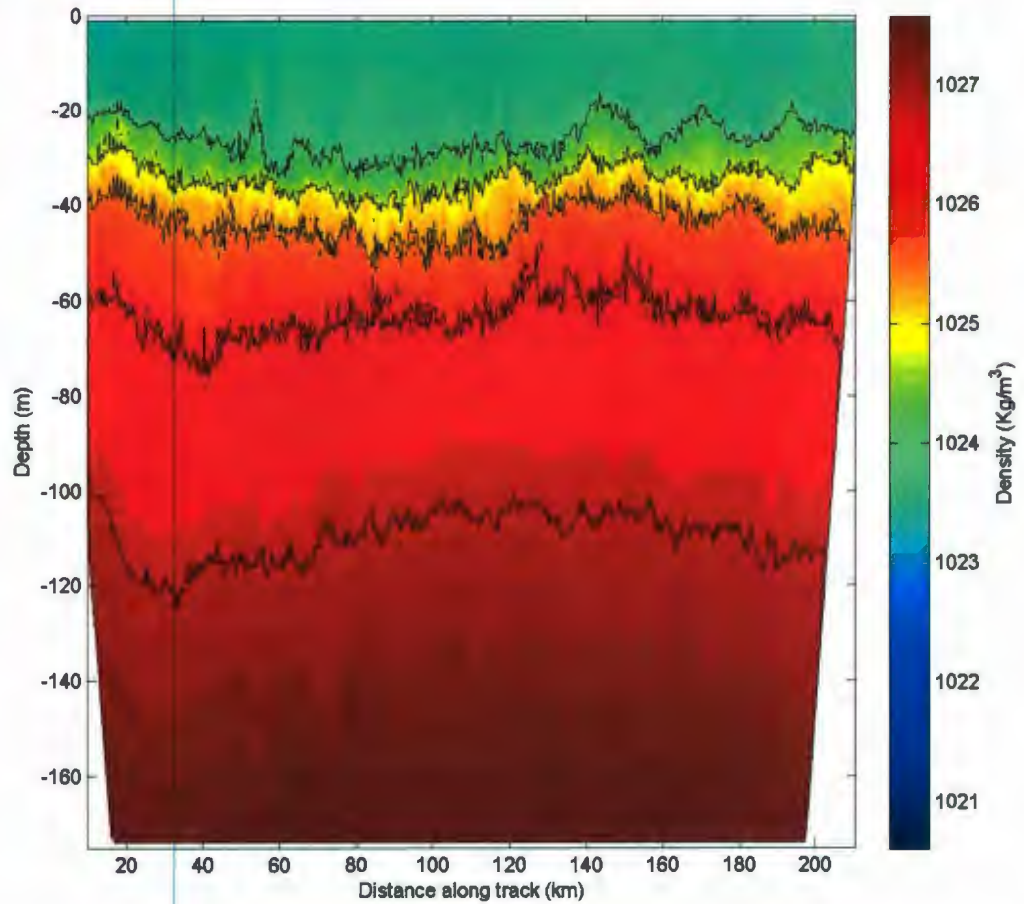


Figure 2.8: Density contour showing the clear stratification in Conception Bay South where the testing was done. Date recorded: September 24th to October 2nd, 2006. Distance Covered: 211 km. See figure 2.1 (middle) for map of location. Contour levels are specified at 1023.3, 1024, 1024.7, 1025.5, 1026.2, and 1026.9 kg/m^3 respectively.

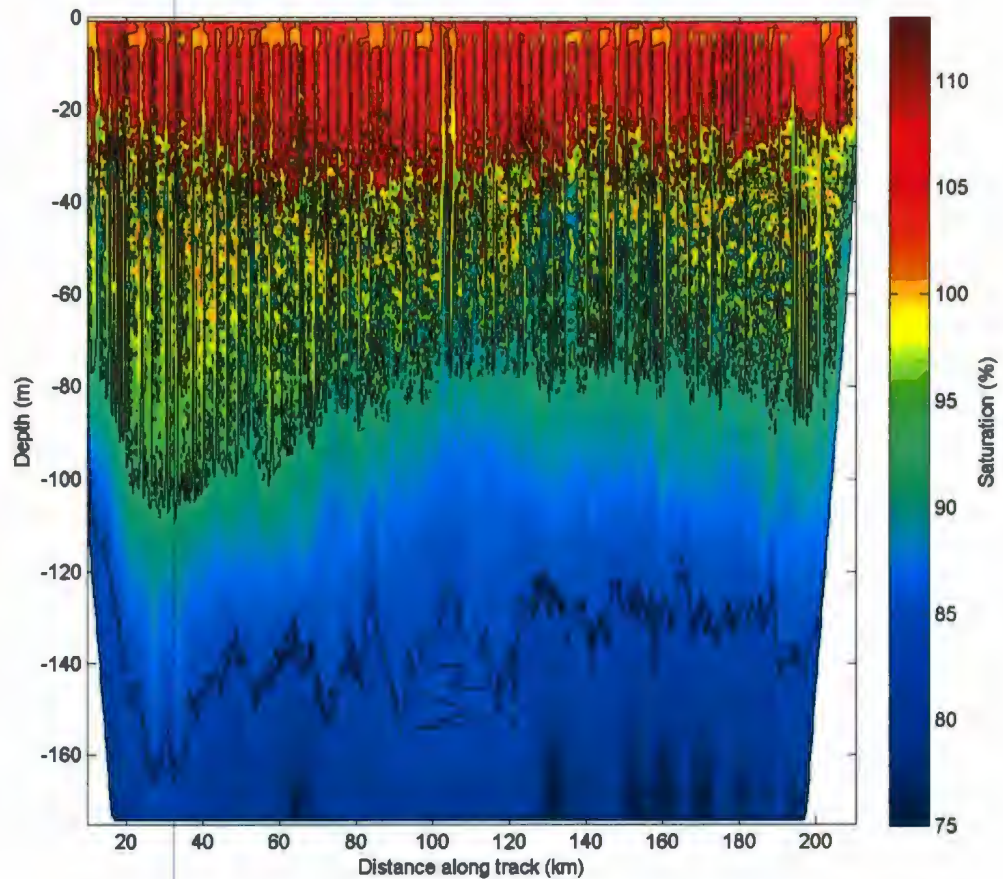


Figure 2.9: Oxygen saturation data recorded from the oxygen optode test. This figure shows an immense amount of vertical banding which is due to sensor dynamics issues, these are corrected for in Chapter 4. Date recorded: September 24th to October 2nd, 2006. Distance Covered: 211 km. See figure 2.1 (middle) for map of location. Contour levels are specified at 74.2, 83.7, 93.1, and 102.6% respectively.

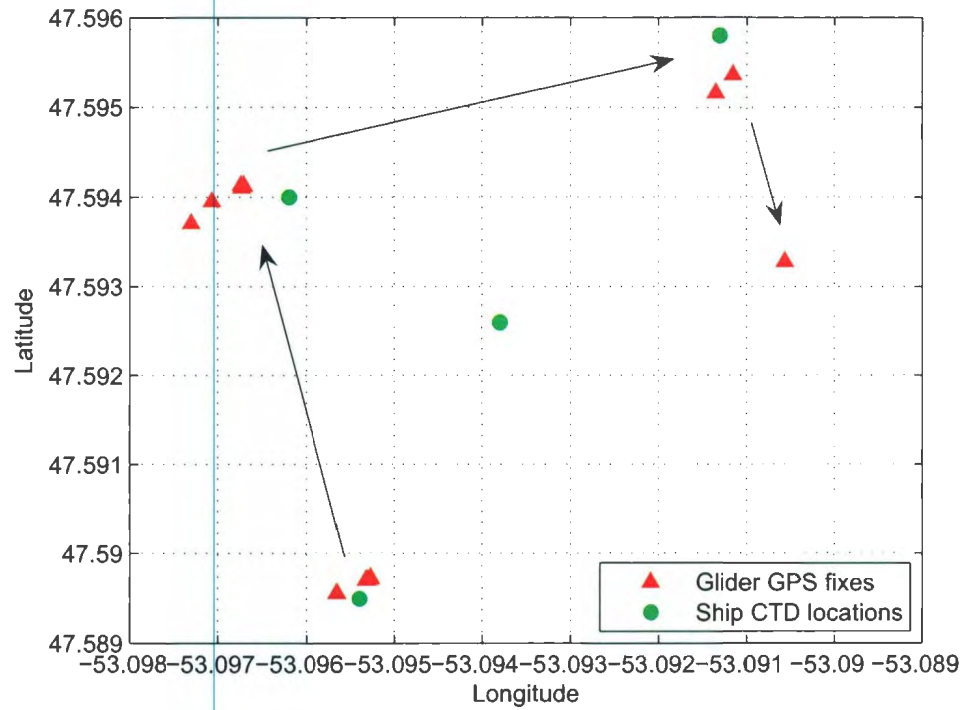


Figure 2.10: Green dots show where the CTD was lowered from the ship while red triangles show where the Slocum surfaced. Black arrows approximate the path traveled by both the ship and Slocum.

Results of the Deployment

The instrument chosen for the comparison was the SeaBird Electronics (SBE) 19+ SEACAT Profiler with an auxiliary SBE43 Dissolved oxygen Sensor (Figure 2.11). SBE CTDs are considered to be the industry standard for sampling oceanographic data.



Figure 2.11: The Slocum glider and SBE19+ CTD.

The comparison of our correction algorithms to the SBE19+ data can be found in sections 3.4.3 and 4.4.6.

2.2 Collected Data

2.2.1 Preparation of the Data

Before any correction algorithms in the following chapters can be applied, the raw Slocum data require considerable pre-processing. First, the Slocum inserts 'Not a Number' (NaN) into the data stream whenever it fails to take a measurement with any specific sensor - all these NaNs must be removed. Second, original glider data is collected at 0.25 Hz, but once the NaN's are removed, it may no longer be evenly spaced. To correct for the uneven data set, we linearly interpolate the entire data set to a sampling frequency of 0.50 Hz. Once the data is evenly spaced we can apply correction algorithms and plot the data.

2.2.2 Data Distribution

During glider deployments, new data are received on each surfacing - typically every few hours. A web page was created to present the data collected from the glider missions (<http://www.physics.mun.ca/glider/>). A suite of MatLab scripts was written to aid in the analysis and distribution of the data (these scripts were designed to automate the process of examining data). A data archive was created and linked to the web page. New data are continuously updated and processed for placement into the archive [2].

The benefits of using automated scripts to analyze and store the data online are evident, as it allows researchers not directly involved with deployments access to near-real-time data from anywhere via an internet connection [2].

2.2.3 Tool Boxes

When a new glider mission takes place and new data are received, a sequence of analysis takes place. First, the longitude and latitude positions are extracted from the GPS and a map is created. The map is placed on the web page and allows for the approximate location of the vehicle to be known at any time. Second, a series of plots are created from the CTD data collected (temperature, salinity, and pressure as a function of depth), as well as from the gliders internal sensors (heading, pitch, and roll). Third, correction algorithms are used to correct for sensor dynamics issues (Chapters 3, 4, and 5). Fourth, a new section is created inside the data archive with the glider mission specifics (date launched, present location, etc.) and the generated figures are automatically updated on the web page [2].

To aid in the analysis of glider data, a series of MatLab ‘toolboxes’ were created (see Appendix 1 for MatLab code):

Distance Calculator and Contouring - this script is used to determine the correct horizontal spacing for Slocum data to be used for contouring purposes.

CTD Corrections - algorithms to correct for lagged response and for heat build up in the conductivity cell of the glider (see Chapter 3).

optode Corrections - an algorithm to correct for the slow response time of the oxygen optode along with corrections for salinity and pressure (see Chapter 4).

Water Velocity Calculator - algorithms to estimate the surface water velocity (see Chapter 5).

Chapter 3

Analysis of the CTD Sensor

3.1 Introduction

The Slocum glider is typically configured with a non-pumped, low drag Conductivity Temperature Depth recorder (CTD) (Figure 3.1), which is optimized for low power consumption. There is a well defined history of sensor dynamics issues with CTD's to which the Slocum is not immune ([5, 6, 7, 8, 9]). The Slocum's CTD configuration, combined with slow horizontal and vertical speeds inherent to gliders, results in significant spiking in the salinity profiles [10], and also causes a differential to exist between the Slocum's downcast and corresponding upcast.

3.1.1 Why Measure Temperature and Salinity?

Oceanographers need to know the distribution of temperature and salinity for many reasons. When surface waters sink into the deep ocean, they retain a distinctive relationship between temperature and salinity which can act as a tracer to help track the source of ocean waters. Temperature and salinity are also needed to compute the density of seawater. Since density is also related to the horizontal pressure gradients



Figure 3.1: A) By default, the Slocum glider comes with a non-pumped SBE41CP CTD which is installed under the wing. B) A close-up view of the CTD.

and ocean currents, knowledge of temperature and salinity provides a powerful tool for understanding the world's oceans [11].

Traditionally, oceanographers have measured these fundamental properties of seawater through the use of a CTD probe.

3.2 Theory of Operation

While temperature and pressure are usually measured directly, the measurement of salinity is based on the conductivity of seawater [12]. Temperature is measured with a pressure-protected, fast-response thermistor, while conductivity is sensed inside a long, narrow, three-electrode cell [5]. Conductivity is determined by measuring the current that flows when there is a known voltage between the electrodes [11]. For a detailed description of CTD's and the type of data available, refer to the *UNESCO Technical Papers in Marine Science*, volumes 44 and 54 ([13] and [12]).

3.3 Sensor Anomalies

Anomalous salinity readings were first noticed in the initial tethered test deployments of the Slocums early in the summer of 2006, and have remained constant throughout all deployments carried out to date. Initially discovered when plotting salinity contours, there appeared to be a consistent offset between the Slocum's downcast data and corresponding upcast.

Examining vertical profiles for temperature and salinity during the second field deployment reveals the anomalous sensor data (Figure 3.2). Large discrepancies of ≈ 0.3 psu exist between the salinity data obtained on the vehicles downcast and the data obtained on the following upcast; temperature data for the same profile shows no

mismatch. This data can be considered to be representative of all the data collected throughout various deployments, and are used below to illustrate our observations.

The two problems we address here, in relation to the CTD, are 1) the temperature probe and conductivity sensor have different response times, and 2) thermal-lag in the conductivity cell of the CTD, which results in significant salinity spiking in our data due to slow vertical velocities and sharp gradients. The thermal-lag issue is the most problematic - as the slow profiling speed of the Slocum helps adjust for its slow sensor response, while the thermal-lag remains an issue at all sampling velocities.

3.3.1 The Sensor Response Problem

Sensors do not change their output immediately for a sudden change in input. Rather, sensors change their output to the new state over a period of time, called the response time.

To deal with the varying response of the Slocum's sensors, we shall generalize the concept of the 'time constant' and define it as the time taken for the response to reach 63% of the amplitude of the variable being measured (Equation 3.4) [13].

Problems occur within our data sets because the individual sensors on the Slocum have different, non-ideal, dynamic response functions with varying time constants. These varying responses cause the CTD temperature sensor, conductivity sensor, and pressure sensor to become mismatched and thus a time-lag is introduced.

The purpose of sensor response corrections is to minimize or remove the mismatch in time constants between the temperature, conductivity, and pressure sensors. Two basic approaches can be used to ensure these sensors align temporally: 1. removal of the shift from the measured sensor values with the most lag, or 2. adding a shift to the other sensor values so the time lags of all the sensors are equal.

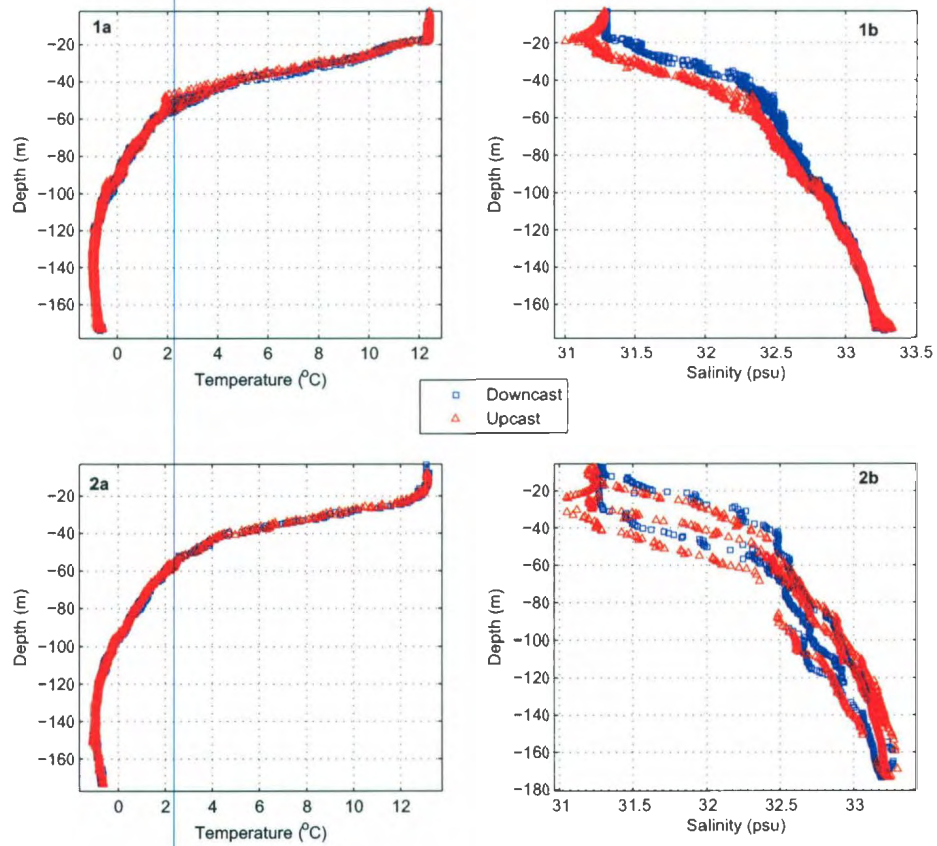


Figure 3.2: Differences in downcast and upcast in salinity obtained from Glider unit: 48, Julian Day: 268, 2007. Plots 1 and 2 show the same information but are taken from different sampling areas at different times. 1a,2a) Downcast (blue squares) and upcast (red triangles) of temperature. 1b,2b) Downcast (blue squares) and upcast (red triangles) of salinity.

The approach historically has been to remove the shift in the data itself, which is the method we use in this section. These methods for removing sensor mismatch in CTDs are well tested and documented and here we use a filter developed by Fofonoff *et al.* [14] for our corrections.

3.3.2 The Thermal Lag Problem

Another problem with the CTD, which causes the majority of discrepancies in our CTD data, is the thermal-lag in the conductivity cell. During the Slocum's downcast, the probe moves from warm to cold waters through a sharp thermocline. As it is lowered, the heat stored in the sensor body diffuses into the water being sampled in the vicinity of the conductivity sensor, artificially raising conductivity, and consequently salinity. Conversely, when the probe moves upward from cold to warm waters, conductivity and salinity are artificially lowered [15]. The existence of a systematic offset in salinity between down and upcast (Figure 3.2) is in agreement with the theory of thermal-lag effect affecting SBE CTDs crossing sharp temperature gradients. Much work has been done to attempt to resolve the thermal-lag problem [16, 17, 9, 15].

The theoretical thermal model for a hollow circular cylinder by Lueck and Picklo [17] predicts that the heat stored in the walls of the SBE CTD will produce a detectable error in the measure of conductivity. This error is characterized by an initial magnitude of the thermal fluid anomaly, α , and a relaxation time constant, τ .

Both Lueck and Picklo [17] and Morison *et al.* [16] state that empirical formulas can be used to calculate values for α and τ in cases where it is difficult to determine them directly. These formulas were based on data gathered from a SBE9 CTD and the equations are:

$$\alpha = 0.0264V^{-1} + 0.0135 \quad (3.1)$$

and

$$\tau = 2.7858V^{-\frac{1}{2}} + 7.1499 \quad (3.2)$$

where V is the velocity of the sensor through the water.

Morison *et al.* [16] notes that for V less than 0.5 m/s, the performance degrades rapidly and any estimates of α and τ will probably be more uncertain. This dependence of α and τ on V pose a significant problem for our Slocums, because our mean vertical speed through the water is ≈ 0.20 m/s (See section 3.4.2 for further details on α and τ).

Work by Pinot *et al.* [15] suggests that the characteristic timescale of the thermal-lag error is usually long (tens of seconds) [15]. It can be diagnosed from the observation of a systematic offset between salinity down and upcasts (Figure 3.2). Work by Johnson *et al.* [5] suggests that the model parameters α and τ depend mostly on the flow rate through the cell, and the physical properties of the cell and its protective jacket. As cell flow rate is increased (velocity of the profiler is increased), the values of α and τ will both be reduced - however, in our case the opposite is true: slow Slocum vertical speeds result in larger α and τ values. The Temperature-Salinity (TS) plots from the optode test show the degree to which down and upcast water mass characteristics are inconsistent in the thermocline (Figure 3.3).

The following section details algorithms to correct for the sensor anomalies.

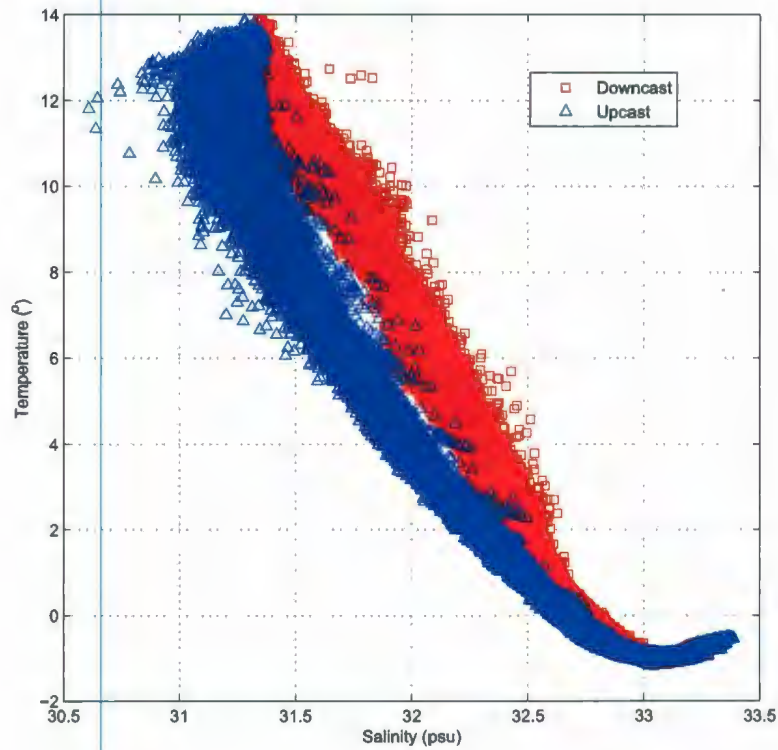


Figure 3.3: Temperature-Salinity data for the optode test conducted in CBS from Glider unit: 48, Julian Days: 267-275, 2007. The existence of an offset between downcast (red squares) and corresponding upcast (blue triangles) data is in agreement with the existence of a thermal-lag issue in the conductivity cell.

3.4 Corrections

Accurate salinity data requires corrections for temporal mismatches in the sensor response, along with corrections for the related problem of heat build-up in the conductivity cell wall as described in the previous sections [17, 16].

3.4.1 Correcting for Sensor Response

Fofonoff *et al.* [14] developed an algorithm for correcting for the finite response of an instrument by using a single pole filter (Equation 3.3). This lag-correction procedure estimates the true temperature at a point by calculating the time rate of change of temperature over several neighboring points [14].

$$X_{true} = X + \tau_X * \frac{dX}{dt} \quad (3.3)$$

where X_{true} is the true variable (temperature or conductivity), X is the measured variable, and τ_X is the corresponding time constant.

Johnson *et al.* [5] calculated rough estimates of the sensor response, τ , for both the thermistor and the conductivity cell in a SBE41CP CTD, using empirical formulas developed and used by Seabird Electronics [5]. The CTD on the Slocum is a modified version of the one from this work. Using this method, they obtained estimates of $\tau_{Temp}=0.53$ s and $\tau_{Cond}=0.20$ s. Work done by Kerfoot *et al.* [10] attempted to calculate values for the Slocum CTD with limited success. Kerfoot's values were $\tau_{Temp}=1.4$ s and $\tau_{Cond}=2.0$ s.

For our purposes, Fofonoff's correction algorithm is applied directly to the CTD data. Standard first difference techniques can be used, but often results in considerable noise. Thus, smoothing of the temperature series is accomplished by a least squares linear regression to estimate $\frac{\delta T}{\delta t}$. This allows for the correct calculation of the

true temperature at any time. The degree of smoothing of the measured temperature series is set by the number of points, N , used in the least squares regression [14]; Here we use $N = 3$ data points.

To correctly determine values for τ_{Temp} and τ_{Cond} we apply equation 3.3 in an iterative fashion to the optode data set (Glider unit: 48, Julian days: 267-275, 2007) - which contains several hundred yo's (the Operational data set cannot be used as the CTD was not always sampling on both up and downcast). 100 separate yo's (each containing one downcast and upcast) were selected at random for testing. Ranging the values of τ_{Temp} and τ_{Cond} from 0 to 2.0 s in increments of 0.1 s, and calculating the root mean square (RMS) error between the corrected downcast and upcast allowed us to minimize the differential. Using this procedure we obtain a value of $\tau_{Temp}=1.02$ s with a standard deviation of 0.86 s, and variance of 0.75 s. Applying the same method to the conductivity data gives us a value of $\tau_{Cond}=1.86$ s with a standard deviation of 0.45 s, and variance of 0.21 s.

3.4.2 Correcting Salinity for Thermal Lag

The methods of Lueck and Picklo [17] and Morison *et al.* [16] are used to correct for the thermal lag in the conductivity cell wall in the following manner:

The thermal response due to a unit step change in temperature, $T(t)$, inside the cell wall can be modeled as:

$$T(t) = 1 - \alpha e^{-\frac{t}{\tau}} \quad (3.4)$$

where α and τ are the magnitude and time constant of the error. A recursive filter developed by Morison *et al.* [16] to estimate the temperature correction inside the conductivity cell is given as:

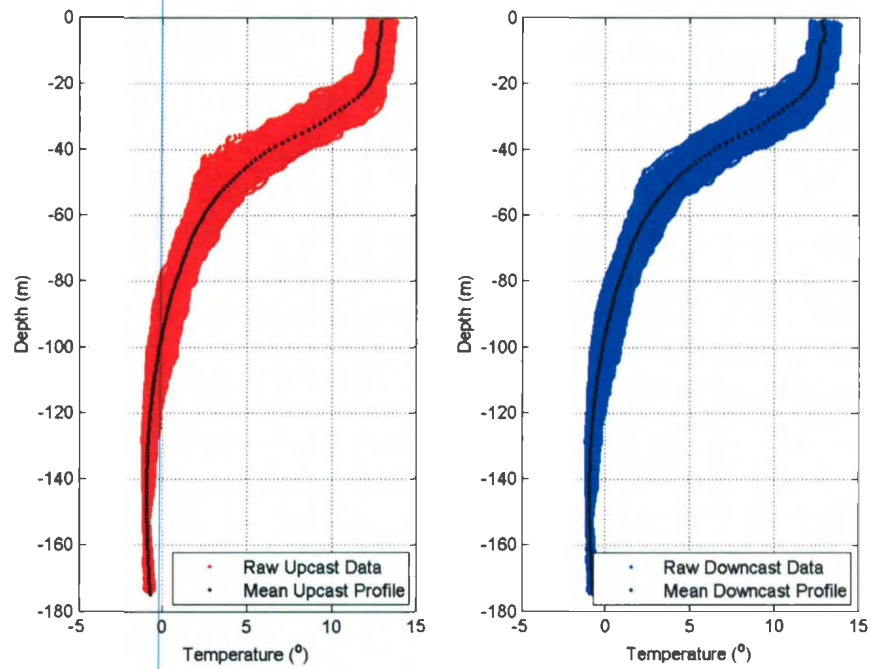


Figure 3.4: Left) Temperature data collected on the upcast (red) and the mean profile (black). Right) Temperature data collected on the downcast (blue) and the mean profile (black). Data obtained from Glider Unit: 48, Julian days: 267-275, 2006. The difference between the upcast and downcast is minimized by applying equation 3.3 to each yo.

$$T_n^C = -bT_{n-1}^C + a(T_n - T_{n-1}) \quad (3.5)$$

where T^C is the temperature correction, T is the measured temperature, n is the sample index, and the constants a and b are given by:

$$a = \frac{4f_n\alpha\tau}{1 + f_n\tau} \quad \text{and} \quad b = 1 - \frac{2a}{\alpha}$$

where f_n is the Nyquist frequency (which corresponds to half the CTD sampling interval), and τ is a time constant.

The temperature correction obtained from equation 3.5 is subtracted from the original temperature data to give a more accurate estimate of a temperature time-series inside the conductivity cell. This new temperature data is then used in the calculation of salinity.

Application of equations 3.1 and 3.2 using the mean vertical speed of the Slocum gives values of $0.10 \text{ } ^\circ\text{C}$ and 12.24 s for α and τ respectively. However, since these equations were determined specifically with a pumped CTD, direct application of these formulas to the non-pumped CTD on board the Slocum glider is questionable [5].

To correctly identify values for our constants we use the same iterative process as outlined by Kerfoot *et al.* [10]. Here we assume that since the horizontal distance covered by 1 yo is on the order of 200 m, and the time required to travel this distance is only $\approx 20 \text{ min}$, the TS data on the downcast should be approximately equal to the TS data on the following upcast. By making this assumption we can now test several values of α and τ iteratively and check to see which values give the lowest discrepancy between downcast and upcast. Similar to the sensor response corrections, we again use 100 randomly selected yo's and calculate values for α and τ in an iterative fashion.

The values for α ranged from 0 to 2.0 $^{\circ}C$ in increments of 0.01 $^{\circ}C$ while the values of τ ranged from 2.0 to 30.0 s in increments of 0.1 s. Using these ranges we are able to calculate corrected salinity profiles using ≈ 28000 different combinations of α and τ using an exhaustive search algorithm. Corrected temperature and salinity time-series are calculated for each set of α and τ , the resulting TS relationship for the mean down/upcast are then compared. To compare the downcast and upcast of a yo, we calculate the difference between the two by using the RMS difference. The value found for α , the magnitude of the effect, is 0.11 $^{\circ}C$. with a standard deviation of 0.044 $^{\circ}C$ and variance of 0.0019 $^{\circ}C$. The value found for τ , the time constant of the effect, is 7.12 s, with a standard deviation of 3.44 s, and variance of 11.85 s.

Application of our correction algorithms to the TS data reduces the mismatch between downcast and upcast from ≈ 0.5 psu to ≈ 0.1 psu (Figure 3.5). A comparison of original salinity profile to the corrected salinity profile shows that mismatch between downcast and upcast is nearly eliminated (Figure 3.6). Our corrections not only help to correct the mismatch between TS relationships, and the vertical salinity profile, but also help to smooth perturbations in the density profile (Figure 3.7).

3.4.3 Comparison of Corrected Data

Using information collected in our Validation Deployment (Section 2.1) we are able to compare our corrected salinity data to data provided by an independent calibrated instrument, the SBE19+ CTD (refer to Chapter 2 for information on this deployment and the comparing instrument).

The result of applying the sensor response corrections followed by the corrections for thermal-lag in the conductivity cell to our data shows good agreement with the independent data set (Figure 3.8). These corrections were applied to the Validation

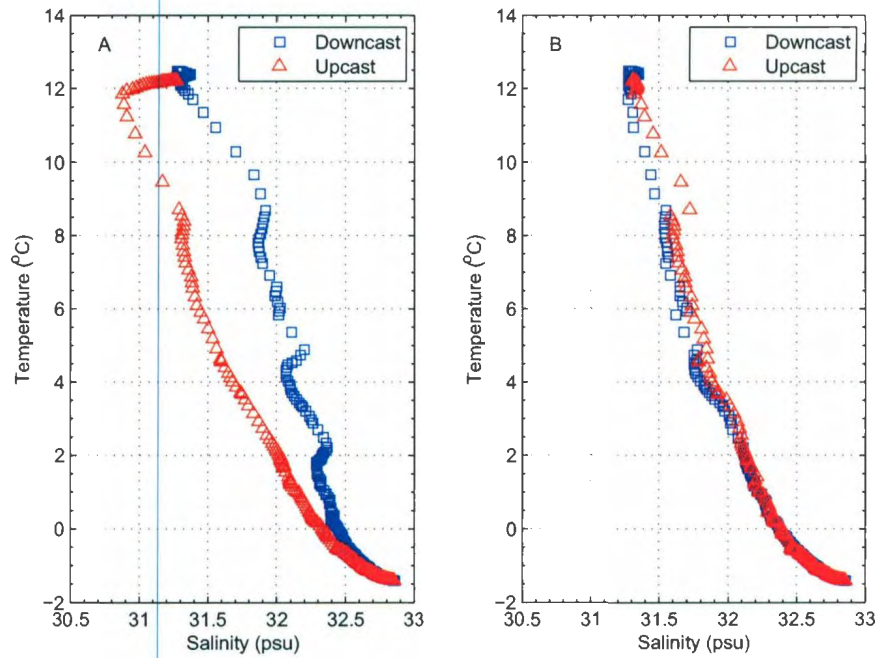


Figure 3.5: Comparison of original TS to corrected TS data obtained from Glider unit: 48, Julian day: 268, 2007. A) Original TS data shows great variation between downcast and upcast data. B) Using correction algorithms detailed previously for both sensor response, and thermal-lag, the deviation between downcast and upcast is all but eliminated.

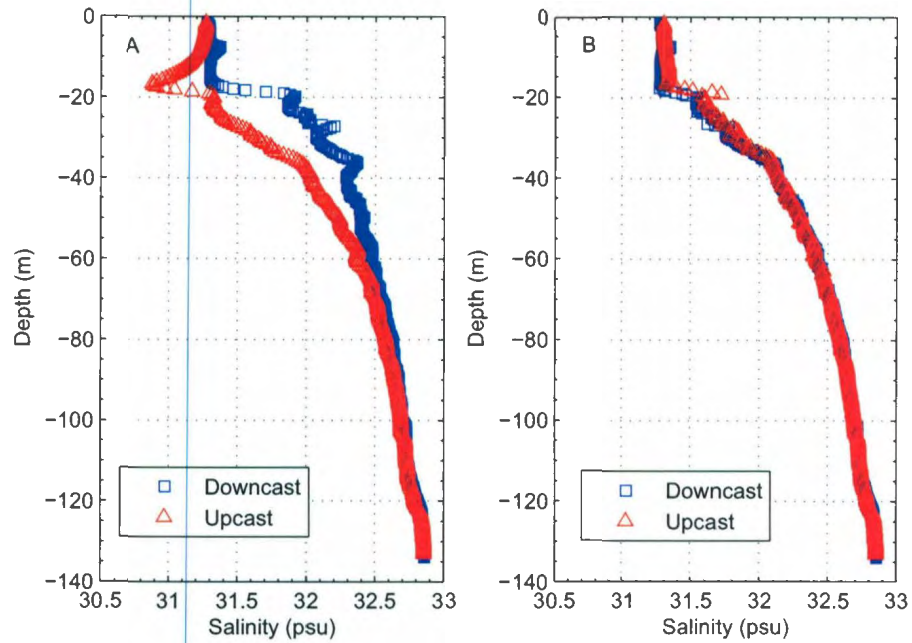


Figure 3.6: Comparison of original salinity values to new corrected values using data obtained from Glider unit: 48, Julian day: 268, 2007. A) Raw salinity data shows a large mismatch between downcast and upcast, on the order of 0.15 psu. B) Corrected salinity data using sensor response algorithms and correction for the thermal-lag problem. Discrepancies between down and upcast have all but disappeared.

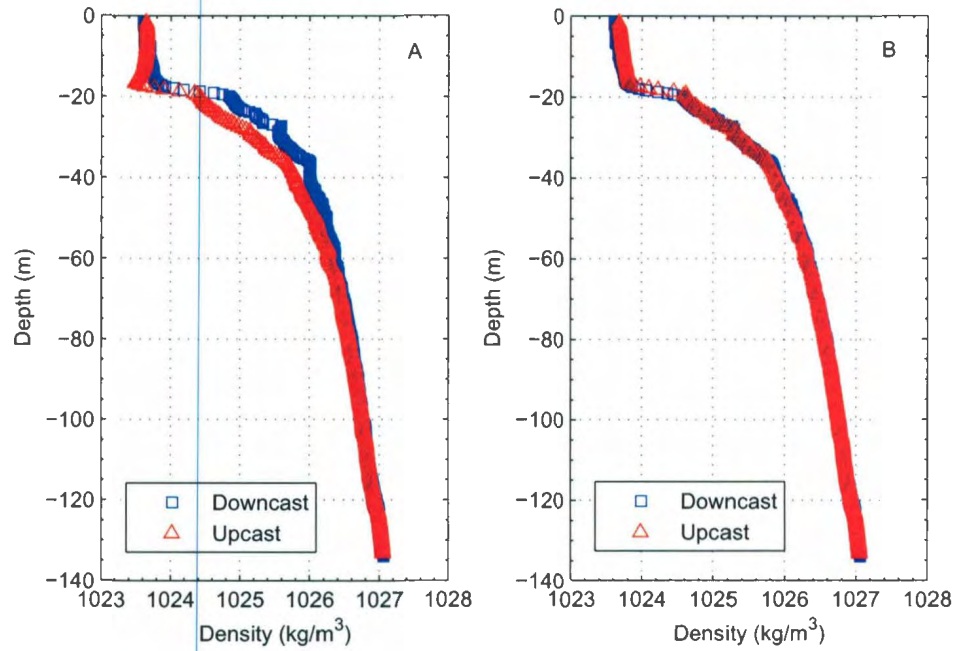


Figure 3.7: Comparison of original density values to new corrected values using data obtained from Glider unit: 48, Julian day: 268, 2007. A) The raw density data shows a mismatch between downcast and upcast, on the order of 0.5 kg/m^3 . B) Corrected density data using sensor response algorithms and correction for the thermal-lag problem bring the downcast and upcast into better alignment.

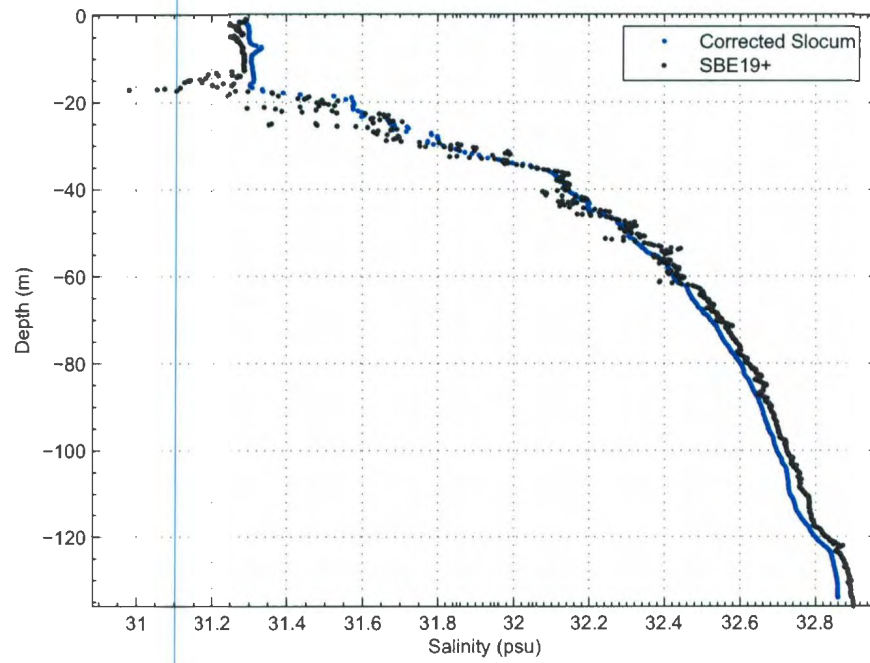


Figure 3.8: Raw salinity data recorded by a SBE19+ CTD (black) as compared to corrected salinity data (blue) from Glider unit: 48, Julian day: 268, 2007. SBE19+ exhibits signs of thermal-lag issues itself. The RMS error between corrected glider data and the SBE instrument is 0.05 psu.

Deployment data. The RMS difference between the corrected Slocum data and the data obtained from the SBE19+ CTD is 0.05 psu - this indicates good agreement between our corrected data and the SBE19+ instrument.

A differential exists between the downcast and upcast data for both the original salinity and also for the corrected salinity using our correction algorithms (Figure 3.9). The raw salinity data shows a difference of 0.7 psu in the area of the pycnocline. After application of our algorithms, this anomaly is reduced by over half to a difference of 0.3 psu.

In Chapter 2, we presented a contour plot of salinity (Figure 2.7) which contained a considerable offset between downcast and upcast which resulted in noisy perturbations in the contour lines. Application of the correction algorithms outlined in this chapter help to smooth out these contours (Figure 3.10).

3.5 Discussion

The first step in correcting our CTD data was to correct for the lagged response of the temperature and conductivity sensors. The values for the sensor response corrections determined for the Slocum CTD are approximately $2 - 3\times$ higher (Table 3.1) than those specified by the Seabird estimates and work done by Johnson *et al.* [5], however, this could be contributed to the modified non-pumped CTD of the Slocum glider. Kerfoot *et al.* [10] showed that the sensor response values with regards to the Slocum CTD are slightly larger than the ones found in this work. Personal communication with Dr. Kerfoot revealed low confidence in these reported values and an examination of his work revealed slight errors in the correction algorithms used.

The large uncertainty associated with our value of τ_{Temp} can be attributed to several of the yo's used for testing which needed no response corrections. Approximately

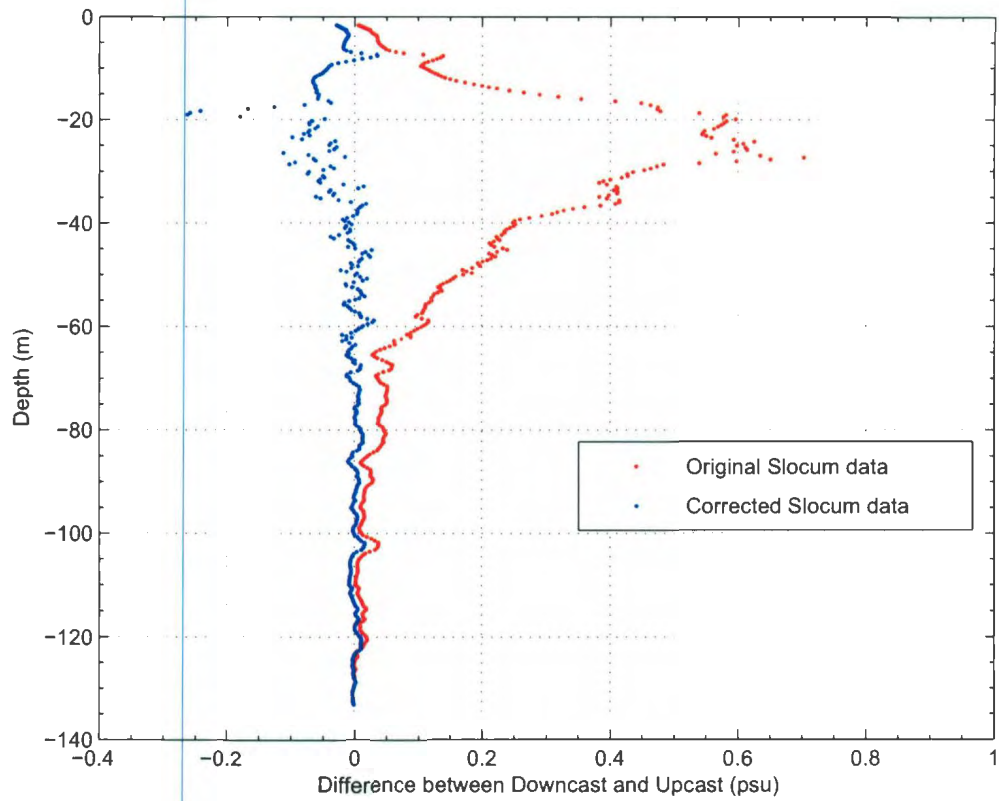


Figure 3.9: The difference between downcast and upcast for original (red) and corrected salinity data (blue) from Glider unit: 48, Julian day: 268, 2007. A differential still exists in the area of the pycnocline of ≈ 0.26 psu in the corrected salinity data - however, this has been reduced from a differential of ≈ 0.70 psu in the original data.

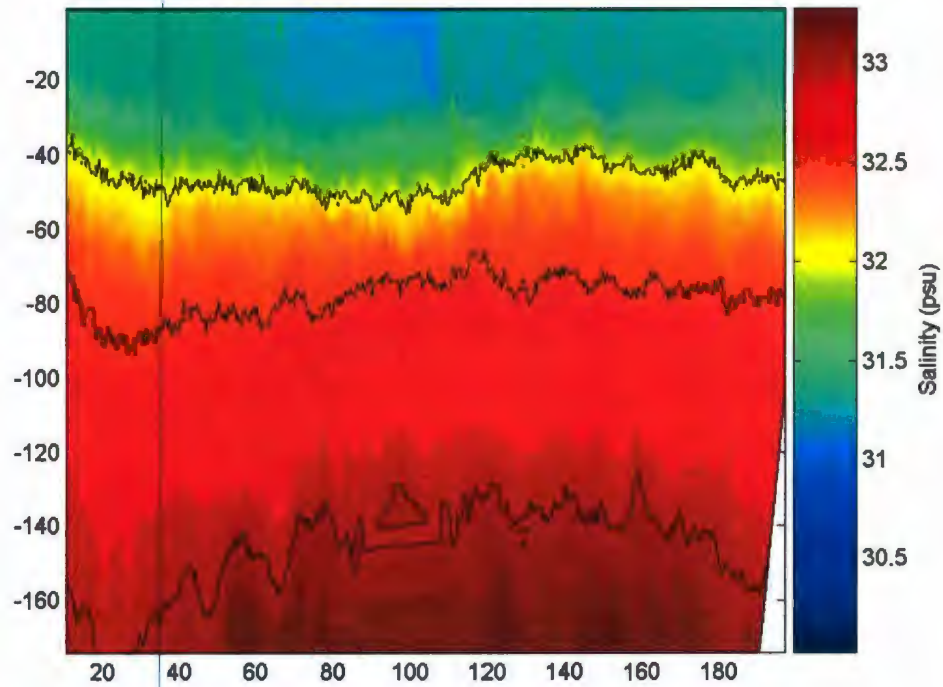


Figure 3.10: Corrected salinity data from the optode deployment using all correction algorithms outlined in this chapter. Data obtained from Glider Unit: 48, Julian days: 267-275, 2006. Comparing this contour to the previous figure 2.7 (raw data) shows that most of the perturbations have been eliminated. Contour levels are at 32, 32.5, and 33 psu respectively.

Source:	τ_{Temp} (s)	τ_{Cond} (s)
Johnson <i>et al.</i> [5]	0.53	0.20
Kerfoot <i>et al.</i> [10]	1.4	2.0
This Work	1.02 ± 0.87 (63% conf.)	1.86 ± 0.45 (63% conf.)

Table 3.1: Differing values for τ_{Temp} and τ_{Cond} from other sources.

28% of the yo's tested had a minimum offset between downcast and upcast before any corrections were applied.

The second step of corrections required is correcting for the thermal-lag problem. We determined α to be $4 \times$ larger, and τ to be $0.6 \times$ smaller than those reported by Lueck and Picklo [17]. Comparing our values to those reported by Kerfoot *et al.* [10] shows good agreement between the value for α but our computed value for τ is $\approx 4 \times$ smaller. When we compare our values to those determined by the theoretical equations 3.1 and 3.2 we see that our value of α is again approximately equal to the theoretical, but our value for τ is just slightly smaller (Table 3.2). The larger values are most likely due to the slower vertical profiling speed of the Slocum glider of ≈ 35 cm/s as opposed to the speed of 1.75 m/s used in Lueck and Picklo's [17] testing (the slower the vertical speed the more time there is for heat to build up in the conductivity cell walls). To summarize, there is more confidence in our calculated value for α , then there is in our value for τ . The large error associated with τ can be attributed to different yo's having different velocities while sampling; even though the error is as large as the value itself, Johnson *et al.* [5] suggests that making the corrections is worthwhile if only for the fact that it smooths out perturbations in the density profiles.

Not only is the speed of the Slocum glider below the recommended range of 0.5 m/s threshold specified by Morison *et al.* [16], we also found that there is a discrepancy

Source:	α ($^{\circ}C$)	τ (s)
Lueck and Picklo [17]	.028	10
Kerfoot <i>et al.</i> [10]	0.13	25.51
Theoretical	0.10	12.24
This Work	0.11 ± 0.044 (63% conf.)	7.12 ± 3.44 (63% conf.)

Table 3.2: Differing values for α and τ from other sources.

between the downcast velocity of a Slocum and the corresponding upcast velocity. Analysis showed that a typical descent occurred over 8.9 minutes, while a typical ascent only took 7.2 minutes, corresponding to vertical velocities of 39 - 53 cm/s and 42 - 56 cm/s respectively [18]. This discrepancy in downcast/upcast velocities calls into question if the methods developed for correcting the thermal-lag can be used in the case of our Slocum glider. Perhaps separate values for α and τ should be specified for each individual downcast and upcast to account for their differing speeds.

Due to the varying speeds during sampling, Morison *et al.* [16] suggest that the values for α and τ should be calculated at each station, therefore we cannot use one set of values for all data collected - each segment of data must thus be dealt with separately. In the future, the processing of each database file obtained from the Slocum could include steps to determine the parameters of α and τ .

Even though these correction methods appear to correct for most of the mismatch between downcast and upcast Temperature-Salinity data, there remains a differential in salinity values (Figure 3.9) in the area of the pycnocline which suggests these correction algorithms may not apply to the Slocum CTD. Calculation of the difference in salinity between the original data and the corrected data reveals that corrected salinity upcast data has values higher than the original upcast, while corrected downcast data is lower than original downcast values (Figure 3.11).

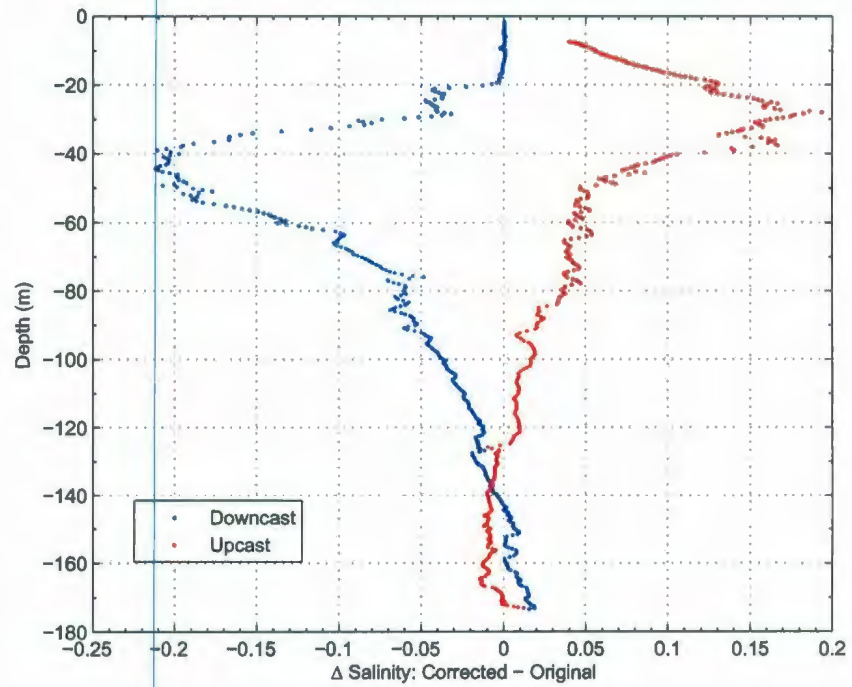


Figure 3.11: Δ Salinity, calculated by subtracting original salinity downcast/upcast from corrected salinity downcast/upcast. Data obtained from Glider unit: 48, Julian day: 268, 2007.

In the future, work should be done to determine if one can use the same values of α and τ for the downcast and corresponding upcast even if the vertical velocities of the profiles differ. While our correction algorithms do minimize the difference between downcast and upcast data, there remains some noise and outlying points in the final data - further work will have to be done to resolve these issues.

Chapter 4

Analysis of the Oxygen Optode Sensor

4.1 Introduction

When a gas comes into contact with water, some gas molecules dissolve in the fluid. Water in nature contains dissolved gases, including oxygen, nitrogen, carbon dioxide and other gases present in air.

The ambient concentration of dissolved oxygen DO_2 in oceanic, shelf and coastal water varies in time and in the vertical and horizontal dimensions for natural reasons. The oceans ability to dissolve oxygen is mainly dependant upon natural factors such as the temperature, the salinity, and the partial pressure of oxygen. DO_2 is also highly affected by biological processes, including the production of oxygen by phytoplankton, and the utilization of oxygen by respiration. The dominant factor determining the potential concentration is temperature, since this exerts the primary control on the solubility of oxygen in water, and therefore the saturation concentration [19]. At every combination of pressure, temperature, and salinity, there is an equilibrium solution at

which point water is saturated with oxygen. Solubility increases with partial pressure and diminishes with increasing temperature and salinity.

4.1.1 Why Measure Dissolved Oxygen?

Both plants and animals consume oxygen as chemical bonds are broken - a process known as respiration. During respiration, carbon and hydrogen food molecules become reconverted to carbon dioxide, water, and recuperated energy; this process requires the presence of oxygen. Marine life must receive enough oxygen for their life processes, without enough oxygen respiration ceases.

Life in the ocean needs DO_2 to survive, the ocean itself has no internal source of oxygen. Oxygen enters the ocean at mid to high latitudes where subduction and deep convection allow the deep ocean waters access to atmospheric gases. Therefore, the DO_2 concentration in the oceans interior reflects a balance between supply through circulation and loss through respiration [20].

Since oxygen responds to both physical and biological stimuli, it can be a very sensitive indicator of environmental change in the ocean. Global ocean data compiled by Kortzinger *et al.* [21] suggest a consistent decreasing trend in oxygen concentrations, which means accurate measurements of DO_2 will have positive implications on understanding global climate change.

4.1.2 A Brief History of Oxygen Sensors

The standard approach to measure oxygen content in water is a two-step wet chemistry precipitation of the DO_2 followed by a titration which was first developed by Winkler [22] and has remained the overall standard [23].

Attempts to complement this classical chemistry method with a sensor based mea-

surement technique started in the 1950's when Clark *et al.* [24] published their paper on the oxygen electrode for analysis on the human body (this electrochemical sensor has long since been adapted for oceanographic purposes ([21] and [24])). Studies such as Berntsson *et al.* [25] have shown that regardless of the design of these sensors, they suffer irreversible pressure effects (hysteresis), cross-sensitivity, and contamination by hydrogen sulfide (H_2S) ([23] and [25]).

Optode technology, which measures oxygen optically using the process of fluorescence, has been known for many years, but has only recently been applied to oceanographic research; this technology may provide a more suitable measurement of DO_2 [23]. Optode's have a number of advantages over electrochemical cells. 1) They come factory calibrated with no need for repeated calibrations. 2) The pressure behavior is fully predictable and reversible. 3) As no oxygen is consumed it does not require stirring. 4) Sensitivity to bio-fouling is reduced as none of the internal optics are exposed to seawater. 5) The fluorescence-lifetime-based measurement principle and luminophores aging properties suggest long-term stability [21].

The optode installed on the Slocum glider is the Aanderaa Instruments oxygen optode 3835 (Figure 4.1). The Aanderaa Optode is based on the ability of certain substances to act as dynamic fluorescence quenchers.

4.2 Theory of Operation

Fluorescence is the ability of a molecule to absorb light of a certain energy and later emit that light with lower energy which corresponds to a longer wavelength. Such a molecule, which we refer to as a luminophore, will enter an excited state after absorbing a photon with high enough energy. After some time, the luminophore will emit a photon of lower energy and return to its initial state. The theory of



Figure 4.1: The Aanderaa oxygen Optode 3835.

operation behind the oxygen optode is based on the principle of dynamic luminescence quenching (Figure 4.2) - the ability of certain molecules to influence the fluorescence of other molecules [26].

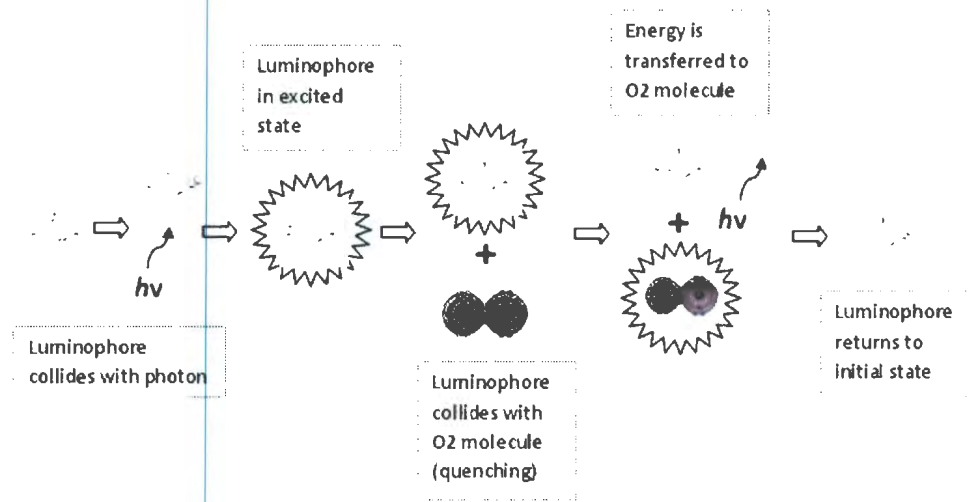


Figure 4.2: The process of Dynamic Luminescence Quenching.

When a luminophore collides with another molecule (oxygen in our case) it transfers part of its excitation energy, which results in less photons (or none at all) being emitted from the luminophore - this effect is known as dynamic luminescence quenching. The luminophore used in our optode is a special molecule called platinum porphyrine [26].

The luminophore is excited with a blue-green light (505 nm) from inside the optical chamber and produces a red fluorescence that is measured by a photodiode in the same chamber; if oxygen is present in the water, the red fluorescence will be quenched [21]. To avoid potential interference with other fluorescent material in the water, or direct sunlight when in the photic zone, the foil is also equipped with a gas permeable

coating which gives optical isolation between the indicator layer and the surroundings [26].

The intensity of light detected by the photodiode depends on the amount of oxygen in the water; however it is not the optimal detection method for oxygen since the intensity is dependent on numerous other factors. Instead, the excitation light is modulated at 5 kHz and the oxygen's fluorescence lifetime is measured [21]. The oxygen lifetime is a measure of how quickly the fluorescence decays.

Following Tengberg *et al.* [23] the relationship between oxygen concentration and the luminescent decay time can be described by the Stern-Volmer equation:

$$[O_2] = \frac{1}{K_{sv}} \left(\frac{\tau_0}{\tau} - 1 \right) \quad (4.1)$$

where τ is a decay time, τ_0 is the decay time in the presence of oxygen, and K_{sv} is the Stern-Volmer constant (the quenching efficiency).

The decay time is a direct function of the phase of the received red luminescent light, which is used directly for oxygen detection. The basic working principles of dynamic luminescence quenching and lifetime based optodes can be found in Klimant *et al.* [27].

4.3 Sensor Anomalies

Similar to the data received from the Slocum's CTD (Chapter 3), anomalous DO_2 data were also detected (Figures 4.3 and 4.4) in the early stages of this project during the initial testing of the oxygen optode (Chapter 2 - oxygen optode test), and have remained constant throughout all deployments since. In order to use DO_2 for modeling purposes, or as an oceanographic tracer, these anomalies must be corrected.

Examining saturation time-series data recorded by the optode (Figure 4.3) show

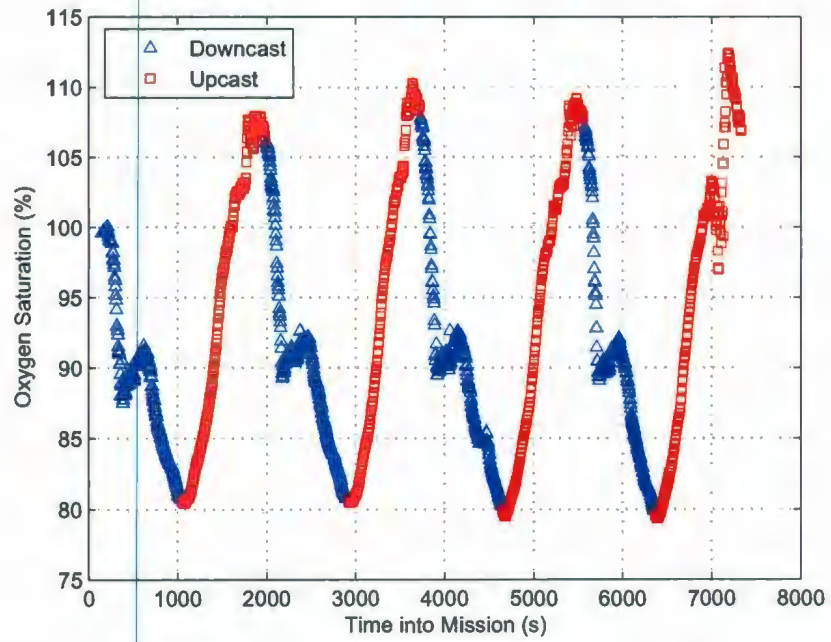


Figure 4.3: A time-series showing oxygen Saturation data of a segment in Conception Bay South. The downcast (blue triangles) shows a distinct anomaly throughout the entire series that is not replicated in the corresponding upcast (red squares).

a distinct difference between the downcast saturation and corresponding upcast saturation. If we look at the vertical profile of saturation (Figure 4.4) we again see the difference between downcast and upcast.

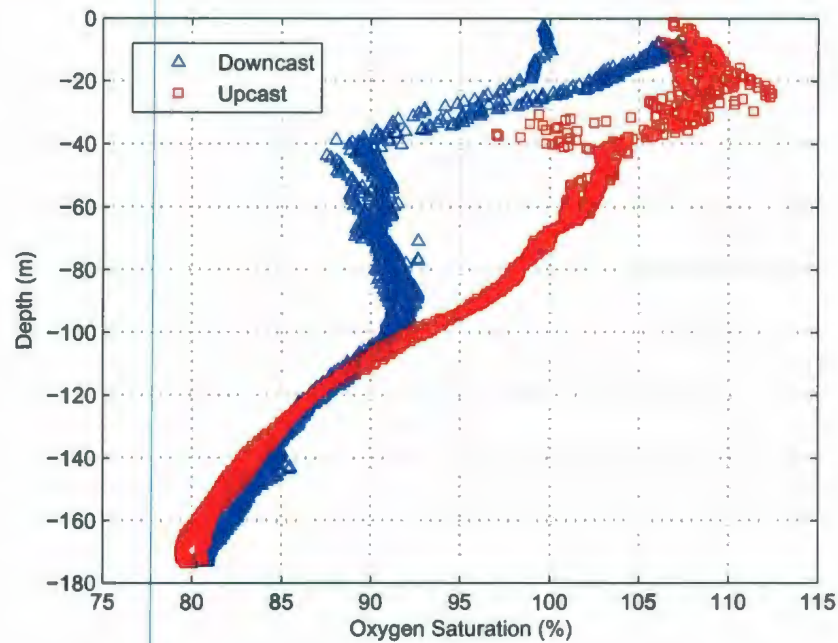


Figure 4.4: A vertical profile of a segment in Conception Bay South. The difference in profiles between the downcast (blue triangles) and upcast (red squares) is prevalent in all collected data.

4.3.1 Sensor Response Problems

As in section 3.3.1, the data obtained from the oxygen optode is also influenced by sensor response problems. Both the optode, and the optode's temperature sensor have somewhat long and different response times, and are therefore out of sync with one another (and also out of sync with the CTD data). When these data sets are combined

to form an estimate of DO_2 , the resulting calculated values will be considerably different from the real values.

The manufacturers specify a time constant for the optode phase data of $\tau_{optode}=25$ s, and a time constant for the temperature sensor as $\tau_{optodeTemp}=10$ s.

4.3.2 Sensitivity to Temperature

Temperature is perhaps the most important factor in determining the amount of dissolved oxygen in water, as the solubility of oxygen in a liquid is inversely proportional to the temperature of the solution (Figure 4.5 A).

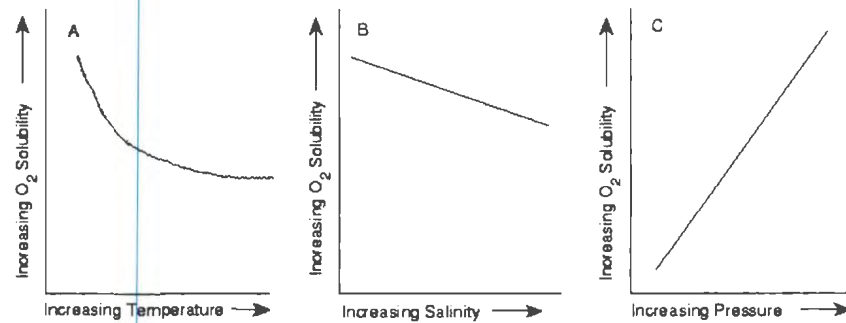


Figure 4.5: The variation of oxygen solubility with regards to a) Temperature, b) Salinity and c) Pressure. For further information refer to *Process Measurement and Analysis*, 2003 [28].

4.3.3 Sensitivity to Salinity

The DO_2 concentration recorded by the optode is the partial pressure of the DO_2 . Due to the physical design of the optode, it cannot sense the effect of dissolved salts in the water because the foil is only permeable to gas. Therefore, the optode

always behaves as if it were submerged in fresh water [26] (if the salinity in our test waters were constant this would not pose a problem). However, there must be post-compensation of collected data since the measured salinity variation is several practical salinity units (31-35 psu).

The solubility of oxygen decreases linearly with increasing salinity. For example, in salt water at 20 °C and 1 atm, the solubility of oxygen would be 7.3 mg/l. In contrast, at the same temperature and pressure, the solubility of oxygen in pure water would be 9.3 mg/l. If salinity compensation is ignored, the error in oxygen solubility can be as great as 20% [28] (Figure 4.5 B).

4.3.4 Sensitivity to Pressure

The oxygen optode sensor responds to the amount of oxygen that is present in water. Oxygen is a gas under normal conditions, thus the amount of oxygen in a liquid is expressed as a partial pressure (P_{O_2}), or as a mole fraction (X_{O_2}). Partial pressure and mole fractions are related through the total gas pressure (P_T) as follows:

$$P_{O_2} = X_{O_2}P_T \quad (4.2)$$

The solubility (or concentration) of a gas dissolved in water, oxygen in our case, S_{O_2} , at a given temperature and pressure follows Henry's law:

$$S_{O_2} = K_H P_{O_2} = K_H X_{O_2} P_T \quad (4.3)$$

where K_H is a constant that depends on temperature and the liquids composition [28] (Figure 4.5 C).

4.4 Corrections

Since the oxygen concentration and saturation data are a function of temperature, salinity, and depth, corrections must be applied to the CTD data before corrections can be made to the oxygen values themselves. Then, the correction of oxygen data involves several steps (Figure 4.6):

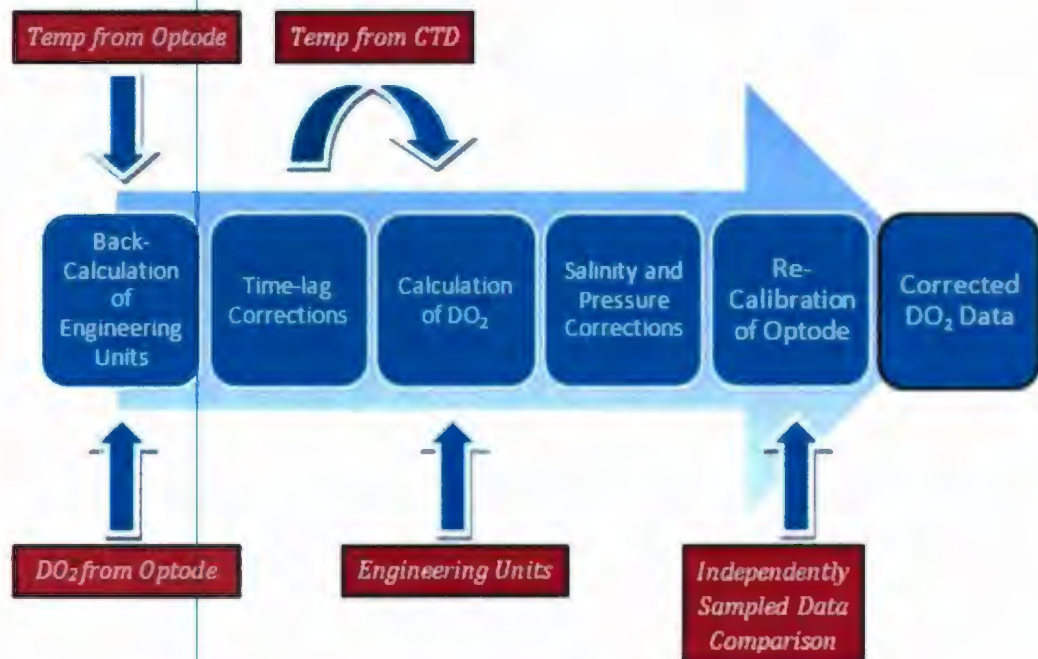


Figure 4.6: The correction of DO_2 data requires several steps. Blue boxes highlight the various algorithms applied; red boxes show the different inputs of data.

1. Decomposition of the original oxygen concentration (μmol) data into physical engineering units ($^{\circ}$).
2. Time lag corrections so that all variables (Temperature, Salinity, Phase data)

correspond.

3. Re-calculation of oxygen concentration using temperature data recorded by the CTD.
4. Corrections for Salinity.
5. Corrections for Pressure.
6. Re-calculation of Sensing Foil Calibration Coefficients.

The original profile of oxygen concentration (Figure 4.7) shows the mismatch between downcast and upcast, and also an asymmetry in the time-series data. This data is for 1 yo during the Validation test, but is broadly representative of all collected data. Corrections applied to this data must not only eliminate the asymmetry problem, but must also eliminate the offset between downcast and corresponding upcast.

4.4.1 Decomposition of Oxygen Concentration Data

Oxygen concentration is calculated using the following formula:

$$[O_2] = C0_{Coef} + C1_{Coef} * P + C2_{Coef} * P^2 + C3_{Coef} * P^3 + C4_{Coef} * P^4 \quad (4.4)$$

where P is the measured phase shift, and the C0Coef to C4Coef are temperature dependent coefficients calculated as:

$$Cx_{Coef} = Cx_{Coef0} + Cx_{Coef1} * T + Cx_{Coef2} * T^2 + Cx_{Coef3} * T^3 \quad (4.5)$$

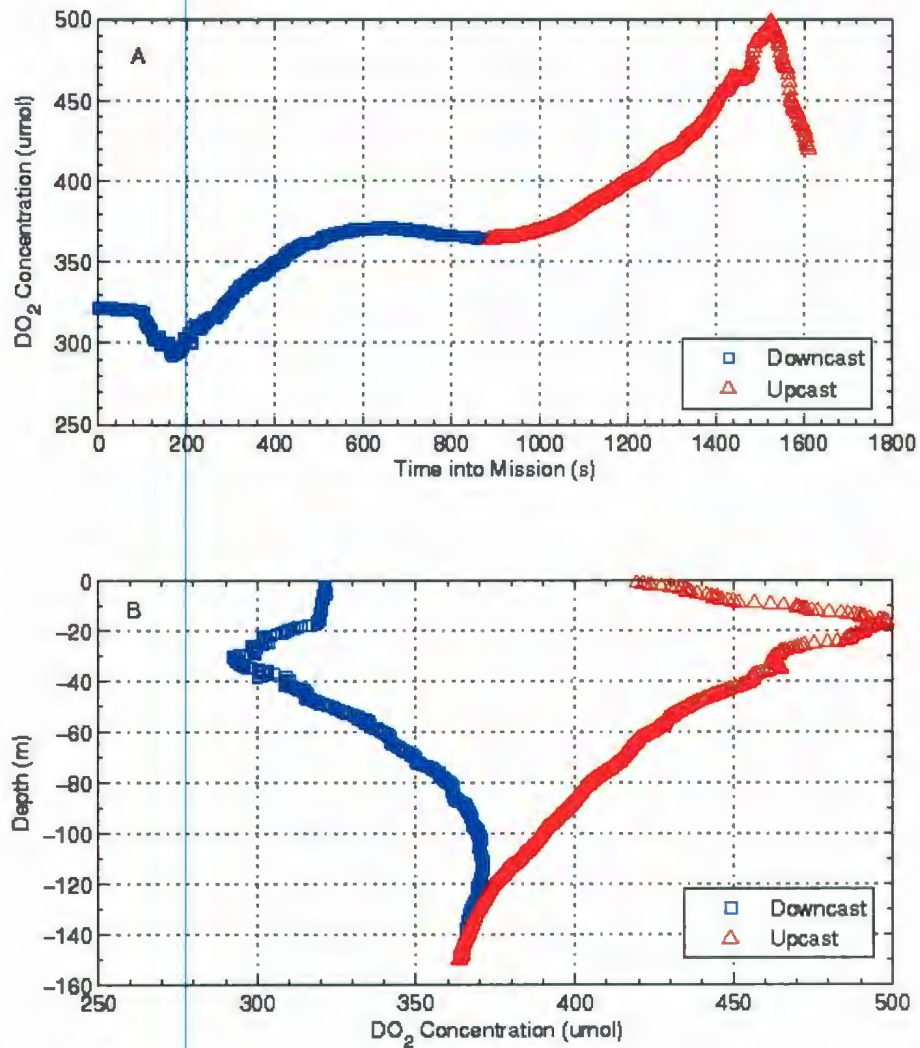


Figure 4.7: Original DO_2 concentration data from Glider unit 48: Julian Day 268, 2007. A) Time series plot shows an asymmetry between DO_2 data collected on the downcast (blue squares) and corresponding upcast (red triangles). B) Vertical profile of DO_2 data also shows major deviation between Downcast (blue squares) and corresponding Upcast (red triangles).

Index	0	1	2	3
C0 Coefficient	3.17242E+03	-1.07261E+02	2.13316E+00	-1.79234E-02
C1 Coefficient	-1.73981E+02	5.10262E+00	-9.85758E-02	8.02240E-04
C2 Coefficient	3.95600E+00	-9.81040E-02	-1.85346E-03	-1.42536E-05
C3 Coefficient	-4.26337E-02	8.78820E-04	-1.64409E-05	1.13709E-07
C4 Coefficient	1.76869E-04	-2.95502E-06	5.55039E-08	-3.08493E-10

Table 4.1: Sensing Foil Calibration Coefficients.

where $Cx_{Coe\text{fo}-3}$ (Table 4.1) are coefficients based on the sensing foil used with the optode (which are supplied by the manufacturer); and T is the external temperature in $^{\circ}C$ [26].

The first step involved in the correction of the oxygen data involves back-calculating the original phase data collected by the optode. The Slocun records the oxygen data in units of concentration (μmol) and saturation (%), which is a function of temperature and phase units. Phase data must be separated from the temperature data so that algorithms can be applied to each set of data. This separation is accomplished by finding the roots of the polynomial (Equation 4.4) which correspond to the phase information. Using the ROOTS command in MatLab, combined with the oxygen concentration and temperature supplied by the optode we obtain the original phase information (Figure 4.8).

The oxygen data collected in CBS during the Validation test can be considered representative of all back-calculated phase data.

4.4.2 Correction for Sensor Response

In section 3.3.1 we corrected varying sensor responses by using the historical method of removing the shift from the temperature and conductivity sensors so that they

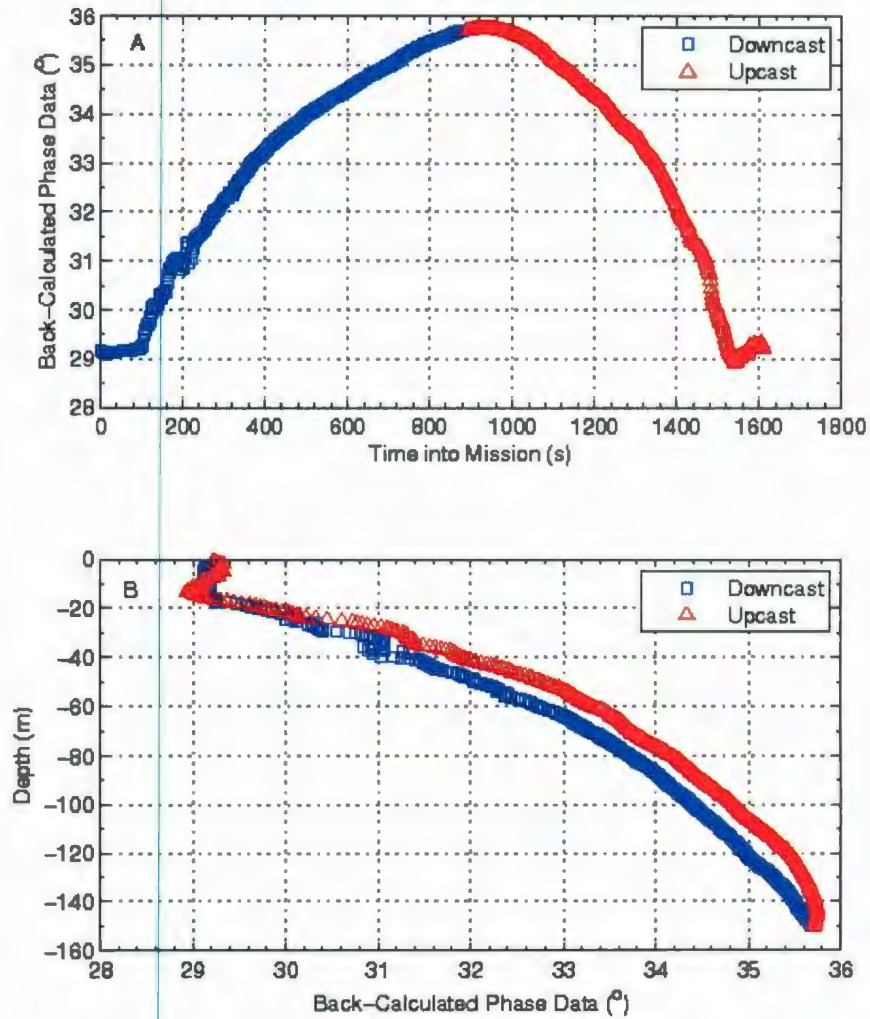


Figure 4.8: Back-calculated Phase data from Glider unit 48: Julian Day 268, 2007. A) The time-series shows good symmetry between phase data collected on the downcast (blue squares) and corresponding upcast (red triangles). B) Vertical profile of phase data also shows good agreement between downcast (blue squares) and corresponding upcast (red triangles).

align with the values for pressure. These methods give adequate results, as the time constants in question are about 1 second. Since the oxygen sensor time constant is on the order of tens of seconds, we use a different method in this section.

More recently in computational oceanography, the trend for dealing with sensor mismatch has been to add a time shift to the other faster responding sensors, since computationally it is simpler and noise amplification is eliminated [13]. This is the approach we take here.

Following the procedure outlined in the *UNESCO Technical Papers in Marine Science: The acquisition, calibration, and analysis of CTD data* [13], the general application to add simple exponential time lag response to data is by using a recursive digital filter:

$$X'(n) = W(0)X(n) + \sum_{k=1}^{k=K} W(k)X'(n-k) \quad (4.6)$$

where the sum of the filter weights, $W(k)$ is equal to unity.

The response function of the previous equation is given by:

$$R_1(f) = \frac{W(0)}{1 - \sum_{k=1}^{k=K} W(k)\exp(-i^2\pi f k \Delta t)} \quad (4.7)$$

where f is in units of cycles per sampling interval.

Simple exponential lag response for a time constant of τ seconds and a sampling interval of Δt seconds can be achieved from equation 4.7 by letting $K = 1$, $W(0) = 1 - \exp(-\frac{\Delta t}{\tau})$, and $W(k) = \exp(-\frac{\Delta t}{\tau})$, thus giving us:

$$X'(n) = [1 - \exp(-\frac{\Delta t}{\tau})]X(n) + \exp(-\frac{\Delta t}{\tau})X'(n-1) \quad (4.8)$$

The oxygen optode has the slowest response time of all our sensors at a value of $\tau_{O_2}=25$ s. Using equation 4.8, appropriate lag can be added to our other sensors to

minimize the temporal mismatching (Figure 4.9).

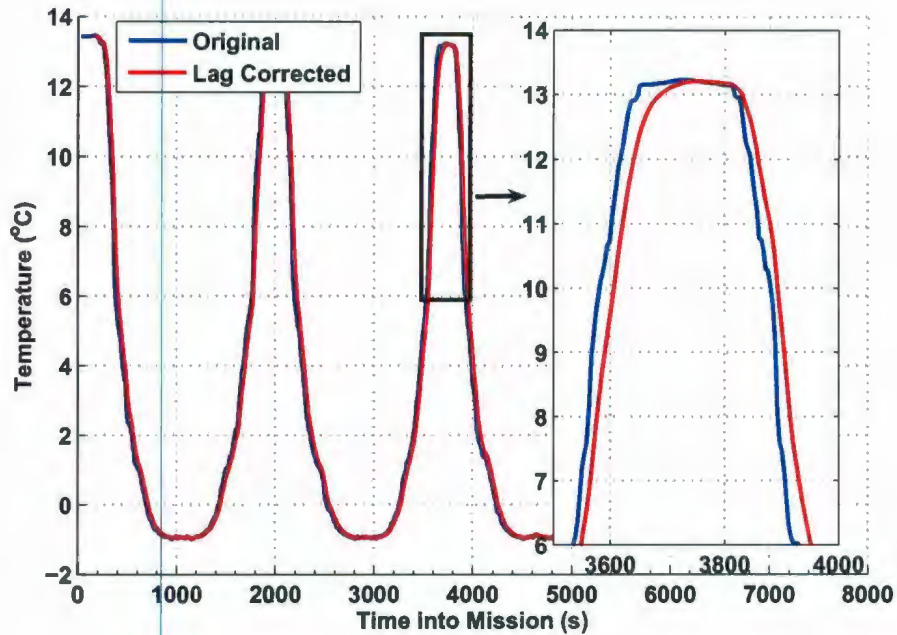


Figure 4.9: Original temperature data (blue) and the same data after being processed using equation 4.8. All the data has shifted forward in time (blue), essentially adding the same lag which is found in the oxygen data.

4.4.3 Replacing Optode Temperature with CTD Temperature

The difference between the temperatures calculated from both the CTD and the oxygen optode may disagree by as much as 3 °C. Also, the temperature recorded by the optode fails to reach the maximum temperature recorded by the onboard CTD (Figure 4.10). It is this erroneous temperature data from the optode which leads to

some of the asymmetry between calculated downcast and upcast DO_2 values.

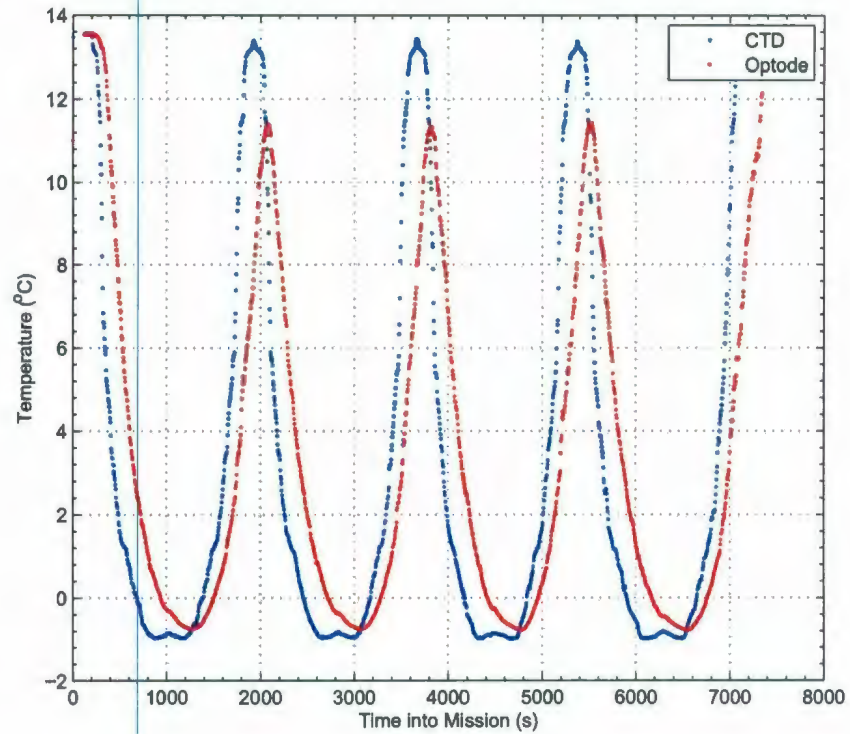


Figure 4.10: Temperature recorded by the oxygen optode (blue) clearly lags the temperature from the CTD (red).

Corrected oxygen data recalculated using temperatures from the CTD, as opposed to that of the optode, show much better agreement between downcast and upcast (Figure 4.11). We use the CTD temperatures because the sensor has a smaller time constant than the temperature sensor on the optode itself, hence being more accurate.

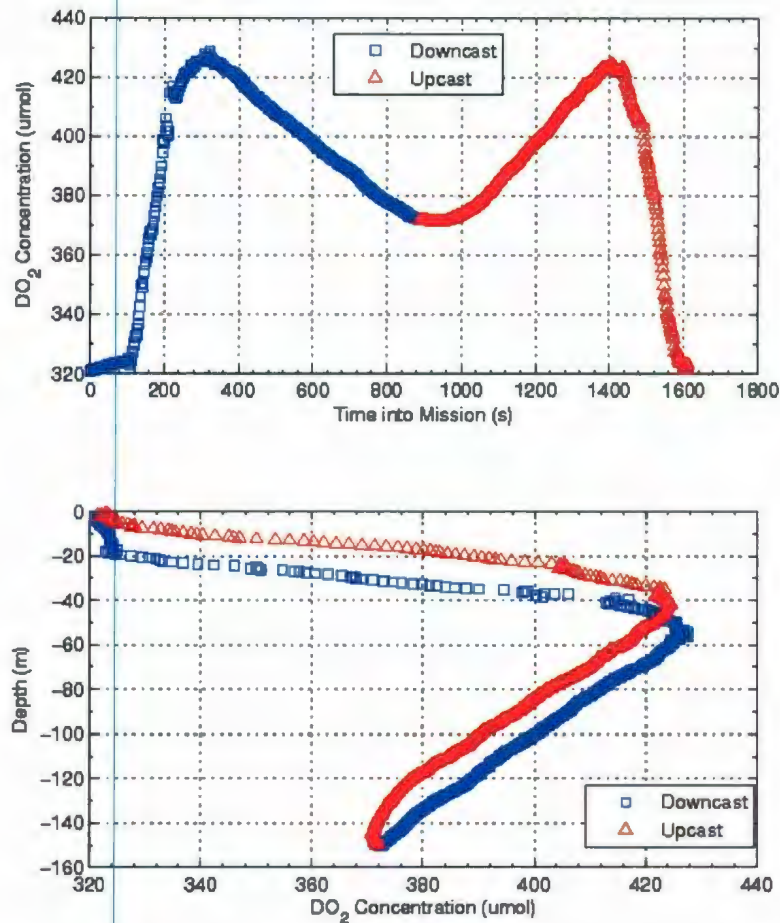


Figure 4.11: Corrected DO_2 concentration data using lag-corrected CTD temperature values from Glider unit 48: Julian Day 268, 2007. A) Time-series plot of corrected DO_2 shows a good symmetry between data collected on the downcast (blue squares) and corresponding upcast (red triangles). B) Vertical profile of corrected DO_2 data also shows good agreement between downcast (blue squares) and corresponding upcast (red triangles). Using lag-corrected temperature data from CTD as opposed to temperature data from the optode has eliminated most of the miss match in the data set.

Constant B_x	Value
B_0	$-6.24097e - 3$
B_1	$-6.93498e - 3$
B_2	$-6.90358e - 3$
B_3	$-4.29155e - 3$
B_4	$-3.11680e - 7$

Table 4.2: Oxygen Optode Constants for Salinity Corrections.

4.4.4 Adjusting Oxygen Data for Salinity

Since DO_2 saturation depends on Salinity, we must first correct the CTD data using correction routines outlined in section 3.4. Once this is accomplished we use the new corrected salinity for our oxygen corrections.

According to the optode manual [26] an accurate correction may be obtained by multiplying the recorded DO_2 concentration, given as micro-molar, by the following factor:

$$O_2^S = [O_2]e^{S(B_0+B_1T_S+B_1T_S^2+B_1T_S^3)+C_0S^2} \quad (4.9)$$

where:

S = salinity in psu

T_S = scaled temperature = $\ln(\frac{298.15-t}{273.15+t})$, t = temperature, °C

B_0 - B_4 are given in table 4.2.

Application of the salinity corrections to the lag-corrected DO_2 data has the effect of lowering DO_2 concentration values by up to 55 μmol (Figure 4.12).

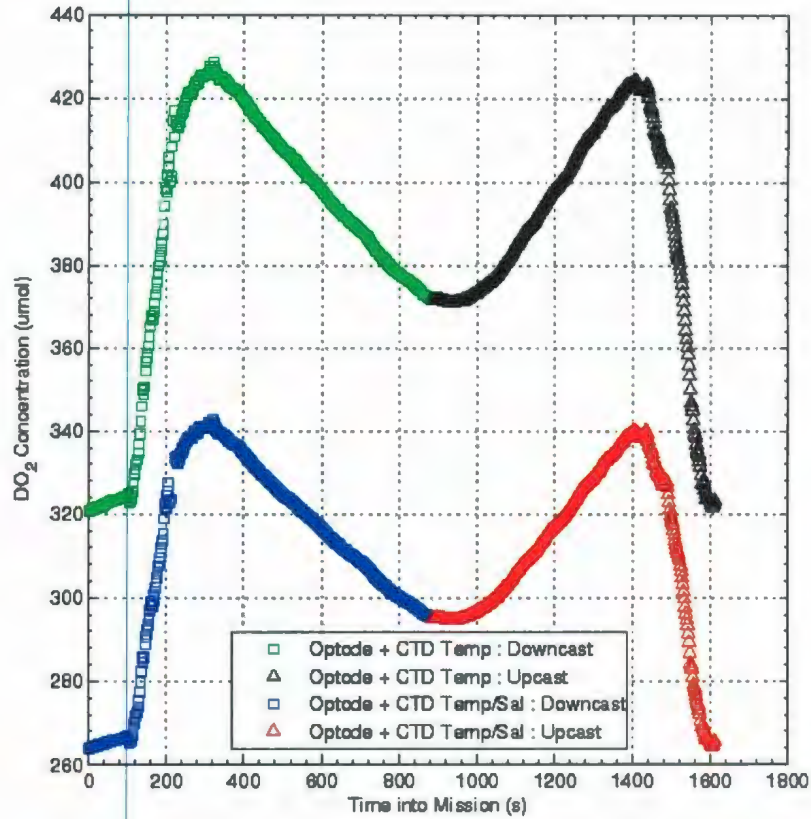


Figure 4.12: A comparison of corrected DO_2 concentration time-series data using lag-corrected CTD temperature and salinity corrections from Glider unit 48: Julian Day 268, 2007. Downcast (green squares) and upcast (black triangles) represent DO_2 calculated using CTD temperature values. Downcast (blue squares) and upcast (red triangles) represent DO_2 calculated using CTD temperature values followed by corrections for salinity. Salinity corrections lower DO_2 concentration values by up to $55 \mu\text{mol}$.

4.4.5 Adjusting Oxygen Data for Pressure

Due to limitations in the physical design of the optode, the response of the sensing foil decreases with the ambient water pressure at about 4% lower response per 1000 m of water depth.

Our glider is restricted to coastal waters (max 200 m) which poses a minor problem that is easily compensated for by using the following equation [26]:

$$O_2^P = [O_2](1 + \frac{0.4d}{1000}) \quad (4.10)$$

where:

d is depth in meters

O_2^P is compensated O_2 -concentration in either micro-molar or percent saturation depending on the input.

The effects of our pressure correction algorithm on our data is almost negligible (Figure 4.13). Comparing our original raw optode data to that of the corrected data (processed using our correction algorithms for lagged CTD temperature, salinity, and pressure), shows that our corrections eliminate most of the asymmetry in the time-series (Figure 4.14) - the corrected data show good agreement between the downcast and corresponding upcast.

4.4.6 Comparison of Corrected Data

Using information collected in our Validation Deployment (Section 2.1) we are able to compare our corrected oxygen concentration data to data provided by an independent measuring device (the SBE43 oxygen sensor). A comparison of the raw data from both the Slocum's oxygen optode, and the independent SBE43 oxygen sensor (which was lowered from the sampling vessel), show considerable offset before corrections are

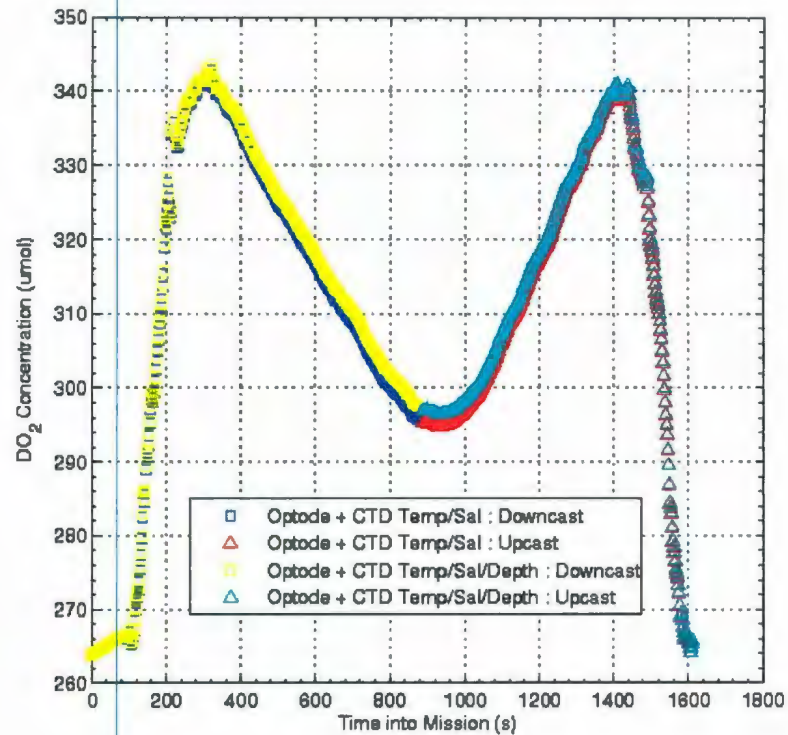


Figure 4.13: A comparison of corrected DO_2 concentration time-series data using lag-corrected CTD temperature, salinity corrections, and pressure corrections from Glider unit 48: Julian Day 268, 2007. Downcast (blue squares) and upcast (red triangles) represent DO_2 calculated using CTD temperature values followed by corrections for salinity. Downcast (yellow squares) and upcast (cyan triangles) represent DO_2 calculated using CTD temperature values, corrections for salinity, and corrections for pressure. Pressure corrections have a negligible effect of raising DO_2 concentration values by 2-3 μmol .

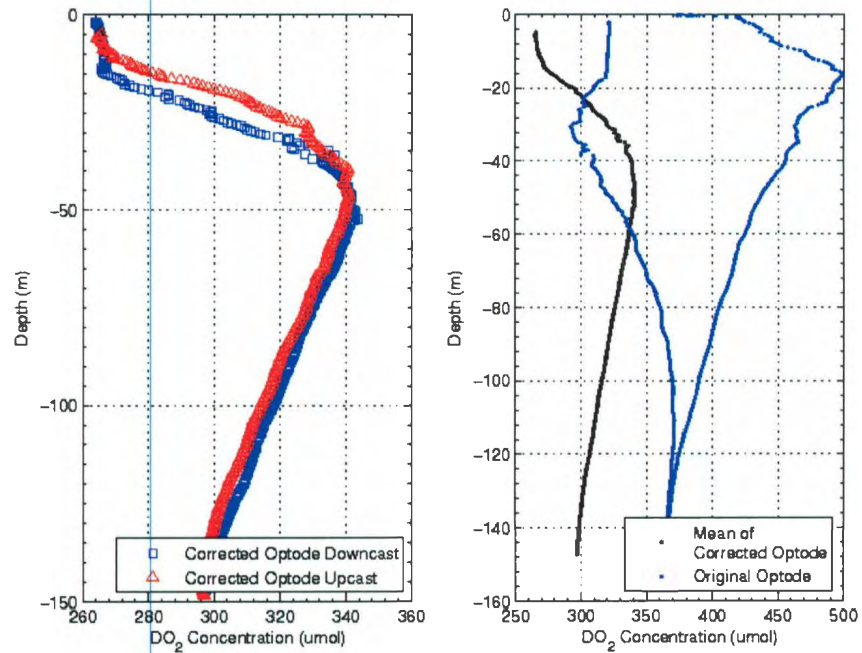


Figure 4.14: A comparison of original DO_2 data to that of corrected DO_2 data using lag-corrected CTD temperature, salinity corrections, and pressure corrections from Glider unit 48: Julian Day 268, 2007. A) Downcast (blue squares) and upcast (red triangles) represent DO_2 corrected for lagged response, using CTD temperature values followed by corrections for salinity, and finally pressure. B) Original optode data (brown) vs the corrected optode data (black) using all correction routines. Corrections eliminate most of the miss match between downcast and upcast.

applied (Figure 4.15). DO_2 data show a complete mismatch throughout the entire water column, however, the pattern observed from the Slocum data visually matches previous data acquired. Since the ship and the glider were never separated by more than 200 m while sampling, we would expect both instruments to record similar data (Figure 2.10).

This DO_2 profile from our Validation deployment shows the same pattern that appeared in our first test of the oxygen optode (and all subsequent deployments) - the fact that the same type of profile appears in two different sets gives evidence that the optode error is systematic in nature and can be corrected. Application of the correction algorithms described in section 4.4 were applied to this data set. While the correction algorithms eliminate the offset between downcast and upcast, bringing the profile into the same shape and range of the SBE43, anomalies still exist. Visual inspection of the corrected optode data (mean profile) versus the SBE43 reveals the existence of a bias in the optode data (Figure 4.16).

Examination of DO_2 in the upper 15 m of both instruments - before any effects are felt due to the strong oxycline - reveals the optode data is consistently $3 \mu\text{mol}$ less than values obtained from the SBE43 instrument (Figure 4.17).

Addition of a bias offset to the corrected optode DO_2 data (Figure 4.17) brings the corrected data into good alignment with SBE43 data in the upper 45 m of depth. However, a constant offset of the data is still noticeable at depths below 50 m due to calibration issues with the instrument.

A statistical comparison of our original optode concentration data to the SBE43 data gives an R^2 value of $8.5849e - 004$ (effectively zero), which indicates no correlation between the data. A comparison of our corrected mean optode data (using all correction algorithms and added bias) with the SBE43 data gives $R^2 = 0.97$ which explains 94% of the variance.

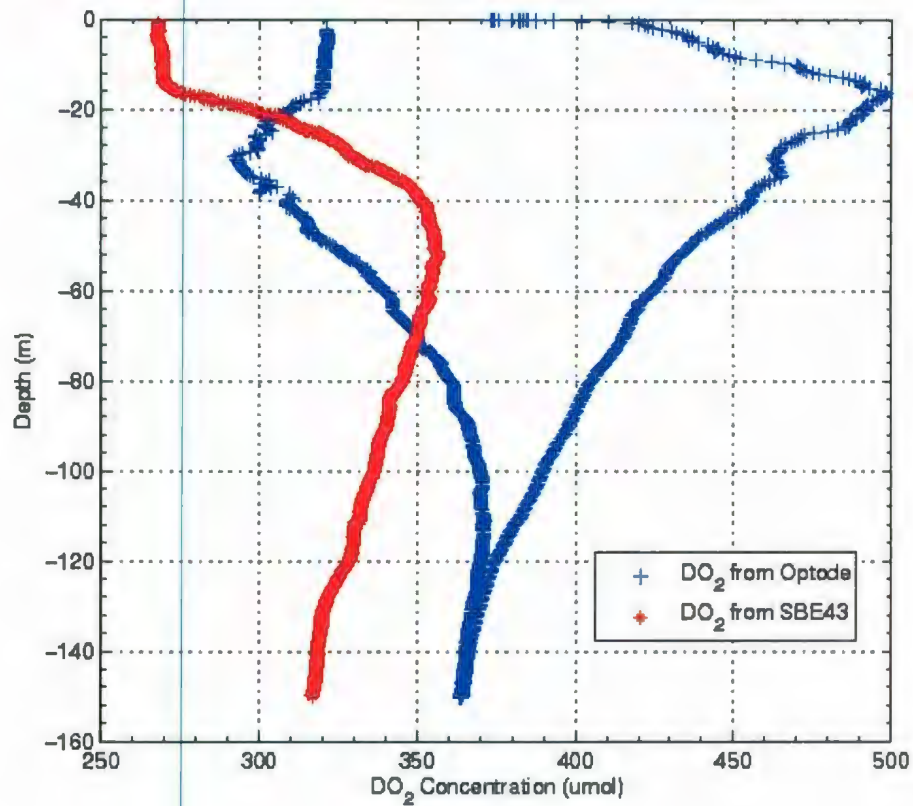


Figure 4.15: Raw DO_2 concentration data from the optode (blue +) compared to DO_2 concentration data from the independent sampling platform, the SBE43 oxygen sensor (red *), obtained during the Validation test from Glider unit 48: Julian Day 268, 2007.

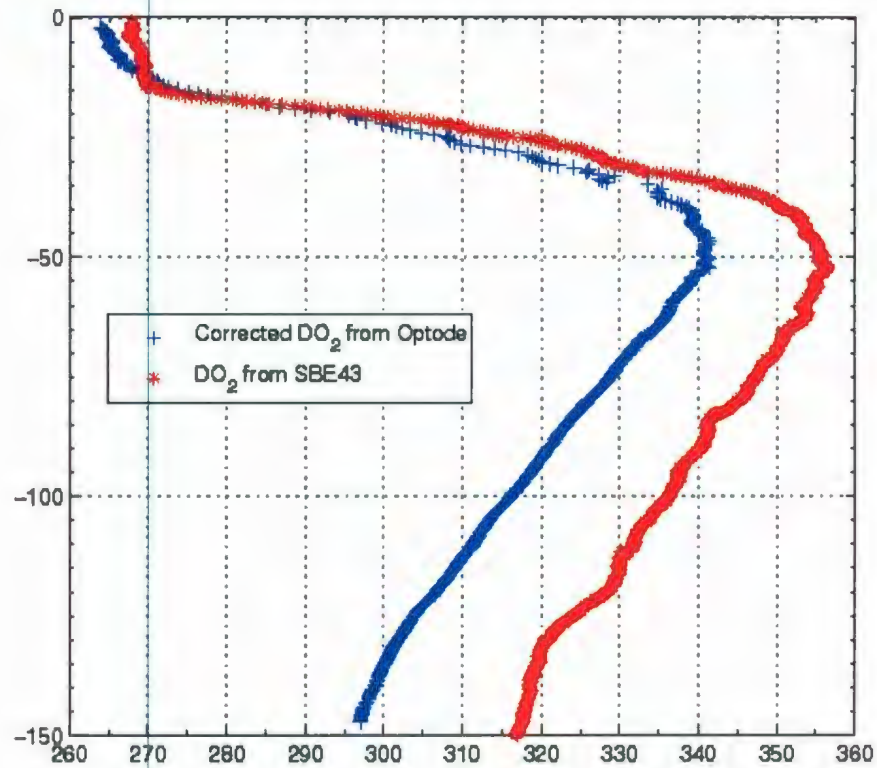


Figure 4.16: Corrected optode DO_2 data (blue) as compared to SBE43 DO_2 data (red) obtained during the Validation test from Glider unit 48: Julian Day 268, 2007. Optode data is corrected for lagged response, temperature, salinity, and depth as described in the previous section. Both profiles now show the same shape, but the optode data appears to be offset by 10-20 μmol below 40 m of depth.

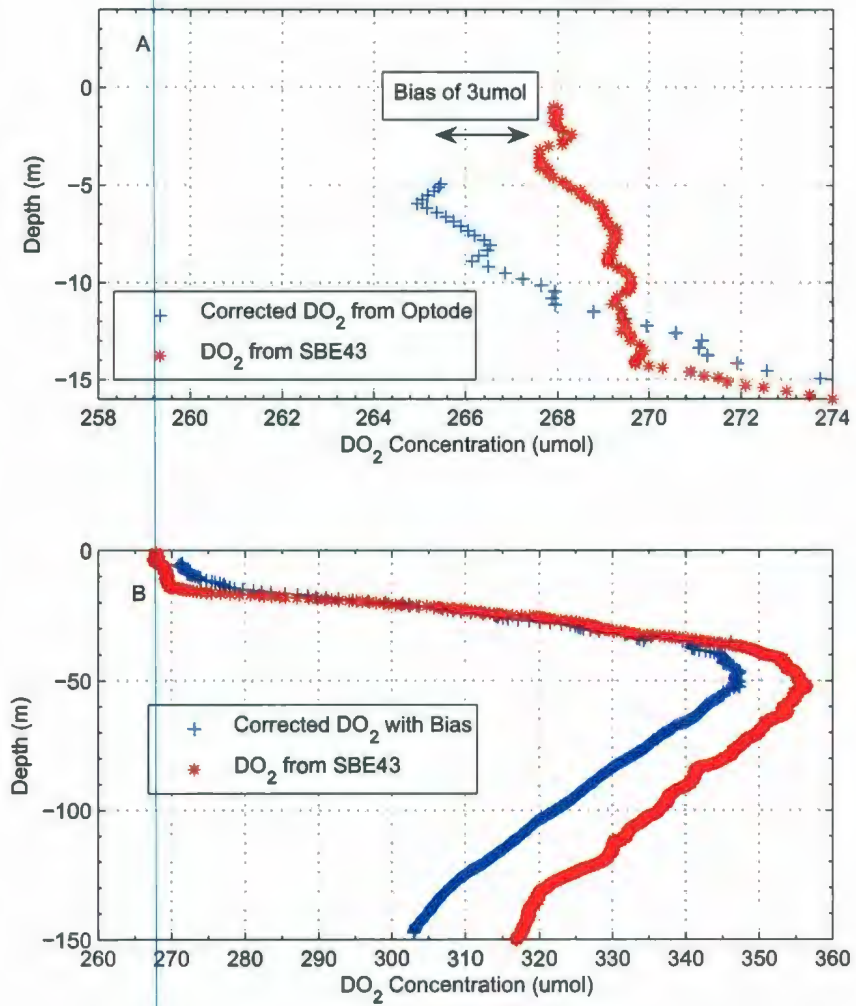


Figure 4.17: A) A bias of 3 μmol is initially present between corrected optode data and SBE43 data obtained during the Validation test from Glider unit 48: Julian Day 268, 2007. B) Corrected DO_2 with added bias (blue +) now aligns much better with SBE43 data (red *) in the upper 45 m but there still exists a constant offset below these depths.

Optode Error Analysis

Aanderraa specifications for the oxygen optode 3835 list the accuracy of the optode as $\pm 8 \mu\text{mol}$ or 5%, whichever is greater - 5% being the greater number in our data set. Visual inspection shows data obtained from the SBE43 instrument falls within the error range specified for our mean optode data (Figure 4.18). The root mean squared error (RMSE) between our corrected data and the SBE43 data is $14.01 \mu\text{mol}$.

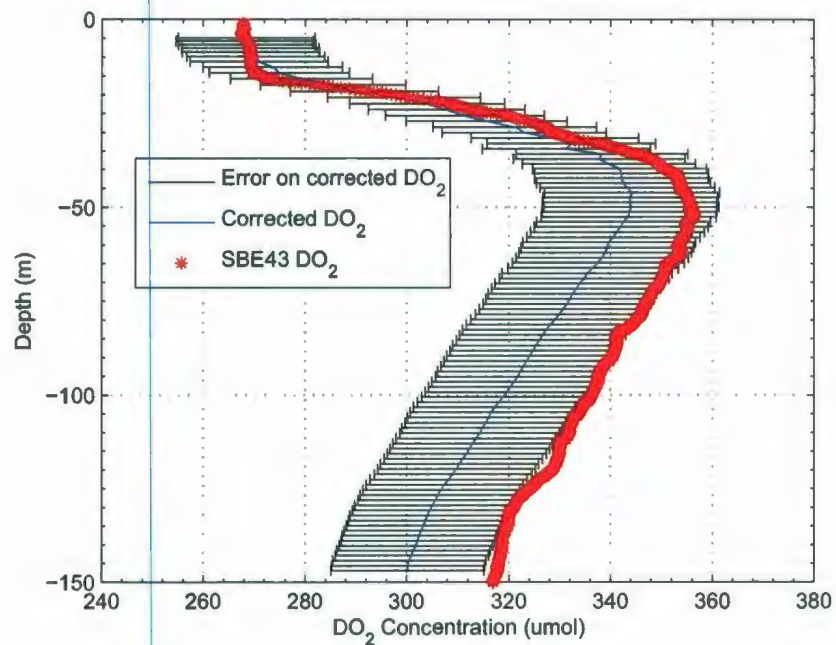


Figure 4.18: The upper and lower bounds of our corrected optode DO_2 data encompass the majority of data supplied by our independent measuring device.

In Chapter 2, we presented a contour plot of raw oxygen saturation (Figure 2.9) which contained a considerable vertical banding in the upper 60 meters of depth - a result of the slow response of the optode. Application of the correction algorithms

outlined in this chapter help to smooth out these contours (Figure 4.19).

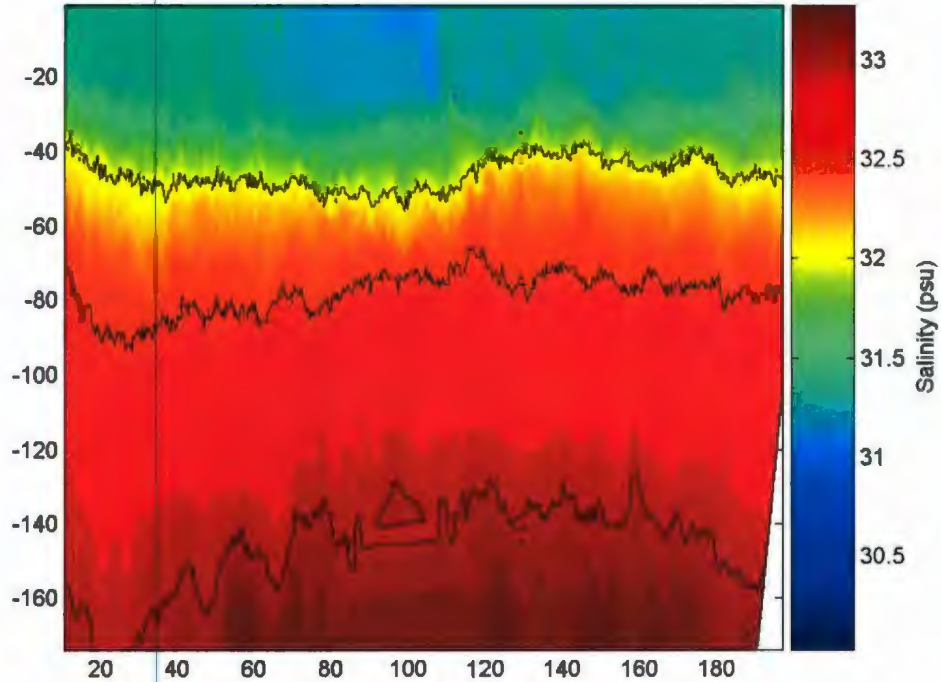


Figure 4.19: Corrected oxygen saturation data from the optode deployment using all correction algorithms outlined in this chapter. Data obtained from Glider Unit: 48, Julian days: 267-275, 2006. Comparing this contour to figure 2.9 (raw data) shows that most of the vertical banding has been eliminated. Contour levels are specified as 75, and 92% respectively

4.4.7 Determining new Coefficients for Calculation of DO_2

Our corrected mean DO_2 data profile does give good results when compared to the SBE43 data (Figure 4.20), however, a calibration issue still exists. To solve this

Index	0	1	2	3
C0 Coefficient	-1786556.55	-629130.27	-210824.88	-8747.58
C1 Coefficient	200087.72	75892.68	25412.44	1152.28
C2 Coefficient	-8390.86	-3417.99	-1148.89	-56.65
C3 Coefficient	156.20	68.13	23.09	1.23
C4 Coefficient	-1.10	-0.51	-0.17	-0.01

Table 4.3: Corrected Sensing Foil Calibration Coefficients.

problem we must determine a new set of foil calibration coefficients. Using our corrected DO_2 data we can once again back-calculate a set of phase data; this corrected phase data, along with the lag-corrected CTD temperature data, can be fitted using a general polynomial regression model (Equation 4.4) to the independent DO_2 values obtained from the SBE43 sensor;. Using MatLab's Polyfitn algorithm, we are able to generate a new set of calibration constants (Table 4.3) that can be used in future optode deployments.

For future optode data, once our correction algorithms are applied, we can input our corrected phase data, along with CTD temperature into MatLab's Polyvaln algorithm (with our new coefficients) to determine a new corrected data set which should better align with our independent measurements (Figure 4.20).

4.5 Discussion

The back-calculation of phase data (Figure 4.8) shows a small offset between downcast and upcast data which is most likely due to the temperature data, supplied from the optode, and also the optode's slow response time. This suggests it is not the phase data recorded by the optode, but instead the temperature data which leads

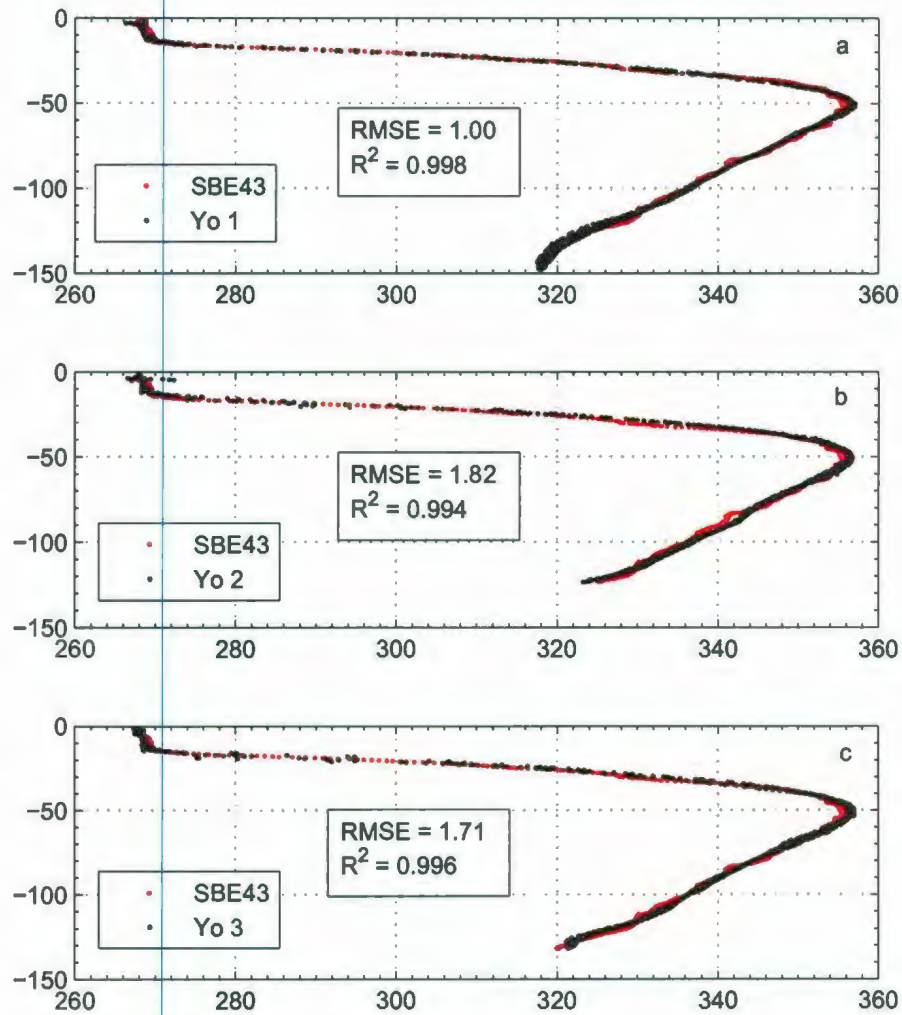


Figure 4.20: Dissolved oxygen calculated using new corrected sensing foil calibration coefficients. a) Yo 1 data is used to determine a new set of calibration coefficients. b) New coefficients are applied to Yo 2 with good results. c) New coefficients are applied to Yo 3, also giving good results when compared to the SBE43 data.

to the deviations in calculated DO_2 . The optode manual states that if a faster responding temperature probe is available, it should be used in replacement of the optode temperature data [26]. The CTD on the Slocum has a time constant of about 1 s, which is much faster than the optode's temperature sensor time constant of 12 s. The application of the digital filter (Equation 4.8) on temperature data recorded by the onboard CTD brings this data into proper alignment with the lagged back-calculated phase data.

Recalculating DO_2 using lagged CTD temperature and phase data eliminates the asymmetry initially seen in the DO_2 time-series (Figure 4.11). This new corrected DO_2 data also eliminates most of the discrepancy initially seen between the downcast and corresponding upcast data.

The corrections for salinity and pressure are carried out on the DO_2 data once the CTD data has been corrected for thermal lag effects (refer to Chapter 3). While the affects of salinity and pressure are less important than those of temperature, they are still responsible for changing DO_2 values by a considerable amount. Salinity corrections effectively reduce the DO_2 levels by up to 20%, while the pressure corrections show a minimal change, which raise values by 2 μmol (Figure 4.12 and 4.13).

Application of the correction algorithms, including the addition of a bias offset of 4.5 μmol , lead to the discovery of a calibration problem with the instrument - the oxygen optode has an operating temperature range of 0-40 $^{\circ}\text{C}$ [26] and is not calibrated for use in subzero temperatures. This problem did not appear to be an issue for the first tests of the optode since these deployments occurred in the warmer month of July, where the water becomes subzero at a depth of ≈ 110 m. However, the Validation deployment occurred in October wherein the waters in CBS became subzero at a depth of ≈ 60 m. The largest discrepancy between corrected optode data and the SBE43 data occurs below 60 m of depth (Figure 4.18) - corresponding to the

Comparison (vs. Ship)	RMSE	Correlation Coefficient
Raw Slocum Upcast	100.62	0.050
Raw Slocum Downcast	36.87	0.034
Mean of Raw Slocum	59.31	0.044
Corrected Glider Upcast	18.97	0.852
Corrected Glider Downcast	18.25	0.935
Mean of Corrected Data with added Bias	13.91	0.963
Corrected Slocum w/ Calibration	≈ 1.0	≈ 0.99

Table 4.4: Comparison of Raw and Corrected Glider Data to Ship-Based Data.

depth at which the temperature of the water becomes subzero.

The corrected sensing foil calibration coefficients determined by fitting our corrected data to the SBE43 data give good results. Both Slocum downcast and upcast now align with each other, and are in good agreement with SBE43 data (Table 4.4).

Uchida *et al.* [29] outline a procedure for the re-calibration of the Aanderaa oxygen optode using extensive field trials at sea [29]. The methods we have developed and outlined here are quicker and more cost-effective to implement and are able to account for 99% of the variance in our data when compared to other independent instruments. In the future, however, it may prove necessary to recalibrate the optode to a lower temperature range.

Chapter 5

Analysis of Attitude Sensor and GPS

5.1 Introduction

Ocean currents flow for thousands of kilometers and play an important role in determining the Earth's climate. These currents are important in the dispersal of many life forms, for example, strongly influencing the recruitment of both pelagic and ground-fish resources in Atlantic Canada [30]. With growing evidence of climate change, it is becoming increasingly important to measure how major ocean currents such as the Labrador current (found off of the coast of Newfoundland and Labrador) may be affected.

For these reasons, we are attempting to determine how well the Slocum glider performs in measuring depth-averaged and surface currents, how the glider responds to wind forcing, and examining the accuracy of its onboard Attitude sensor.

5.2 Estimation of Depth-Averaged Currents

While underwater, the Slocum navigates by measuring its vertical motion through the water column, its pitch, and its heading. The vertical speed adjusted by the tangent of the pitch angle gives a horizontal speed (relative to the water), while the heading from the compass gives a direction; this navigation is referred to as 'dead-reckoning'.

The glider dead-reckons its position relative to the water (Figure 5.1). While surfaced, the glider receives a precise location from its GPS. Assuming that the dead-reckoning and GPS are perfect, any errors between the GPS fix and the final dead-reckoned position must be due to water currents while the glider is underwater - these currents are herein referred to as the depth-averaged currents.

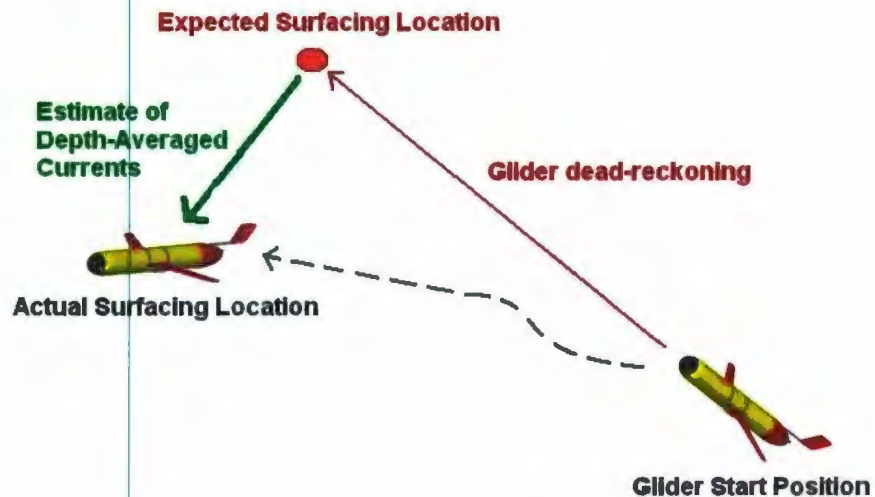


Figure 5.1: A simplified version of dead-reckoning done by the Slocum.

A detailed explanation of how the internal calculations of depth-averaged currents are done can be found in the glider documentation produced by Webb Research [3].

Depth-Averaged currents as recorded by the Slocum for the Operational test in

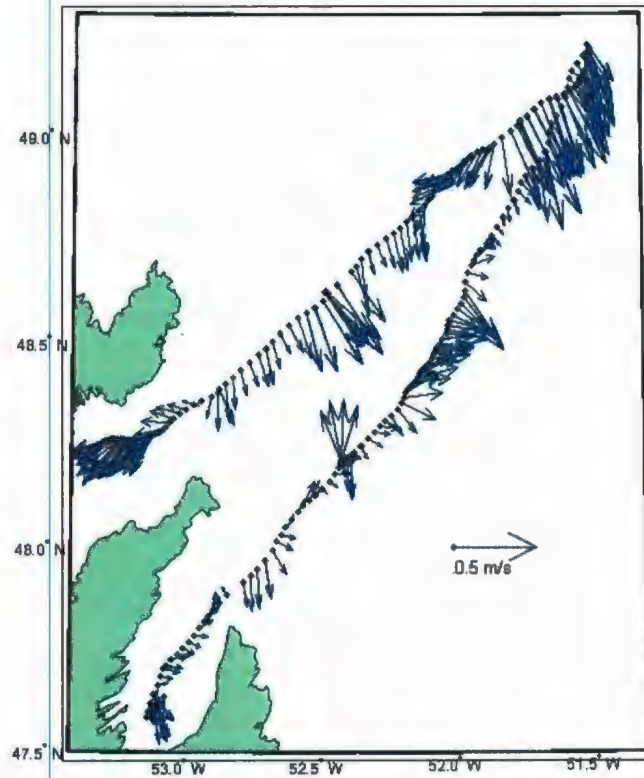


Figure 5.2: Depth-averaged currents recorded by the Slocum for the Operational Test. Data obtained from Glider unit: 49, Julian Days: 205-226, 2006. Velocities range from 0 cm/s to 30 cm/s; the later of which are found near the edge of the continental shelf, due predominantly to the Labrador current.

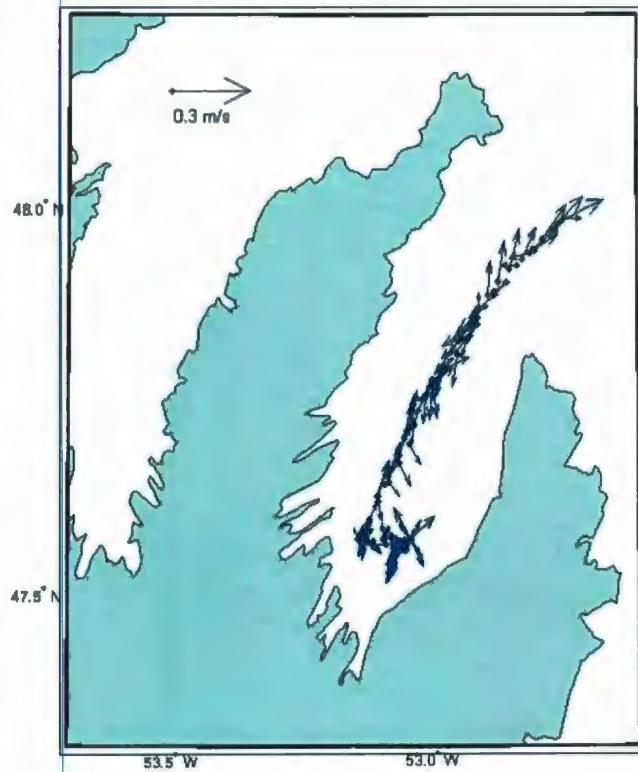


Figure 5.3: Depth-averaged currents recorded by the Slocum for the optode Test obtained from Glider unit: 48, Julian Days: 267-275, 2006. Velocities range from 0cm/s to 20cm/s, and are smaller than those recorded on the Operational test - due to shelter of the bay.

Velocity (m/s)	Min	Max	Mean
$ U $	0	0.325	0.120
$ V $	0	0.371	0.114
$\sqrt{U^2 + V^2}$	0.002	0.3947	0.180

Table 5.1: Depth-Averaged Ocean Currents - Operational Test. Data obtained from Glider unit: 49, Julian Days: 205-226, 2006.

Velocity (m/s)	Min	Max	Mean
$ U $	0.002	0.164	0.044
$ V $	0	0.110	0.049
$\sqrt{U^2 + V^2}$	0.017	0.174	0.072

Table 5.2: Depth-Averaged Ocean Currents - Optode Test. Data obtained from Glider unit: 48, Julian Days: 267-275, 2006.

Trinity bay range from 0 m/s (in the shelter of Trinity Bay) to a maximum of 0.40 m/s (approaching the inner branch of Labrador current), while the mean currents experienced over the entire deployment are approximately 0.18 m/s (Figure 5.2 and Table 5.1). Depth-Averaged currents recorded for the optode test in CBS are smaller in magnitude, ranging from 0 m/s to a maximum of nearly 0.20 m/s (just outside the mouth of CBS); the mean currents experienced over the entire deployment are approximately 0.07 m/s (Figure 5.3 and Table 5.2).

5.3 Estimation of Surface Currents

When the glider surfaces at pre-determined intervals to transmit data, it may be sitting at the surface for a period of 6-10 minutes, during which a series of GPS fixes are taken. Knowing the change in longitude and latitude, and the time over which the drift occurs, we are able to calculate the eastward and northward components of the surface water velocity, U and V , respectively.

Using the formulae:

$$U = \frac{\Delta x}{\Delta t} = \frac{\text{change in longitude (in meters)}}{\text{time at the surface}} \quad (5.1)$$

and

$$V = \frac{\Delta y}{\Delta t} = \frac{\text{change in latitude (in meters)}}{\text{time at the surface}} \quad (5.2)$$

Conversion of the longitude and latitude into meters was done using the standardized method [31].

An example of calculated surface currents from our first two deployments (Figure 2.1 for deployment areas) can be seen in figures 5.4 and 5.5 respectively.

Surface currents calculated for the Operational test in Trinity bay range from 0 m/s (in the shelter of Trinity Bay), to a maximum of nearly 1 m/s (approaching the edge of the continental shelf), while the mean currents experienced over the entire deployment are approximately 0.22 m/s (Table 5.3). Surface currents calculated for the optode test in CBS are smaller in magnitude, ranging from 0 m/s, to a maximum of nearly 0.30 m/s (just outside the mouth of CBS), while the mean currents experienced over the entire deployment are approximately 0.09 m/s (Table 5.4). These very low currents in CBS make it an ideal location for testing of the Slocum gliders

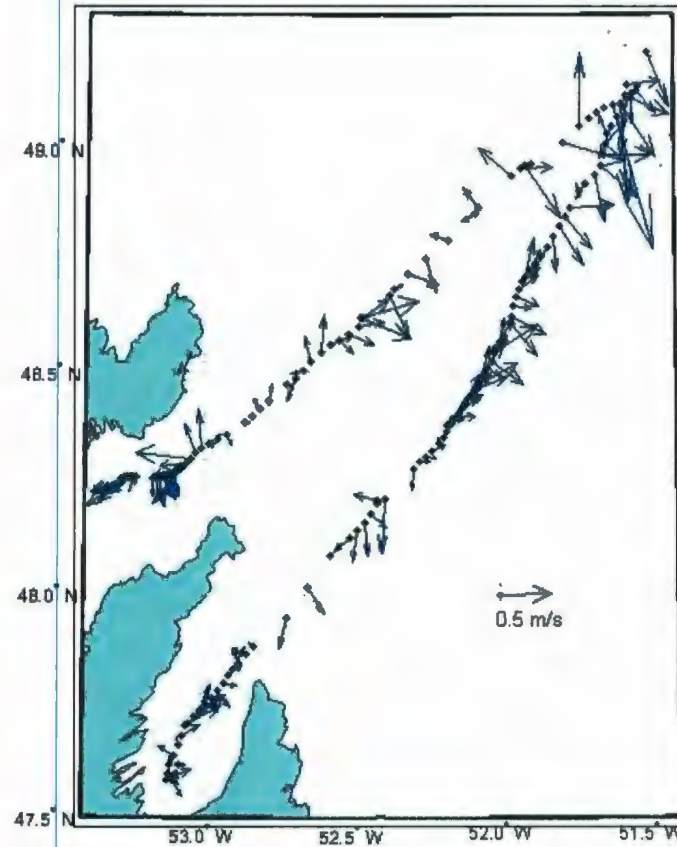


Figure 5.4: Surface currents recorded during the Operational test are twice as large as depth-averaged currents. Data obtained from Glider unit: 49, Julian Days: 205-226, 2006. The largest of these currents (1 m/s) are occurring at the edge of the continental shelf.

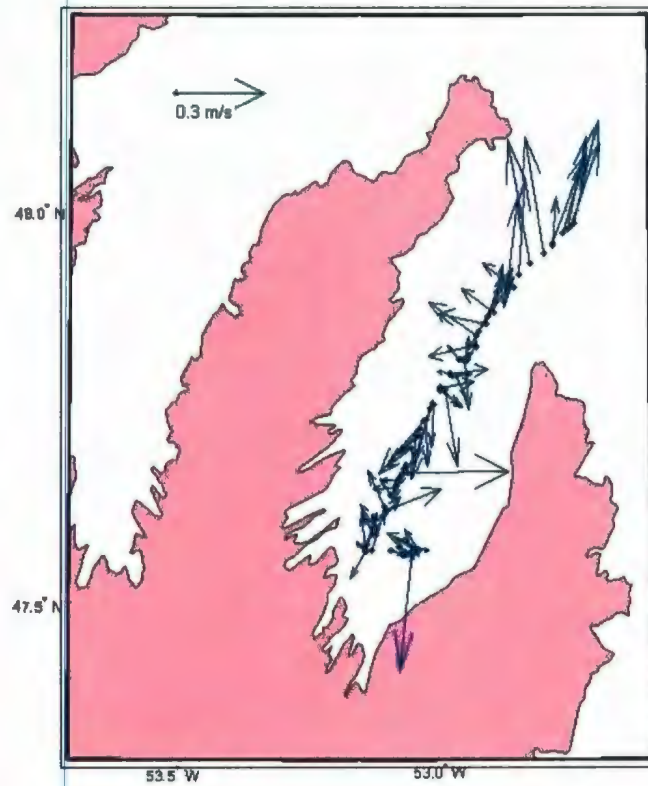


Figure 5.5: Surface currents recorded during the optode test are comparative to the depth-averaged currents, and are primarily tidal in origin. Data obtained from Glider unit: 48, Julian Days: 267-275, 2006. Currents range from 0 to 30 cm/s.

Velocity (m/s)	Min	Max	Mean
U	0.001	0.7264	0.151
V	0.002	0.744	0.135
$\sqrt{U^2 + V^2}$	0.034	0.807	0.224

Table 5.3: Surface Ocean Currents - Operational Test. Data obtained from Glider unit: 49, Julian Days: 205-226, 2006.

Velocity (m/s)	Min	Max	Mean
U	0	0.267	0.054
V	0	0.229	0.063
$\sqrt{U^2 + V^2}$	0	0.267	0.095

Table 5.4: Surface Ocean Currents - Optode Test. Data obtained from Glider unit: 48, Julian Days: 267-275, 2006

as it allows for easy deployment, and the glider does not expend extra energy fighting against strong currents.

5.3.1 Error Analysis

Using standard error analysis techniques, we can calculate the error associated with our U and V velocities - the only uncertainty in these calculations comes directly from uncertainty in the measurements of latitude and longitude. Using the following formula to calculate for V :

$$V = \frac{\Delta x}{\Delta t} = \frac{\text{latitude}_{final} - \text{latitude}_{initial}}{t_{final} - t_{initial}} \quad (5.3)$$

the associated error in V is given by:

$$\frac{\delta V}{V} = \frac{\delta(\Delta latitude)}{\Delta latitude} + \frac{\delta(\Delta t)}{\Delta t} \quad (5.4)$$

however, $\delta(\Delta t)$ approaches 0 and $\delta(\Delta latitude) = \delta(latitude_{final}) + \delta(latitude_{initial})$

therefore our final estimate of the error is given by:

$$\delta V = \frac{\delta(latitude_{final}) + \delta(latitude_{initial})}{\Delta latitude} V \quad (5.5)$$

Slocum documentation [3] specifies the error in a longitude/latitude GPS fix as ± 3 m. Using this error, if the Slocum drifts 200m in a northward direction over a time interval of 11 minutes, it's speed V will equal (0.300 ± 0.009) m/s. This error is quite small at 3 % of the velocity, and indicates the Slocum may give fairly accurate drift information. The error in U can be calculated in the same way by replacing latitude with longitude. The errors in velocity from the Operational deployment are approximately equal in both the U and V directions at ± 0.01 m/s (Figure 5.6). The question now becomes, does the Slocum's measured drift correlate to the surface currents, or to the wind direction?

5.4 Slocum Gliders and Wind

Estimates of surface current based on the gliders drift assume that it is primarily driven by the surface current, and not because of the wind - even though the two are related. Since the Slocum's tail sticks out of the water while transmitting data, it is possible that the rudder may catch the wind, thus rotating the vehicle in due course.

By examining the heading information during different surfacing events, we hope to reveal details of how quickly the glider rights itself with respect to the direction of the wind, if at all. Furthermore, if after the glider rights itself, does it drift with the current, or does the wind still play a role?

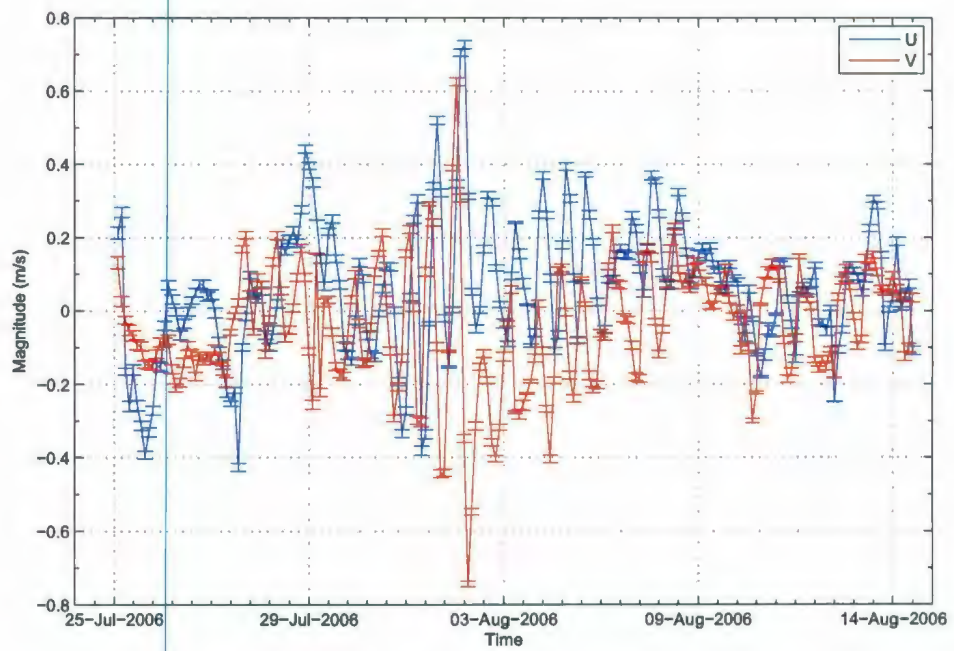


Figure 5.6: Time series of U (blue) and V (red) velocities from Operational deployment with error bars. Data obtained from Glider unit: 49, Julian Days: 205-226, 2006.

Visual inspection of the glider at the surface during various deployments makes one believe that the glider does right itself with respect to wind direction within minutes of reaching the surface. However, these deployments were specifically carried out on days of light wind, so our experiences may not tell the entire story - we have yet to visually inspect a surfacing event of a Slocum in rough weather.

5.4.1 Heading Information from the Attitude Sensor

During the Operational test, 781,061 individual sampling points were recorded. Of this total, only 6101 of these points occurred at the surface of the ocean. Of these surface points, only 1637 contain valid measurements for heading from the Attitude sensor. Bad data points are identified by searching for all 'NaN' and removing them. Thus, only 27% of the surfacing data has valid heading information.

As well, 250,626 individual sampling points were recorded in total during the optode test. Of this total amount, only 2950 of these points occurred at the surface of the ocean. Of these surface points, only 1637 contain valid measurements for heading from the Attitude sensor. Here, only 32% of the surfacing data contain valid heading information. The reason for so few heading data is due to the fact that the once surfaced, the attitude sensor takes several minutes to come online, and then promptly goes offline several minutes before diving.

The following analysis was carried out on the Operational data set but can be considered representative of all our data sets collected to date.

A typical surfacing event consists of 70 data points, and lasts approximately 6-10 minutes (Figure 5.7). Keeping in mind that we only have valid heading data $\approx 30\%$ of the time, we can plot heading versus time during different surfacing events to learn what direction the glider is pointed, and if the wind (or sea-state) may be causing

it to rotate. Heading data from six randomly selected surfacing events (Figure 5.8) shows the characteristic patterns of heading associated with surfacing events. When comparing the last subplot to the first five, we see an example of a surfacing event where there are many gaps in the heading data, which is often the case. From these heading plots we see that the Attitude sensor may take up to two minutes to start recording data once the Slocum has surfaced, and that there is often a gap in heading information at the end of a surfacing event.

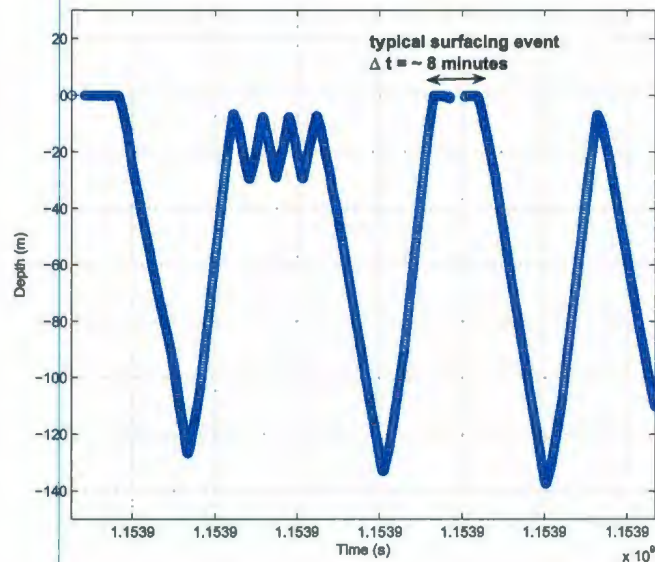


Figure 5.7: A typical surfacing event only lasts 6-10 minutes.

The heading information obtained from the Attitude sensor makes it nearly impossible to tell how quickly the glider rights itself with respect to wind direction. In fact, the data suggests that while at the surface the Slocum may wobble back and forth and change its heading by 20° to 40° - indicating that wind, or surface waves, may be playing more of a role than was first anticipated. However, not knowing the

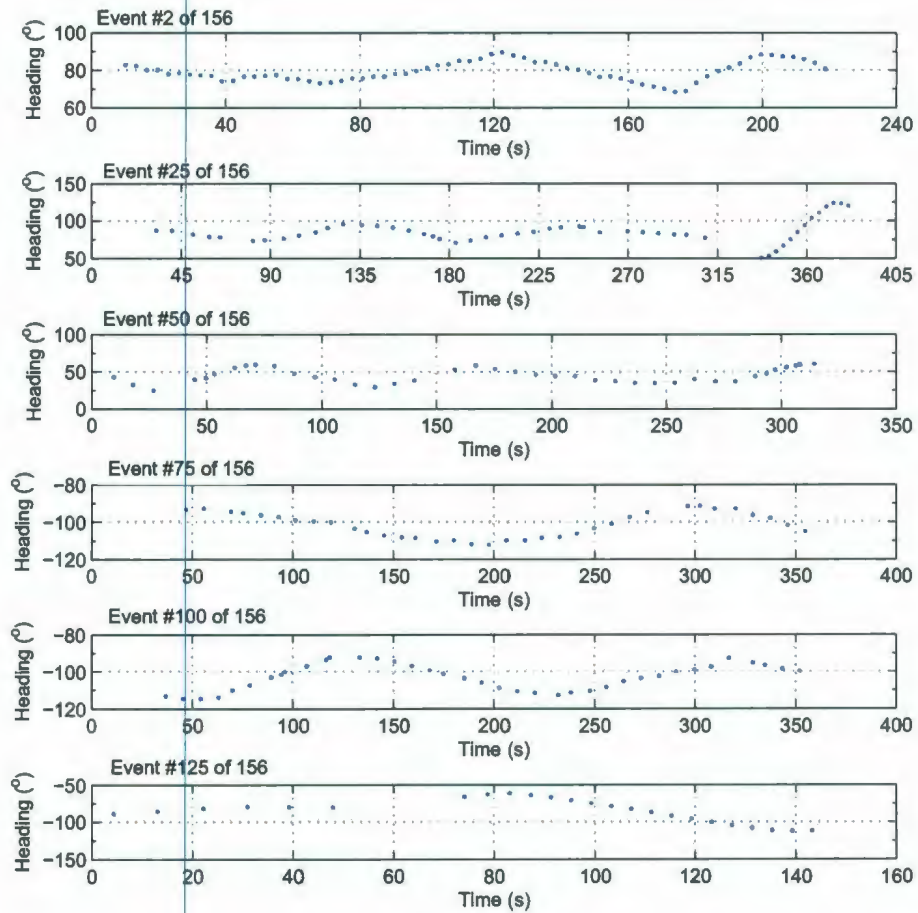


Figure 5.8: Six randomly selected surfacing events (out of a possible 156) ranging from the beginning of the Operational test to the end. Heading may change between 20° to 40° while at the surface. Data obtained from Glider unit: 49, Julian Days: 205-226, 2006.

sea-state at the time when the glider surfaced, this information is inconclusive and further testing must be done.

5.4.2 Testing the Slocum's Compass

After seeing evidence of a strong variation in heading while the Slocum is at the surface, an experiment was designed to test the validity of the Slocum's compass to ensure the heading data was reliable.

Using a hand held compass and starting at North, divisions were marked on the laboratory floor every 10° . The Slocum was manually rotated around in a circle and compass data was recorded at these 10° intervals (Figure 5.9). The recorded data does not show the large deviation that was expected; in actuality the Slocum compass, a Precision Navigation TCM2, shows a small non-linear offset of $\approx 5^\circ$ (Figure 5.10). This deviation should be accounted for when dealing with surface heading data in future deployments. While the test was conducted inside, several compass tests conducted there in the past suggests that the room is free of any interfering magnetic fields.

5.4.3 Comparison to Environment Canada Wind Data

For comparison purposes, wind velocity data was obtained from the *Environment Canada National Climate Data and Information Archive* [32]. These data were gathered from the St. John's Airport weather station (the Bonavista station data would be geographically closer to our Slocum data but was not available for the time period in question) for the days corresponding to our Operational test. Using this wind data we are able to compare it to our Slocum drift information to see if the two are related.

Two separate days worth of data selected from the Operational test are presented



Figure 5.9: An experiment was performed to test the Slocum compass on January 16th, 2008. The Slocum was placed on an aluminium (non-magnetic) table and was manually rotated around in a circle, stopping every 10° to record its heading.

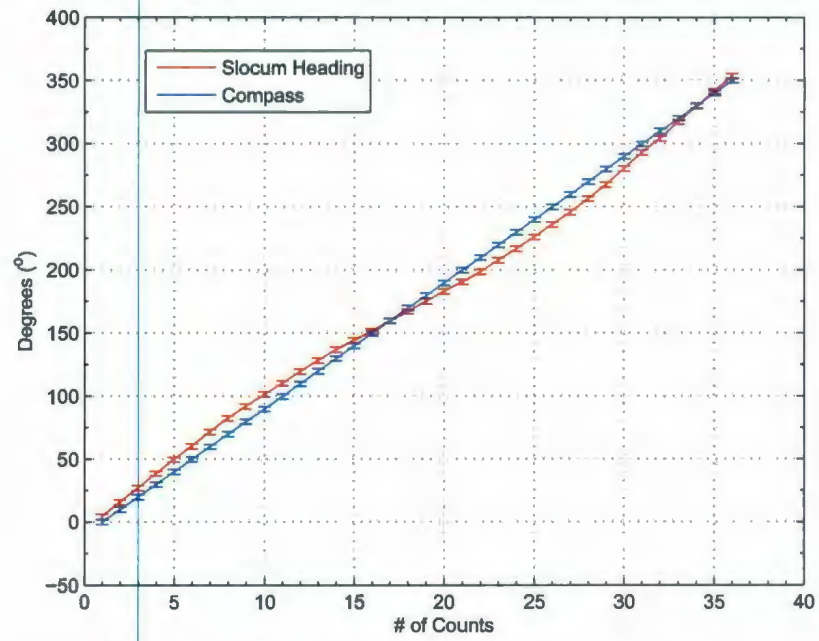


Figure 5.10: The results of the Slocum compass test show a small non-linear deviation of 5° from expected. This deviation should be accounted for in future deployments.

for comparison with the available wind data (Figure 5.11) - August 1st, 2006 (the glider was traveling across the shelf), and August 5th, 2006 (wherein the glider was nearest the inner branch of the Labrador current). According to the Environment Canada Climate Data (ECCD), on August 1st, the wind was blowing from the West at an average speed of 22 km/hr (6 m/s), while on August 5th the wind was blowing from the South at an average speed of 14 km/hr (3.89 m/s). A direct comparison of ECCD wind data, to the Slocum's heading, to the calculated surface drift on August 1st, and August 5th respectively reveal that on these days the Slocum was drifting in the opposite direction to that of the wind. These figures can be considered representative of the entire data set (Figures 5.12 and 5.13). When looking at an individual days worth of data, it can be seen that the Slocum sometimes points into the wind direction, but not always, due to varying sea-states at the time. We must examine data from the entire mission to determine if any relation indeed exists.

A series of scatter plots were created from all surfacing data available (over 100 separate surfacing events) from the Operational deployment in order to determine if there was indeed a relationship between the wind, the recorded Slocum heading, and the direction of its drift. A scatter plot of the mean heading of the Slocum while at the surface vs. the direction of its drift shows no apparent relationship (Figure 5.14). A scatter plot of the Slocum's surface drift vs. the direction from which the wind is blowing again shows no apparent relationship - suggesting the Slocum's drift may be more strongly influenced by the ocean currents rather than the wind (Figure 5.15). A final scatter plot showing the mean Slocum heading vs. the direction from which the wind is blowing gives strong evidence that the Slocum often acts like an anemometer (while at the surface), and faces into the direction from which the wind is blowing (Figure 5.16); the values not falling on the line of best fit are primarily due to issues with wrap-around.

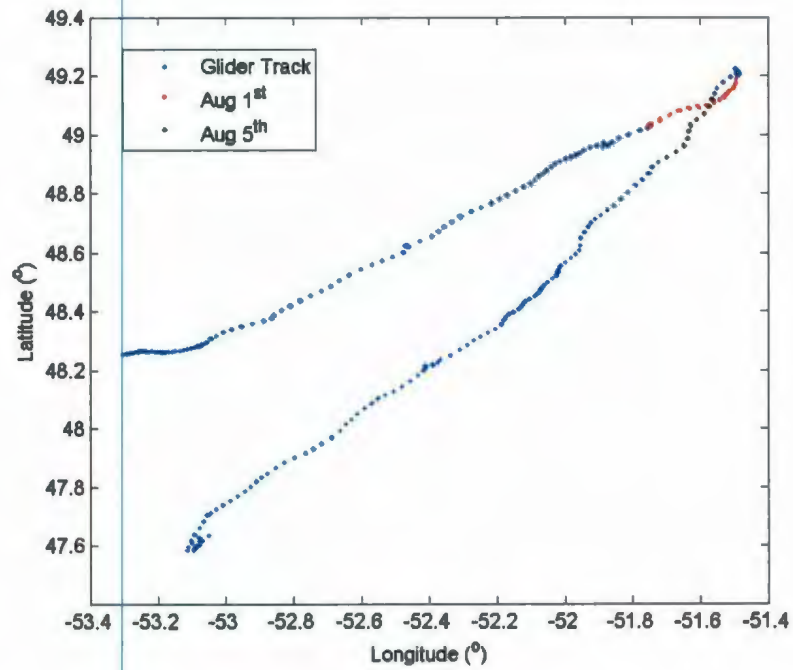


Figure 5.11: The location of the Slocum during the days tested against available wind data from Environment Canada. See figures 5.12, and 5.13.

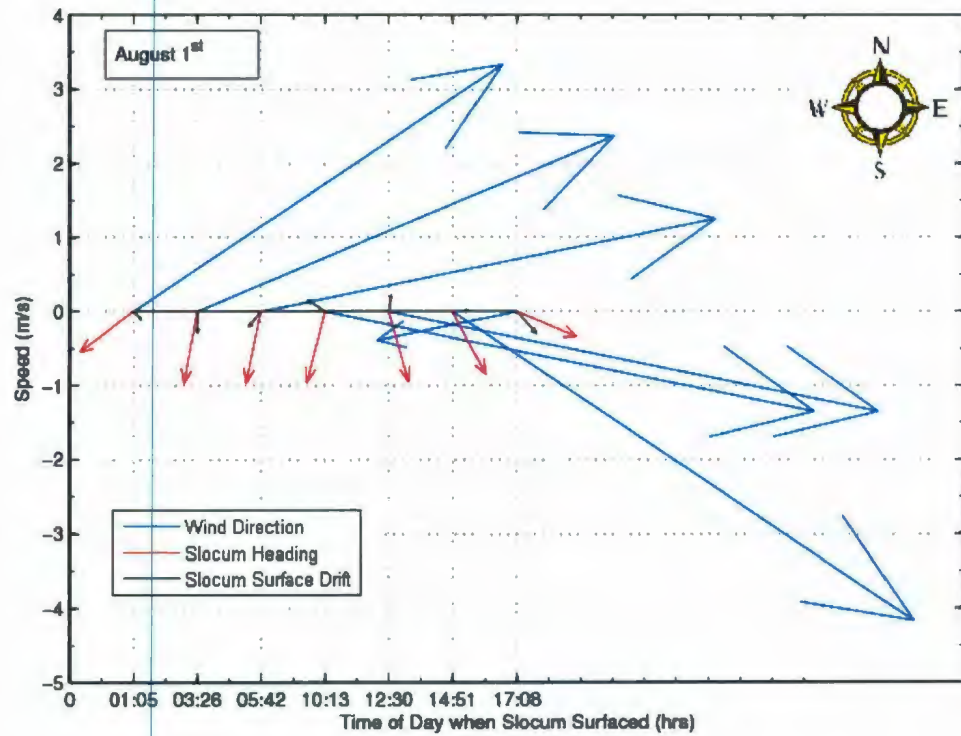


Figure 5.12: A comparison of surfacing data from Glider Unit: 49, Julian Day: 245, 2006. This time series compares wind speed and direction (blue) to the Slocum's mean heading during surfacing (red) to the surface drift of the Slocum (black). No relation between surface drift and the winds is prevalent.

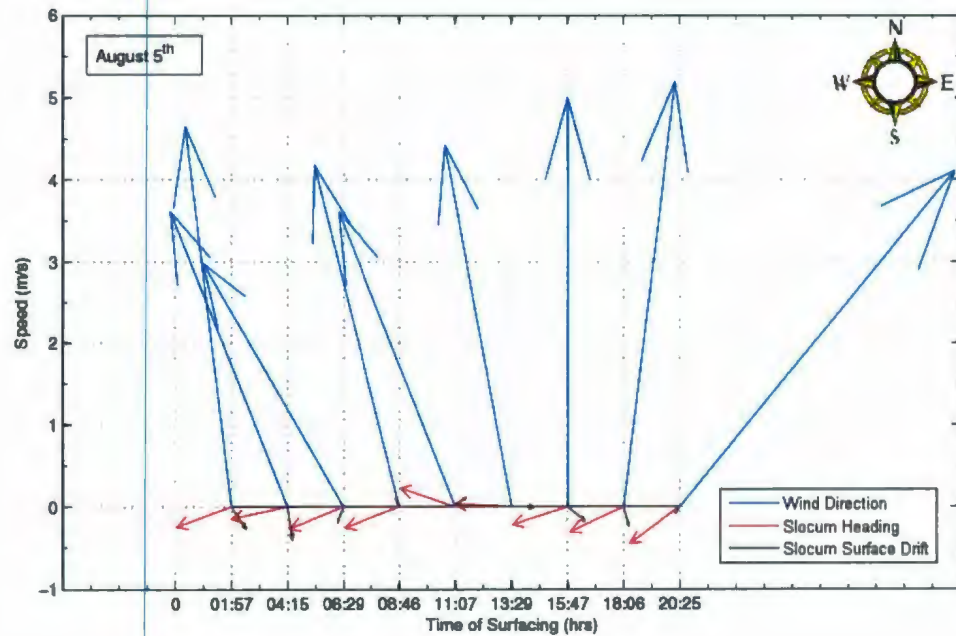


Figure 5.13: A comparison of surfacing data from Glider Unit: 49, Julian Day: 250, 2006. This time series compares wind speed and direction (blue) to the Slocum's mean heading during surfacing (red) to the surface drift of the Slocum (black). No relation between surface drift and the winds is prevalent.

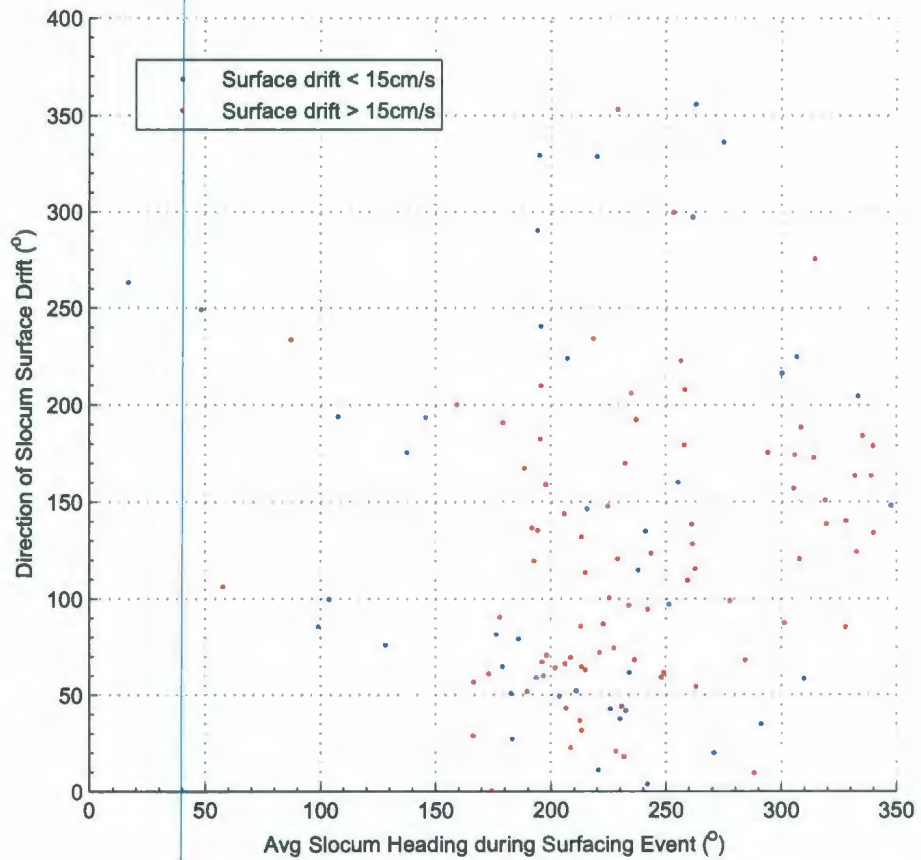


Figure 5.14: A scatter plot of all surfacing events in the month of August, 2006. Data obtained from Glider unit: 49, Julian Days: 205-226, 2006. There is no correlation between surface drift and the mean heading of the Slocum while at the surface for speeds greater, or less than, 15 cm/s.

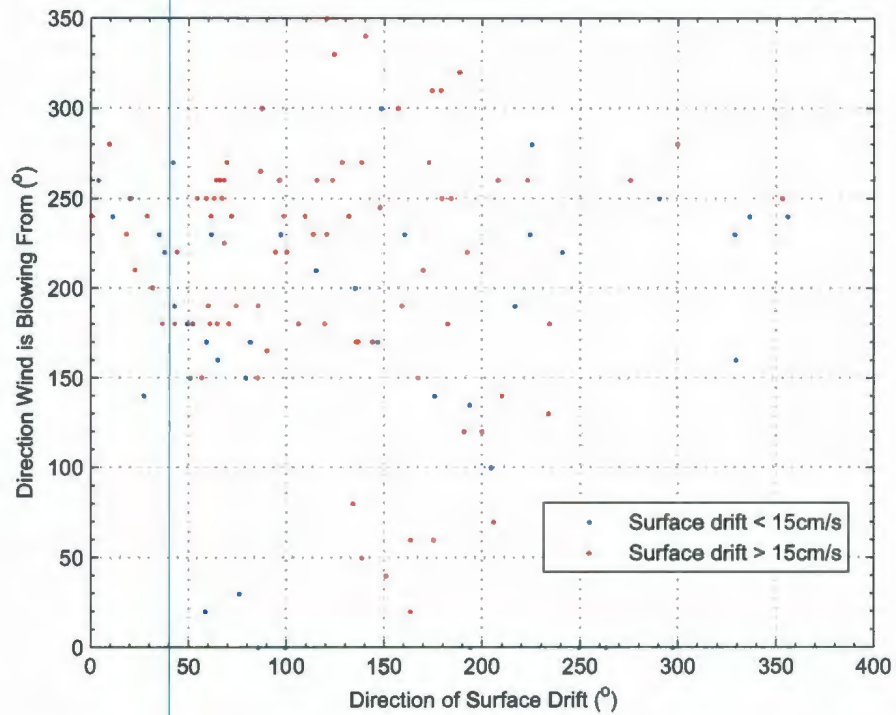


Figure 5.15: A scatter plot of all surfacing events in the month of August, 2006. Data obtained from Glider unit: 49, Julian Days: 205-226, 2006. There is no correlation between surface drift and the direction from which the wind is blowing for speeds greater, or less than, 15 cm/s.

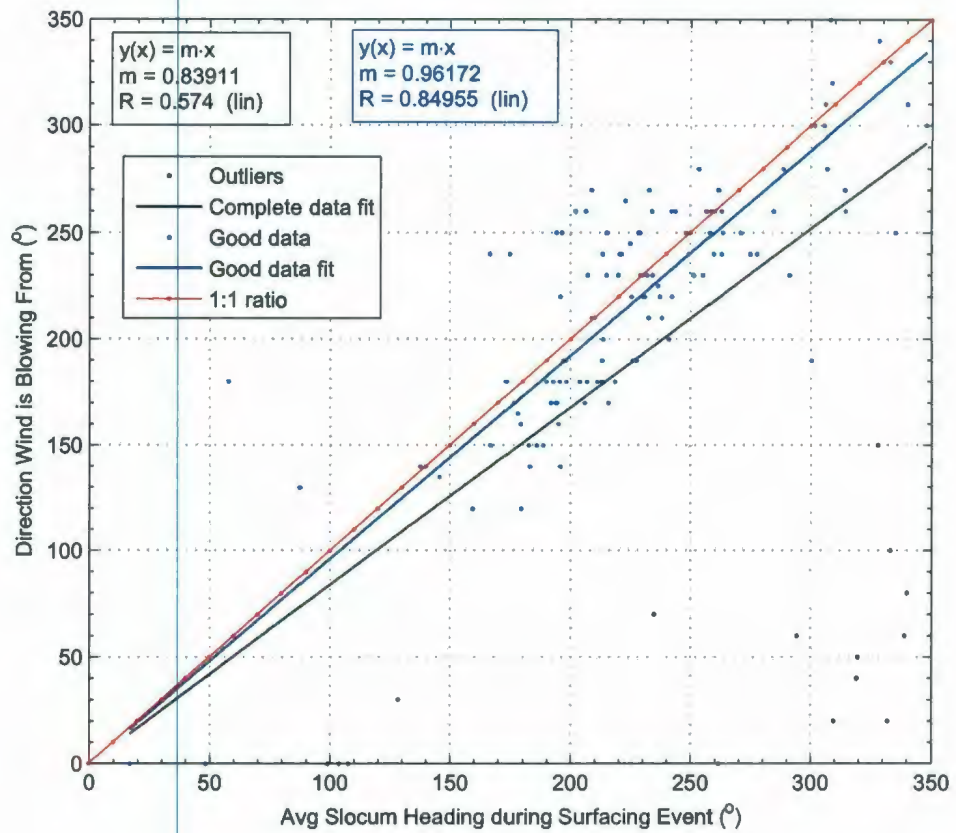


Figure 5.16: A scatter plot of all surfacing events in the month of August, 2006. Data obtained from Glider unit: 49, Julian Days: 205-226, 2006. This scatter plot shows that, while at the surface, the Slocum functions like an anemometer and faces into the wind. The black line shows a fit to all data points, while the blue line shows a fit with the outliers removed (black data points). For comparison a 1:1 ratio line is plotted in red.

5.5 Discussion

The scheme to measure the depth-averaged currents strongly depends on the accuracy of the dead-reckoning, as any error in the dead-reckoning (or the GPS) will cause an erroneous water current to be computed. Since the error in any one of our GPS position fixes may be as great as 3 m, the resulting depth-averaged and calculated surface currents may be off by as much as 3% (this is a small error and may be slightly underestimated).

The estimates of our depth-averaged currents calculated during the optode test correspond well with estimates given by deYoung and Sanderson [33], which state the flow outside the mouth of Conception Bay South as having a mean near-surface speed of roughly 20 cm/s. The depth-averaged currents calculated by the Slocum during the Operational test across the continental shelf vary from 10 to 30 cm/s, with the mean current to the Southeast in good agreement with other measurements of the inner branch of the Labrador Current given by Colbourne *et al.* [30].

Examination of the heading data provided from the Attitude sensor contradicts the hypothesis that the glider is not affected by the wind during surfacing events. In fact, the data shows that while there are some points where the glider drifts with a constant heading, the majority of surfacings show heading data which changes by as much as 40° (Figure 5.8). During consultations with the research engineers responsible for the construction of the Slocum glider at Webb Research, it was learned that the attitude sensor could be affected by RF noise inside the vehicle while at the surface - the sources of the RF noise come from the Iridium, the Argos transmitter, and also from the Freewave modem when it is being used (M. Palanza, research engineer, personal communications). It is due to this noise that the attitude sensor is often not recording while at the surface - thus leading to the gaps in heading data. This

erroneous heading data could be due to the RF interference, or it could be due to wind and wave action while at the surface - the question now becomes: is the Slocum affected by the wind/waves, or is this deviation in heading data a result of some sensor dynamics problem? Our laboratory test of the Slocum's compass suggests that there is only a small error of 5° , which may be attributed to RF interference, or more likely, iron structures causing interference in our testing area - meaning that the wobble of 40° while at the surface is most likely due to the wind and sea state at that time.

Furthermore, examination of the scatter plots of surface drift, mean heading, and wind direction (Figures 5.14, 5.15 and 5.16) give strong evidence that the Slocum indeed faces into the oncoming wind while at the surface, with the caveat that some outlying points in our analysis do not fit. Since the Slocum does point nose-into-wind, this adds to the repertoire of data available from the vehicle; we can now get estimates of wind direction at sea by taking $\approx 180^\circ \pm 20^\circ$ opposite of the Slocum's heading while surfaced [34]. The uncertainty of 20° is due to variations in the surface current acting on the Slocum's center of mass, which pushes the vehicle slightly to the side of the wind direction (Figure 5.17). Though the Slocum is pointed into the wind, a comparison of surface drift to the wind direction shows no relationship, indicating the Slocum's drift is predominantly forced by ocean currents. Future work on the attitude sensor may involve further analysis on how the Slocum vehicle aligns itself in varying wind/wave combinations.

Future work and analysis will need to be carried out on the Slocum's Attitude sensor, as well as a study on how strong winds and rough seas may affect the drift of the glider, and consequently, its estimate of surface currents. Also, we plan to incorporate a high grade orientation sensor with 3 magnetometer, 3 axis angular rates and linear accelerations for further investigation of surfacing behavior.

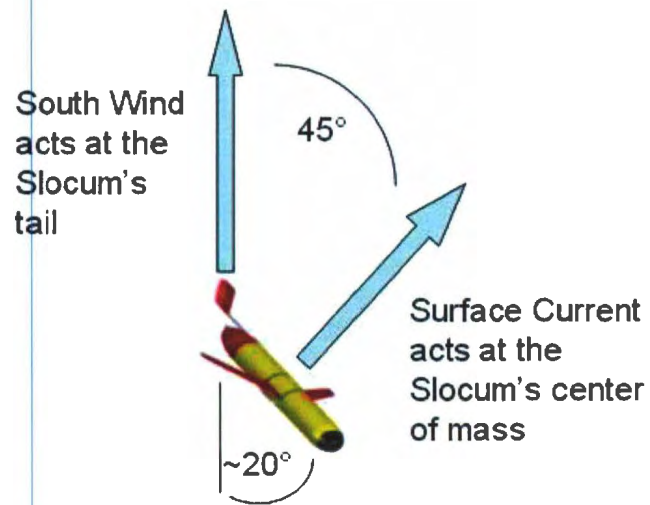


Figure 5.17: Wind acts at the Slocum's tail, causing it to act like a weather-vane and point into the oncoming wind direction, however, the induced surface current acts at 45° to the right of the wind. The currents act on the Slocum's center of mass and cause it to rotate slightly at $\approx 20^\circ$ to the side of the wind. Future work will be done in a wave tank to better understand these dynamical responses.

Chapter 6

Summary

There were three main goals of this project: 1) Analysis of the CTD sensor, 2) Analysis of the oxygen optode, 3) Analysis of the Attitude sensor accompanied by data from the GPS unit.

6.1 Summary of the CTD

The default non-pumped SBE CTD installed on the Slocum glider is affected by the same sensor dynamics issues that seem to affect all CTDs: sensor response problems and thermal-lag issues - the later leading to the majority of our erroneous data. An offset exists between the downcast and upcast in the raw salinity data recorded of up to 0.7 psu; while application of our correction algorithms seem to remove up to half of this error, it does not fully correct the data set.

This calls into question if the application of standard correction techniques for thermal-lag developed by Lueck and Picklo [17], and Morison *et al.* [16] can be used on data recorded by the Slocum glider. As the glider is ballasted and trimmed before every deployment, this will ultimately affect its vertical speed through the

water column; since the determination of the parameters α and τ (Section 3.4.2) for our thermal-lag corrections depend on this vertical speed, we cannot use the same parameters for every data set. Therefore, the data retrieved from each deployment must be dealt with separately, and mission specific values for α and τ should be calculated.

6.1.1 Future Work and Recommendations

The methods described in the previous chapters were based solely on post-calibration of data using correction algorithms. However, perhaps a simpler way to solve these problems would be with better designed hardware. Researchers at the Woods Hole Oceanographic Institute have developed a new fast responding CTD specifically for use on autonomous underwater vehicles [35]. It uses a four-electrode conductivity cell with an internal temperature sensor to achieve excellent dynamic response and high spatial resolution. The design has low drag and is resistant to fouling, is non-pumped and reportedly free of thermal drifts. Results of a comparison with an un-pumped Seabird SBE41CP CTD (the version used on our Slocum) on a glider show superior performance in all temperature gradient situations [35].

The acquisition and installation of such a fast responding CTD would increase the accuracy of data provided by Slocums and eliminate the need of post-correction algorithms. However, the associated cost prohibits wide deployment of these new sensors and thus our sensor corrections will be used in future deployments.

6.2 Summary of the Optode

The Aanderaa oxygen optode 3835 installed on the Slocum glider provides much faster sampling than more traditional oxygen sensors, however, the response time is

still a major issue. The raw data received from the optode cannot be used, as the downcast and upcast are completely different, both of which are considerably offset when compared to other independent instruments (see Chapter 4). Post-processing of this data must be done to account for the sensor response issue.

There is a trade-off to consider when correcting optode data. The slow profiling speed of the Slocum allows for easier correction of the sensor response problem, however, the slow profiling speed increases the issues of thermal-lag inside the conductivity cell.

It appears that the developed correction algorithms correct the offset between downcast and upcast, and also bring the Slocum data into alignment with other independently sampled data - though an offset still exists whenever the optode encounters water with subzero temperatures. This offset is then eliminated using the new calibration coefficients and brings both the downcast and upcast of the Slocum into alignment with the independently sampled data.

6.2.1 Future Work and Recommendations

The first step in working with the optode data was to back-calculate the originally measured phase data, using concentration units and temperature. This step (and the error associated with it) could be eliminated if the Slocum was reprogrammed to record only phase units and temperature, instead of calculating DO_2 concentrations internally. Doing this would allow us to combine temperature values measured by the external CTD to the phase units recorded to obtain a more accurate estimate of oxygen concentration.

A re-calibration of the optode should be considered before any future DO_2 data is collected. Factory calibration of the oxygen optode is done from a minimum of 0 °C.

However, in our sampling areas the water frequently becomes subzero in temperature at depths greater than 50 m. Since the Slocum samples to a maximum depth of 200 m, the majority of the optode data is recorded in waters which are subzero in temperature - leading to anomalous readings. A re-calibration of the optode can be carried out using an adapted version of the process outlined in the optode manual [26], using control water samples with temperatures below 0 °C.

To increase the accuracy of the data obtained, it may also be worthwhile to increase the sampling interval on the Slocum from one measurement every four seconds, to one measurement every two seconds - thus giving more detail in areas with strong gradients.

6.3 Summary of the Attitude/GPS

Examination of the compass data recorded by the Attitude sensor, along with position information recorded by the GPS allows for a good estimation of surface currents. Comparison of the Slocum's drift at the surface to available wind data suggests the Slocum acts like an anemometer by pointing into the direction of the oncoming wind; however, the drift at the surface is not correlated with wind direction. This gives credit to the hypothesis that the Slocum may be used as a current meter whenever it has surfaced to transmit data.

6.3.1 Future Work and Recommendations

Laboratory test of the Slocum's compass data lead to the discovery of a non-linear 5° offset between measured and accepted heading data. A re-calibration of the Slocum compass should be carried out as described in the Slocum documentation [3] to see if this error can be eliminated. Also, recommendations from this experiment are to

develop a degaussing procedure for the battery packs installed on the Slocum, as the magnetic fields built up in these batteries could significantly alter heading data. However, it should be noted that new versions of the Slocum glider come equipped with a better compass that allows for soft and hard iron calibration. Further testing of the Slocum's compass should occur outside, free of large iron objects which may affect the results.

Another worthwhile experiment for the Slocum would be to compare the calculated surface drift against an independent instrument such as a current meter. Having the Slocum sample around a moored current meter over several days, experiencing varying wind conditions, would allow us to better estimate the error in our surface drift data.

6.4 Implications Of This Project

The various sensor dynamics issues which influence the Slocum glider significantly affect its ability to record meaningful data. However, the application of correction algorithms developed, while not fully eliminating these errors, does help to minimize anomalies in the data.

The Slocum glider, at the forefront of new ocean technology, has proven to be an effective instrument for gathering data over the Newfoundland shelf. There exists great potential for the addition of new sensors to the vehicle only continuing to better our understanding of the world's oceans.

Bibliography

- [1] Daniel L. Rudnick, Russ E. Davis, Charles C. Eriksen, David M. Fratantoni, and Mary Jane Perry. Underwater gliders for ocean research. *Marine Technology Society Journal*. 38(1):48–59, 2004.
- [2] Ralf Bachmayer, Brad de Young, Chris Williams, Charlie Bishop, Christian Knapp, and Jack Foley. Development and deployment of ocean gliders on the newfoundland shelf. In *Proceedings of Underwater Vehicle Symposium*. 2006 (IN PRESS).
- [3] Webb Research Corp. Slocum shallow battery glider operations manual. East Falmouth, Massachusetts, USA, 2005.
- [4] William J. Emery and Richard E. Thomson. *Data Analysis Methods in Physical Oceanography*. Elsevier, 2004.
- [5] Gregory C. Johnson, John M. Toole, and Nordeen G. Larson. Sensor Corrections for Sea-Bird SBE-41CP and SBE-41 CTDs. *Journal of Atmospheric and Oceanic Technology*, 24:1117–1130, June 2007.
- [6] Farhad M. Fozdar, Geoffrey J. Parker, and Jrg Imberger. Matching temperature and conductivity sensor response characteristics. *Journal of Physical Oceanography*. 15(11):15571569, 1985.

- [7] David R. Topham and Ronald G. Perkin. Ctd sensor characteristics and their matching for salinity calculations. *IEEE Journal of Oceanic Engineering*, 13(3):107–117, 1988.
- [8] E.P. Horne and J.M. Toole. Sensor response mismatches and lag correction techniques for temperature-salinity profilers. *Journal of Physical Oceanography*, 10:1122–1130, 1980.
- [9] Raymond W. Schmitt, Robert C. Millard, John M. Toole, and W. David Wellwood. A double-diffusive interface tank for dynamic-response studies. *Journal of Marine Research*, 63:263–289, 2005.
- [10] J. Kerfoot, S. Glenn, J. Kohut, O. Schofield, and J.H. Roarty. Correction for thermal lag effects in non-pumped temperature-conductivity sensors on the slocum coastal electric glider. In *Ocean Sci. Meet. Suppl.*, volume 87. Eos Trans. AGU, 2006.
- [11] Robert Stewart. *Introduction to Physical Oceanography*, chapter 1-6, pages 1–103. Texas A&M University, 2003.
- [12] SCOR Working Group 51. Algorithms for computation of fundamental properties of seawater. *Unesco Technical Papers in Marine Science*, (44), 1983.
- [13] SCOR Working Group 51. The acquisition, calibration, analysis of CTD data. *Unesco Technical Papers in Marine Science*, (54), 1988.
- [14] N.P. Fofonoff, S.P. Hayes, and R.C. Millard. Whoi/brown ctd microprofiler: methods of calibration and data handling. Technical Report 64pp, Woods Hole Oceanographic Institution Tech.Rep., 1974.

- [15] Jean-Michel Pinot, Joaquin Tintore Pedro Velez, and Jose Luis Lopez-Jurado. The thermal-lag effect in SBE-25 CTDs: Importance of correcting data collected in the Mediterranean summer thermocline. *Scientia Marina*, 61(2):221–225, 1997.
- [16] J. Morison, R. Andersen, N. Larson, E. D'Asaro, and T. Boyd. The Correction for thermal-lag effects in Sea-Bird CTD data. *Journal of Atmospheric and Oceanic Technology*, 11:1151–1164, 1994.
- [17] Rolf G. Lueck and James J. Picklo. Thermal Inertia of Conductivity Cells: Observations with a Sea-Bird Cell. *Journal of Atmospheric and Oceanic Technology*, 7:756–768, 1990.
- [18] Chris Williams, Ralf Bachmayer, and Brad deYoung. Toward improved predictions of the performance of ocean gliders. In *Proceedings of 8th Canadian Marine Hydromechanics and Structures Conference*, October 2007 (IN PRESS).
- [19] F. Page, H. Losier, R. McCurdy, P. Greenberg, and JB. D. Chaffey. Dissolved oxygen and salmon cage culture in the southwest brunswick portion of the bay of fundy. *Handbook of Environmental Chemsitry*, 5:1–28, 2005.
- [20] Arne Körtzinger, Jens Schimanski, Uwe Send, and Douglas Wallace. The ocean takes a deep breath. *Science*, 306:1337, November 2004.
- [21] Arne Körtzinger and Jens Schimanski. High quality oxygen measurements from profiling floats: A promising new technique. *Journal of Atmospheric and Oceanic Technology*, 22:302–308, March 2005.
- [22] L.W. Winkler. Die bestimmung des in wasser gelosten sauerstoffes. *Berichte der Deutschen Chemischen Gesellschaft*, 21:2842–2855, 1888.

- [23] A. Tengberg, J. Hovdenes, H.J. Andersson, O. Brocandel, R. Diaz, D. Hebert, T. Arnerich, C. Huber, A. Kortzinger, A. Khripounoff, F. Rey, C. Ronning, J. Schimanski, S. Sommer, and A. Stangelmayer. Evaluation of a lifetime-based optode to measure oxygen in aquatic systems. *Limnology and Oceanography: Methods*, 4:7-17, February 2006.
- [24] L.C. Clark, R. Wolf, D. Grandger, and Z. Taylor. Continuous recording of blood oxygen tensions by polarography. *Journal of Applied Physiology*, 6:186-193, 1953.
- [25] M. A. Berntsson, P. O. J. Tengberg, and M. Josefsson. Multivariate experimental methodology applied to the calibration of a clark type oxygen sensor. *Anal. Chim. Acta*, 355:43-53, 1997.
- [26] Aanderra Data Instruments. *TD 218 OPERATING MANUAL - Oxygen Optodes*, November 2005.
- [27] I. Klimant, C. Huber, G. Liebsch, G. Neurauter, A. Stangelmayer, and O.S. Wolfbeis. Dual lifetime referencing (DLR): a new scheme for converting fluorescence intensity into a frequency-domain or time-domain information. *Flourescence Spectroscopy: New Methods and Applications.*, 2000.
- [28] Bla G. Liptk. *Process Measurement and Analysis*. Instrument Engineers' Handbook. CRC Press, 4th edition, 2003.
- [29] Hiroshi Uchida, Takeshi Kawano, Ikuo Kaneko, and Masao Fukasawa. In-situ calibration of optode-based oxygen sensors. *Journal of Atmospheric and Oceanic Technology*, December 2007 (IN PRESS).

- [30] E. Colbourne, B. deYoung, S. Narayanan, and J. Helbig. Hydrography and circulation on the newfoundland shelf. *Canadian Journal of Fisheries and Aquatic Sciences*, 54:149–157, 1997.
- [31] Nathaniel Bowditch. *American Practical Navigator*, volume II. Defense Mapping Agency, 1975.
- [32] Environment Canada. National climate data and information archive. *http : //www.climate.weatheroffice.ec.gc.ca/climateData/canada_e.html*, 2007.
- [33] B. deYoung and B. Sanderson. The circulation and hydrography of conception bay, newfoundland. *Atmospheric-Ocean*, 33(1):135–162, 1994.
- [34] E. Creed, J. Kerfoot, C. Mudgal, S. Glenn, and O. Schofield. Automated control of a fleet of slocum gliders within an operational coastal observatory. In *Proceedings of OCEANS'03 MTS/IEEE*, September 22-26 2003.
- [35] Raymond W. Schmitt and Robert A. Petitt. A fast response, stable CTD for gliders and AUVs. In *Proceedings of Oceans'06 mts/ieee*, September 18-21 2006.

A.1 Distance Calculator and Contouring

```
1 %% this script is for finding the horizontal distance for contouring purposes. you must have a DBD file loaded,
2 %% or an entire data set, with the variable named "data"
3
4 %% this script requires: ddm2ddd.m (for lat lon conversion)
5 %%           mll2dist.m (from m.map package)
6
7
8 %create a subset of the data file, easier to work with:
9 subdata=data(:,[m_present_time m_water_temp m_water_cond m_water_pressure m_depth m_lon m_lat sci_oxy3835_saturation]);
10
11 [r c]=find(isnan(subdata)); %get rid of any NaN's we may have
12 subdata(r,:)=[];
13
14
15
16 %this is changed depending on the data we have loaded, sometimes there are erroneous measurements at
17 %the beginning or end of the file, so we drop them accordingly:
18 subdata=subdata(1:end-1,:);
19
20
21 [lat, lon] = ddm2ddd(subdata(:,6),subdata(:,7)); %this converts Lat/lon to proper formatting.
22
23 %%%%%%%%%%%%%%%%%%%%%%%%%%%%%%%%%%%%%%%%%%%%%%%%%%%%%%%%%%%%%%%%%%%%%%%%% This section calculates the distance for the
24 %%%%%%%%%%%%%%%%%%%%%%%%%%%%%%%%%%%%%%%%%%%%%%%%%%%%%%%%%%%%%%%%%%%%%%%%% contouring. We use m_lat, and m_lon because the LMC
25 %%%%%%%%%%%%%%%%%%%%%%%%%%%%%%%%%%%%%%%%%%%%%%%%%%%%%%%%%%%%%%%%%%%%%%%%% system the glider uses has errors.
26
27 range=[0]; %initialize:
28 ΔDist=[0];
29
30 h = waitbar(0,'Please wait...'); %initialize waitbar
31 for x=2:length(lon)
32     LON=[lon(x-1) lon(x)]; %step through our lon,lat vectors
33     LAT=[lat(x-1) lat(x)];
34     Δm_lldist(LON,LAT); %gets the distance
35     ΔΔ(:); %forces column vector
36     ΔDist = [ΔDist; Δ];
37     range = [range; sum(ΔDist(1:x-1))]; %range adds up all the Δ's
38     waitbar(x/length(lon)) %update waitbar
39 end
40 close(h) %close waitbar
41
42
43 range=range*1000; %convert to meters.
44 range=range(:);
45 clear lon1 lat1 LON LAT
46 %%%%%%%%%%%%%%%%%%%%%%%%%%%%%%%%%%%%%%%%%%%%%%%%%%%%%%%%%%%%%%%%%%%%%%%%%
47
```

Appendix 1

```
48
49
50 % CTD data interpolation, plotting, etc.
51
52 depth=subdata(:,5);
53 temp=subdata(:,2);
54 %cond=sortdata(:,12);
55 pressure=subdata(:,4);
56 time=subdata(:,1);
57
58 salt= calculate_glider_salinity(subdata(:,3), subdata(:,2), subdata(:,4)*10); %calc salinity
59 %dens = sw_dens(S,T,P)
60 dens = sw_dens(salt,temp,pressure*10);
61 o2sat=subdata(:,8);
62
63 ind = find(depth ≤ 0.5); %drop the upper 0.5 of meters, makes it look nicer...
64 depth(ind) = [];
65 temp(ind) = [];
66 salt(ind) = [];
67 range(ind) = [];
68 dens(ind)=[];
69 o2sat(ind)=[];
70 clear ind;
71
72 %%% contouring:
73
74 minDist = min(floor(range)); maxDist = max(ceil(range));
75 minDepth = min(floor(depth)); maxDepth = max(ceil(depth));
76 xInc = 50; yInc = 1; %specify our resolution here.
77 xScale = 0.001;
78 depthRange = minDepth:yInc:maxDepth;
79 distRange = minDist:xInc:maxDist;
80 [xi, yi] = meshgrid(distRange, depthRange);
81
82 clear minDist maxDist minDepth maxDepth distRange depthRange xInc yInc
83
84 %contour function craps out sometimes with big numbers, multiply by a scaling factor to make it smaller:
85 xi = xi*xScale; range = range*xScale;
86
87 %this grids the data we want plotted, it can be temp, sal, dens, O2sat, or whatever:
88 toPlot = griddata(range, depth, temp, xi, yi);
89 xi = xi./xScale; range = range./xScale; %undo the scaling..
90
91
92 figure
93
94 pcolor(xi, -yi, toPlot); shading interp; %does a pcolor plot
95 caxis([min(temp) max(temp)]); hold on % "temp" can be changed to whatever variable is being contoured.
96 [c h]=contourf(xi, -yi, toPlot, 8); %adds contour lines to our pcolor plot.
97 colorbar;
98 xlabel('Distance along track (km)'); ylabel('Depth (m)'); %labeling.
```

A.2 CTD Corrections

A.2.1 Fofonoff Correction for Lagged Response

```
1 function lagcorrected_variable=fofonoffcorrect(variable,time,tau) %from fofonoff et al (1974)
2
3 %%% This is the fofonoff correction, see fofonoff et al, 1974, pages 1-18.
4 %%%
5 %%% We have 2 versions here. The first is using linear regression, the second is standard first differences.
6 %%%
7 %%% usage: lagcorrected_variable=fofonoffcorrect(variable,time,tau)
8 %%%
9 %%% where variable is either temperature or conductivity.
10
11
12
13 n=length(variable);
14
15
16 %%%%%%%%%%%%%%%%%%%%%%%%%%%%%%%%%%%%%%%%%%%%%%%%%%%%%%%%%%%%%%%%%%%%%%%%%%%This is fofonoff using linear regression with 3 points:
17
18 N=3;
19 dt=mean(diff(time)); %we should have the data evenly spaced before passing to this algorithm
20
21
22 %this is the calculation of the filter weights (see fofonoff et al, 1974. page18):
23 a=1/N + tau/dt * (12*n - (6*(N+1))) / (N*(N^2 - 1));
24 a=a(:); %force column vector
25
26 for i=1:3:length(a) %every "N" filter weights must sum to 1.
27     test=a(i:i+N-1);
28     test=test./sum(test);
29     a(i:i+N-1)=test;
30 end
31
32 filter.times.variable=a.*variable;
33 for i=1:length(variable)-2
34     lagcorrected_variable(i)=sum(filter.times.variable(i:i+N-1));
35 end
36
37 lagcorrected_variable=lagcorrected_variable(:); %force column
38
39
40 %if our time series isn't a factor of N, we drop the last few points:
41 index=1:length(variable);
42 toofar=find(index>(max(1:3,length(a))));
43 lagcorrected_variable(toofar)=NaN;
44
```

Appendix 1

```
45
46
47 %%%%%%%%%%%%%%%%%%%%%%%%%%%%%%%%%%%%%%%%%%%%%%%%%%%%%%%%%%%%%%%%%%%%%%%%%this is fofonoff using first differences:
48
49
50 % h = waitbar(0,'Please wait...'); %initialize waitbar
51 % for i=1:n
52 %     if i==1 %boundary condition.
53 %         lagcorrected_variable(1)=variable(1);
54 %     if i==n %boundary condition
55 %         dt=time(i)-time(i-1);
56 %         dT=variable(i)-variable(i-1);
57 %         A=variable(i);
58 %         B=tau* dT./dt;
59 %         lagcorrected_variable(i)=A+B;
60 %
61 %     else %main loop
62 %         dt=time(i+1)-time(i);
63 %         dT=variable(i+1)-variable(i);
64 %         A=variable(i);
65 %         B=tau* dT./dt;
66 %         lagcorrected_variable(i)=A+B;
67 %     end
68 %     waitbar(i/n) %update waitbar
69 % end
70 %close(h)
71 %lagcorrected_variable=lagcorrected_variable(:); %force column
72 %end
```

A.2.2 Correction for Thermal-Lag

```
1 function temp_for_salinity_calculation=thermallagcorrection(temp,alpha,tau,nyquist)
2
3
4 %%% algorithm to correct for thermal lag in conductivity.
5 %%% based on morison et al (1994)
6 %%%
7 %%%
8 %%% usage: temp_for_salinity_calculation=thermallagcorrection(temp,alpha,tau,nyquist)
9 %%% you must specify alpha, tau and the nyquist.
10 %%%
11 %%% the output "temp_for_salinity_calculation" can then be used with conductivity values
12 %%% for new salinity calculations
13 %%%
14 %%% Charlie Bishop. 2008. Version 4.
15
16
17 a=(4*nyquist*alpha*tau)/(1+(4*nyquist*tau)); %a and b are parameters for the correction
18 b=1-(2*a)/alpha;
```

Appendix 1

```
19
20
21 %initialize so that it doesnt grow inside the loop. saves a lot of time;
22 temp_correction=zeros(length(temp),1);
23
24
25
26 for i=2:length(temp) %the main loop
27 temp_correction(i)=-b*temp_correction(i-1)+a*(temp(i)-temp(i-1));
28 end
29
30 %set the first equal to the second, so our series stays the same length
31 temp_correction(1)=temp_correction(2);
32
33
34 %take the correction term from the original series:
35 temp_for_salinity_calculation=temp-temp_correction;
```

A.3 Optode Corrections

A.3.1 Back-Calculation of Phase Data

```
1
2 function [Dphase, index]=backcalculate_phasedata(oxygen,T,time,T_CTD);
3
4 % Script to back-calculate phase data for the aanderraa oxygen optode
5 %
6 % in order to properly adjust for the lag in response of the instrument we
7 % must back calculate the phase data, apply our lagged-correction
8 % algorithm, then recalculate oxygen concentrations using the CTD measured
9 % temperatures.
10 %
11 %
12 % If DPHASE length is less than original vector length, use the "index"
13 % output to correct other variables. Index were the finite entries.
14 % example: temperature=temperature(index);
15 %
16 %
17 % *****NaN's should be removed from the data before passing to this script.*****
18 %
19 % Charlie Bishop, May 2007
20 %
21 %
22 %
23
24
```

Appendix 1

```
25
26
27 %declare calibration coefficients. These may
28 %change in the future, they are supplied by manufacturer.
29
30 C00=3.17242E+03;
31 C01=-1.07261E+02;
32 C02=2.13316E+00;
33 C03=-1.79234E-02;
34
35 C10=-1.73981E+02;
36 C11=5.10262E+00;
37 C12=-9.85758E-02;
38 C13=8.02240E-04;
39
40 C20=3.95600E+00;
41 C21=-9.81040E-02;
42 C22=1.85346E-03;
43 C23=-1.42536E-05;
44
45 C30=-4.26337E-02;
46 C31=8.78820E-04;
47 C32=-1.64409E-05;
48 C33=1.13709E-07;
49
50 C40=1.76869E-04;
51 C41=-2.95502E-06;
52 C42=5.55039E-08;
53 C43=-3.08493E-10;
54
55
56 for i=1:length(T); %loop through temperature data.
57
58 C0(i)=C00+C01*T(i)+C02*T(i)^2+C03*T(i)^3;
59 C1(i)=C10+C11*T(i)+C12*T(i)^2+C13*T(i)^3;
60 C2(i)=C20+C21*T(i)+C22*T(i)^2+C23*T(i)^3;
61 C3(i)=C30+C31*T(i)+C32*T(i)^2+C33*T(i)^3;
62 C4(i)=C40+C41*T(i)+C42*T(i)^2+C43*T(i)^3;
63 end
64
65 C0=C0'; %force column vectors
66 C1=C1';
67 C2=C2';
68 C3=C3';
69 C4=C4';
70
71
72 CONSTANT=C0-oxygen; %the following lines set up our polynomial.
73 p=[C4 C3 C2 C1 CONSTANT];
74 index=isfinite(p(:,1));
75 P=p(index,:); %finite entries
76
```

Appendix 1

```
77
78 for i=1:length(P) %%% this is the main loop for solving for the roots.
79     r=roots(P(i,:));
80     b = r(imag(r)==0);
81     a=find(b>10 & b<70);
82     if length(a)==0
83         Dphase(i)=NaN;
84     else
85         Dphase(i)=b(a);
86     end
87 end %%% end the main loop
88
89 Dphase=Dphase(:); %force column vector
```

A.3.2 Adjusting for Lagged Response

```
1 %%% UNESCO SCOR working group calibration for lagged response, case 5.
2 %%%
3 %%% Charlie Bishop, May 2007
4
5
6 function [lagcorrected_variable]=calibrate_variable_wrt_timeconstant(variable,time,tau)
7
8
9
10
11
12 n=length(variable); % our timeseries length.
13
14
15
16 for i=1:n
17     if i==1 %boundary condition
18         lagcorrected_variable(i)=variable(i);
19     elseif i==n %boundary condition
20         dt=time(i)-time(i-1);
21         A=(1-exp(-(dt/tau)))=variable(i);
22         B=exp(-(dt/tau))*lagcorrected_variable(i-1);
23         lagcorrected_variable(i)=A+B;
24
25     else
26         dt=time(i+1)-time(i);
27         A=(1-exp(-(dt/tau)))=variable(i);
28         B=exp(-(dt/tau))*lagcorrected_variable(i-1);
29         lagcorrected_variable(i)=A+B;
30     end
31 end
32
33
```

Appendix 1

```
34 lagcorrected_variable=lagcorrected_variable(:); %force column
35
36
37
38
39
40
41
42 %%%%%%%%%%
```

A.3.3 Re-calculation of DO_2

```
1 function lagcorrected_O2_conc=calculate_O2_corrected(correctedphase,T)
2
3
4 % calculate O2 concentration using the backcalculated phase data.
5 % where T is the lag-corrected CTD temperature :
6 %
7 %
8 % Charlie Bishop. May 2007
9 %
10 % usage: lagcorrected_O2_conc=calculate_O2_corrected(correctedphase,lagcorrected_CTD_temp)
11
12
13 C00=3.17242E+03; % original coefficients
14 C01=-1.07261E+02;
15 C02=2.13316E+00;
16 C03=-1.79234E-02;
17
18 C10=-1.73981E+02;
19 C11=5.10262E+00;
20 C12=-9.85758E-02;
21 C13=8.02240E-04;
22
23 C20=3.95600E+00;
24 C21=-9.81040E-02;
25 C22=1.85346E-03;
26 C23=-1.42536E-05;
27
28 C30=-4.26337E-02;
29 C31=8.78820E-04;
30 C32=-1.64409E-05;
31 C33=1.13709E-07;
32
33 C40=1.76869E-04;
34 C41=-2.95502E-06;
35 C42=5.55039E-08;
36 C43=-3.08493E-10;
37
```

Appendix 1

```
38
39
40 for i=1:length(T); %our main loop
41
42 C0(i)=C00+C01*T(i)+C02*T(i)^2+C03*T(i)^3;
43 C1(i)=C10+C11*T(i)+C12*T(i)^2+C13*T(i)^3;
44 C2(i)=C20+C21*T(i)+C22*T(i)^2+C23*T(i)^3;
45 C3(i)=C30+C31*T(i)+C32*T(i)^2+C33*T(i)^3;
46 C4(i)=C40+C41*T(i)+C42*T(i)^2+C43*T(i)^3;
47
48
49 %new DO2 concentrations:
50 lagcorrected_O2_conc(i)=C0(i)+(C1(i)*correctedphase(i))+(C2(i)*correctedphase(i)^2)+(C3(i)*correctedphase(i)^3)+(C4(i)*correctedphase(i)
51
52 end
53
54
55
56 lagcorrected_O2_conc=lagcorrected_O2_conc(:); %force column vector
```

A.3.4 Adjusting for Salinity

```
1 function [O2_corrected]=correctO2.wrt.salinity(salinity,temp,oxygen);
2
3 %%% oxygen must be in micro-molar
4
5 %this formula is taken from the sanderraa optode manual
6
7
8
9 S=salinity;
10
11 %%declare constants:
12 B0=-6.24097E-3;
13 B1=-6.93498E-3;
14 B2=-6.90358E-3;
15 B3=-4.29155E-3;
16 C=-3.11680E-7;
17
18 %% Ts is our scaled temperature:
19 top=298.15-temp;
20 bottom=273.15+temp;
21 Ts=log(top./bottom);
22
23
24 %%% compensate for salinity:
25 O2_corrected=oxygen.*exp(S.*(B0+(B1.*Ts)+(B1.*Ts.^2)+(B1.*Ts.^3))+C.*S.^2);
```

A.3.5 Adjusting for Pressure

```
1 function [O2.wrt.depth]=correctO2wrtdepth(O2,depth)
2
3 %%% this correction for pressure. the change is negligible because our glider only
4 %%% goes to 200m of depth.
5
6
7
8 O2conc=O2_corrected_salinity.*(1+(.04.*depth/1000)); %simple pressure correction algorithm
```

A.4 Water Velocity Calculator

```
1 %must have a DBD file OR full data set loaded, with all variables declared:
2 %m_depth_state=something, m_present_time=something, etc.
3 %
4 %
5 % This is version 7. Fully working as of Jan. 19th
6 %
7 % this requires the m_map package, also requires ddm2ddd.m (which changes the formatting of the gps coords)
8
9
10
11 surfCur=[]; %initialize our variables.
12 currentINFO=[];
13 gpserror=3; %this is in meters, specified in user manual.
14
15
16 [r c]=find(isnan(data(:,m_depth_state))); %gets rid of the NaNs.
17 data(r,:)=[];
18 data(:,m_heading)=data(:,m_heading)*180/pi; %convert heading to degrees
19
20
21 data(1,m_depth_state)=1; %this is set for formatting purposes.
22
23 data(:,m_heading)=data(:,m_heading)*180/pi; %convert heading to degrees
24
25
26
27
28
29 %convert to proper lat/long
30 [data(:,m_gps_lat), data(:,m_gps_lon)] = ddm2ddd(data(:,m_gps_lat), data(:,m_gps_lon));
31 %get rid of junk in our longitude data:
32 [r]=find(data(:,m_gps_lon)>0);
```

Appendix 1

```
33 data(x,:)=[];
34
35
36 for i=2:length(data) %loop through our data
37     if data(i,m.depth.state)~=0 %find the entries that are not at the surface
38         %this finds anomalies in depth.state while at the surface:
39         if data(i-1,m.depth.state)==0 && data(i+1,m.depth.state)==0
40             %make sure the points are close in time:
41             if data(i+1,m.present.time)-data(i-1,m.present.time)<1100
42                 data(i,m.depth.state)=0; %fix the data point
43             end
44         end
45     end
46 end
47
48
49 i=2;
50 while i<length(data)-1 %the main loop
51
52
53 count=0; %restart the count at every surface event.
54
55     while data(i,m.depth.state)==0 %run through surfacing event
56         count=count+1; %count to see how many values we have at the surface
57         i=i+1;
58     end
59
60     if data(i-1,m.depth.state)==0 %define our surface event
61         % all relevant information from surfacing event:
62         currentINFO=data(i-count:i,[m.present.time m.gps.lon m.gps.lat m.heading]);
63         startpoint=i-count;
64         endpoint=i;
65
66
67         [r c]=find(isnan(currentINFO(:,[2 3]))); %get rid of NaNs in lon/lat
68         currentINFO(r,:)=[];
69         %drop very first entry and last, as often times it is an incorrect
70         %GPS hit:
71         currentINFO=currentINFO(2:end-1,:);
72
73
74
75         [x y]=size(currentINFO); %get the size of the new surf event.
76
77         %if the data isnt empty, we make a new entry:
78         if isempty(currentINFO)==0 & length(currentINFO)>5
79
80             difftime=diff(currentINFO(:,1)); %difference between consecutive gps hits.
81
82             j=1;
83             while difftime(j)<100
84                 j=j+1;
```

Appendix 1

```
85     if j==length(difftime)
86         break
87     end
88 end
89
90 surface_startpoint=1;
91 surface_endpoint=j-1;
92 dive_startpoint=j;
93 dive_endpoint=length(currentINFO);
94
95 maxdifftime=max(difftime);
96
97 if maxdifftime<20
98     surface_endpoint=floor(length(currentINFO)/2);
99     dive_startpoint=floor(length(currentINFO)/2)+1;
100
101 end
102
103
104 %taking averages and standard deviations for calculating DRMS error:
105 surface_avglon=nanmean(currentINFO(surface_startpoint:surface_endpoint,2));
106 surface_avglat=nanmean(currentINFO(surface_startpoint:surface_endpoint,3));
107 dive_avglon=nanmean(currentINFO(dive_startpoint:dive_endpoint,2));
108 dive_avglat=nanmean(currentINFO(dive_startpoint:dive_endpoint,3));
109
110
111 dlon=dive_avglon-surface_avglon; %dlon - longitude difference in degrees
112 alat=nanmean(currentINFO(:,3)); %alat = average latitude between the two fixes
113 dlat=dive_avglat-surface_avglat; %dlat = latitude difference in degrees
114 alon=nanmean(currentINFO(:,2)); %alat = average longitude between the two fixes
115 dx = lon_to_m(dlon, alat); %meters
116 dy = lat_to_m(dlat, alat); %meters
117 dt = currentINFO(x,1)-currentINFO(1,1); %seconds
118
119
120
121 if abs(dx)>35 | abs(dy)>35 % dont take surfacings that travel less than 35m.
122
123 U=dx/dt;
124 V=dy/dt;
125
126 %error using standard error formulas, see Chapter 5 of thesis:
127 errorU=((gpserror+gpserror)/abs(dx))*abs(U);
128 errorV=((gpserror+gpserror)/abs(dy))*abs(V);% " "
129
130
131 %update surface currents vector, surfCur = [longitude,latitude,difference in x,difference
132 % in y, U, V, dt at surface, time it surfaced, startpoint,
133 %endpoint, mean of the heading info during event, variance of heading info
134 %during event. ] :
135
136 surfCur=[surfCur; alon alat dx dy U V dt errorU errorV currentINFO(1,1) startpoint endpoint ...
```

Appendix 1

```
137 nanmean(currentINFO(3:end,4)) nanvar(currentINFO(3:end,4));
138
139
140     end
141
142 end
143
144 end
145
146 i=i+1;
147 end
148
149 start*surfCur(:,10); %times of surfacing events
150 v=datevec(darenum(1970,1,1) + start/86400); %convert our time.
```





